The Role of Endothelial Mechanosensing in Capillary Development and Organization

by

Rahul K. Singh

A dissertation submitted in partial fulfillment
of the requirements for the degree of
Doctor of Philosophy
(Biomedical Engineering)
in the University of Michigan
2015

Doctoral Committee:

Associate Professor Andrew J. Putnam, Chair
Assistant Professor Jianping Fu
Professor Jan P. Stegemann
Professor Stephen J. Weiss

Acknowledgments

I would like to thank my thesis advisor Professor Andrew Putnam and members of my thesis committee, professors Jianping Fu, Jan Stegemann, and Stephen Weiss.

I would also like to thank my colleagues: Drs. Bita Carrion, Jacob Ceccarelli, Stephanie Grainger, Isaac Janson, Suraj Kachgal, Yen Peng Kong, David Lai, Ram Rao, Marina Vigen and (soon-to-be Dr.) Ana Rioja. I also thank my team of undergrads who were critical to completion of the final aim: Evan Chen, Spencer Paris, and Matthew Tan.

This work was partially supported by grants from the US-Israel Binational Science Foundation (Award #2007366) and the National Institutes of Health (R01-HL085339) and National Science Foundation CAREER Award #0968216. RKS was partially supported by a pre-doctoral fellowship from the NIH (NIDCR)-funded Tissue Engineering and Regeneration training program (T32-DE007057) at the University of Michigan.

Finally, I would like to thank my father, Professor Rakesh Singh, my mother, Ms. Sunita Singh, and my sister (soon-to-be Dr.) Supriya Singh for their love and support.

Contents

List of Figures

List of Tables

List of Appendices

Abstract

Ischemic injury is a leading cause of morbidity and mortality with the most common causes being heart attack, stroke, and peripheral artery disease. Therapies attempt to improve healing, in part, by promoting angiogenesis in these ischemic sites. Angiogenic invasion and maturation into a new capillary network may be affected by the altered microstructure and the mechanical properties of the ischemic tissue, in particular, the extracellular matrix (ECM). It is known that endothelial cells (EC) are mechanosensitive and reorient in response to both shear and normal stresses in vessels. Further, they generate traction forces and displacements in 2D culture to coordinate motion. However, the question of whether EC use cell-generated ECM forces to communicate in 3D culture to direct capillary organization and anastomosis is currently unresolved.

Hydrogels formed from natural extracellular matrix (ECM) proteins readily support the formation of vasculature *in vitro.* The ECM is a highly ordered meshwork of various macromolecules. This anisotropic microstructure produces non-linear viscoelastic mechanical properties which confound attempts towards modeling the mechanical environment around cells. To overcome these issues, we developed a biosynthetic hydrogel consisting of polyethylene glycol diacrylamide conjugated to macromolecular type-I collagen. Through acrylamide-based cross-links, these materials allow for independent control of physical properties and bulk ligand concentration.

Photoencapsulation of EC and fibroblasts within this hydrogel material and their subsequent co-culture led to the formation of capillary vessel-like networks with well-defined hollow lumens. Patterned hydrogel constructs were produced to assess angiogenic invasion independently of other stages of EC organization. ECM displacements were observed over time and mechanical modeling was used to compute cell-generated stresses and strains. We found that regions of strain exceeding 9% and stress exceeding 1,500 pN/μm^2 co-localized with regions of capillary invasion (r=0.44). Thus, capillaries were found to generate stresses which propagated though the ECM.

Through these studies, we developed an engineered ECM which enabled the magnitudes of cell-generated stresses during a complex 3D morphogenetic process to be quantified for the first time. These findings could yield a better understanding of the physical principles guiding capillary morphogenesis and provide new strategies for treating ischemic disease.

Chapter 1:

Introduction

Motivation & Significance

Cardiovascular diseases are, worldwide, a leading cause of death (1). Examples of cardiovascular diseases are heart attacks and strokes which produce ischemic scars. In these sites, blood flow to the tissue is blocked and the tissue dies from a lack of oxygen and nutrients, as well as a buildup of waste products. Normally exchange of oxygen, nutrients, and waste occurs in the capillary bed. To resupply the tissue with blood flow, the capillary bed would need to be replaced or reattached to the circularity system. Promoting this process, called angiogenesis, is a promising target for emerging biotechnologies that attempt to heal the tissues (2).

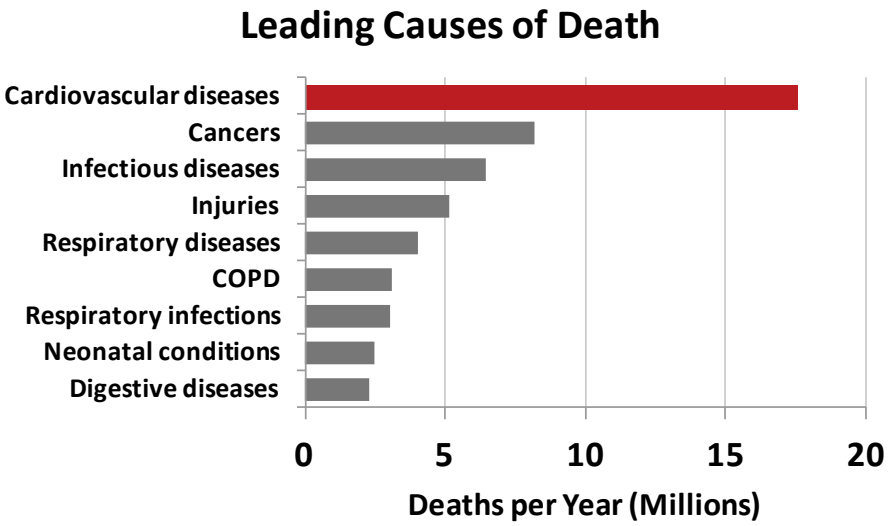

Figure 1: Leading causes of death worldwide

Cardiovascular diseases are the leading cause of death worldwide according to a 2012 WHO report. Cardiovascular diseases are prominent in all geographic and income divisions (1). Thus they are a promising target for improving human heath globally. Angiogenesis is the process by which capillaries grow from existing blood vessels into the surrounding tissue (Figure 2). This occurs at the cellular level wherein a tip cell is activated by angiogenic factors and adopts a migratory phenotype.

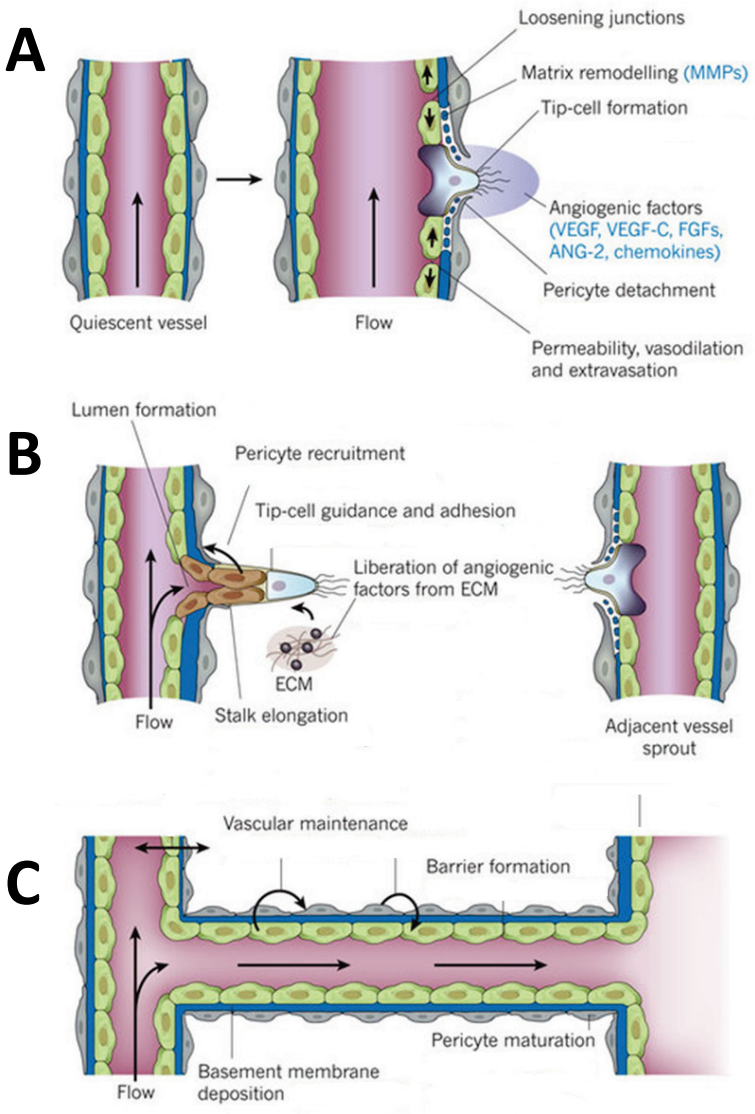

Figure 2: An overview of angiogenesis

A) Selection of a tip cell proceeds in response to angiogenic factors which prompt it to switch to a migratory phenotype while remodel the local matrix. B) The tip cell is followed by stalk cells as it migrates towards an adjacent vessel. C) Ultimately the vessels connect, a continuous lumen forms, and blood flow passes to the adjacent vessel. (Adapted from (3))

The tip cell remodels the matrix and is followed by a stalk of ECs and recruits pericytes. It proceeds to elongate the nascent sprout towards another blood vessel. Ultimately, a continuous lumen is formed connecting the vessels, and blood can pass from one to the

other. This process is known to be promoted by angiogenic factors such as VEGFs, FGFs, Ang2, PDGF, and TGF-β (3). Likewise, there has been much inquiry focused on the cues that promote and direct the migration of endothelial cells (EC) to establish new vasculature (4, 5).

Previous studies have determined the role of soluble factors in promoting angiogenesis and driving EC migration. The role of juxtacrine cues such as cell-cell junctions and Notch signaling have also been well investigated as mechanical mediators of EC phenotype (6). However, soluble factors and juxtracrine signaling do not adequately explain how EC can detect their environment in the neighborhood of a few cell lengths. In anastomosis, the leading EC is in contact with EC in the same capillary but not with EC in a distant capillary with which it is attempting to connect Thus, juxtracrine signaling between capillaries is hampered by their physical separation. Chemotaxis has been demonstrated through single-cell migration studies and likely provides coarse migratory cues to EC (7).

Approaches to producing capillaries *in vitro* have varied in their degree of success, which may be caused by the choices of growth factors, cells, and ECM. Previous work by our group has utilized an assay which produces robust capillary formation. Ghajar et al. (8) have shown that endothelial growth media can induce a co-culture of human umbilical vein EC with mesenchymal stem cells (MSC) in fibrin clots to produce stable capillaries *in vitro*. Further investigation into the effects of matrix density, matrix diffusivity, and stromal cell identity by Kniazeva et al. (9), Ghajar et al. (10), and Grainger et al. (11), revealed their respective influences on sprouting and network

formation within these constructs. Additional studies by Kachgal et al (12) and again by Ghajar et al (13) have interrogated the molecular mechanisms underlying angiogenic sprouting. However, the mechanism by which established capillaries and, in particular, endothelial tip cells can communicate over a distance has not been directly investigated by our group nor by any others.

Traditionally paracrine and juxtacrine factors have been investigated as mechanisms governing EC migration through the extracellular matrix (ECM) while the microstructural and mechanical properties of the ECM have not been as thoroughly interrogated (14). The structure and mechanical properties of these ischemic scars are significantly altered as compared to healthy tissue (15-18). It is known that ECs are mechanosensitive and reorient in response to both shear and normal stresses in vessels; further they can generate traction forces and displacements in 2D culture (19). The question of whether ECs utilize these physical cues to communicate with non-adjacent cells to direct their organization in a 3D tissue remains unresolved.

The hypothesis was first put forth by Thoma in 1893 as "Increase or decrease in the length of a vessel is governed by the tension exerted on the vessel wall in a longitudinal direction by tissues and organs outside the cell" Ref. in, (20). Later studies by Korff & Augustin showed matrix displacements were associated with endothelial cell sprouting (Figure 3). They further found that tensional forces were responsible for directional capillary sprouting (21). However, they were unable to quantify the magnitude of these matrix displacements or determine the underlying forces.

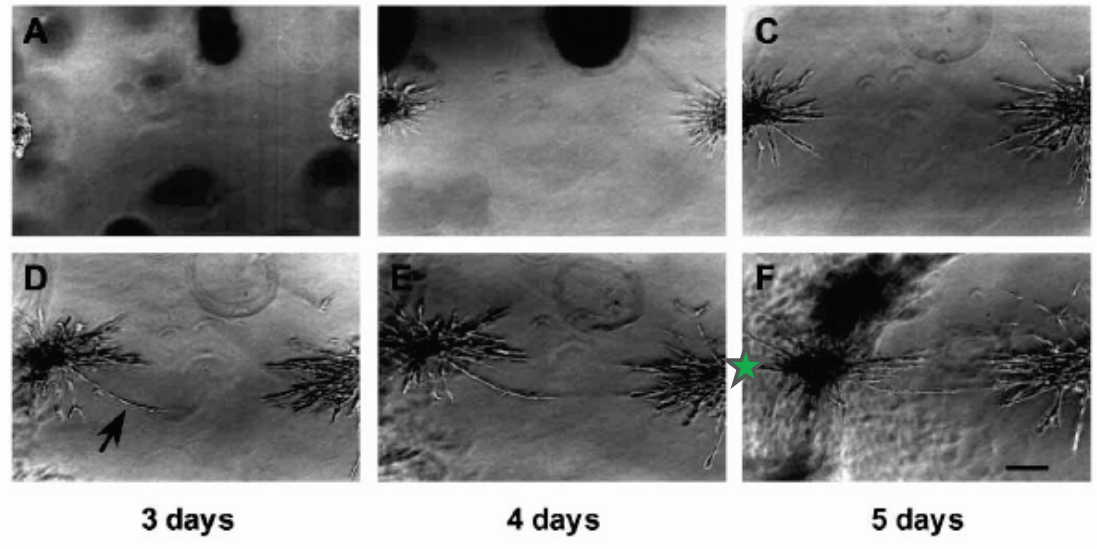

Figure 3: Angiogenesis is accompanied by ECM tension.

Time-lapse images of EC spheroids undergoing sprouting angiogenesis show displacements of the spheroids by day 5 (original location starred). This is attributed to tension between adjacent spheroids. Scale bar is 200 μm, adapted from (21).

Cellular communication at a distance has been demonstrated on fibrin clots Winer et al. (22) with smooth muscle cells and on polyacrylamide by Reinhart-King et al. (23) with endothelial cells, both through 2D traction force studies. Recently, tractional mapping in 3D has been demonstrated in polyethylene glycol (PEG) hydrogels with fibroblasts by Legant et al. (24). In addition, Kniazeva et al. (25) have previously demonstrated local matrix stiffening near angiogenic sprouts. A combination of these approaches would allow investigation as to whether angiogenic sprouts utilize tractional forces as directional cues to guide endothelial alignment, capillary maturation, and anastomosis into a capillary network.

Cellular Migration & Mechanics

Cellular forces were first observed by Harris et. al in 1980 by observing cells cultured on 2D silicone membranes. The cells were found to generate wrinkles on the thin membrane as they grew and this was attributed to cell-generated forces (26). Later work by Dembo et al. established a method wherein small marker particles are embedded in an elastic substrate and the motions of these particles are tracked to determine a displacement field produced by cellular tractions (27). This approach is known as traction force microscopy. Later, Dembo & Wang refined this approach and applied it to mammalian cells (28). Extending this work, Pellham & Wang refined the approach to consist of cells cultured on elastic, collagen-coated polyacrylamide sheets embedded with 0.2-μm fluorescent beads (29). Their approach has remained the mainstay of traction force studies until very recently.

Earlier work by the same two authors established that the rigidity, or more precisely, the elastic modulus of the substrate could affect cellular spreading and motility (30). Thus, generalizable quantity is needed to compare cell responses under different conditions. By measuring the displacement field, normalizing by the modulus, and spreading the force over the cell surface area they arrived at a cell traction force. This value can be easily compared between studies and measurement approaches (Table 1).

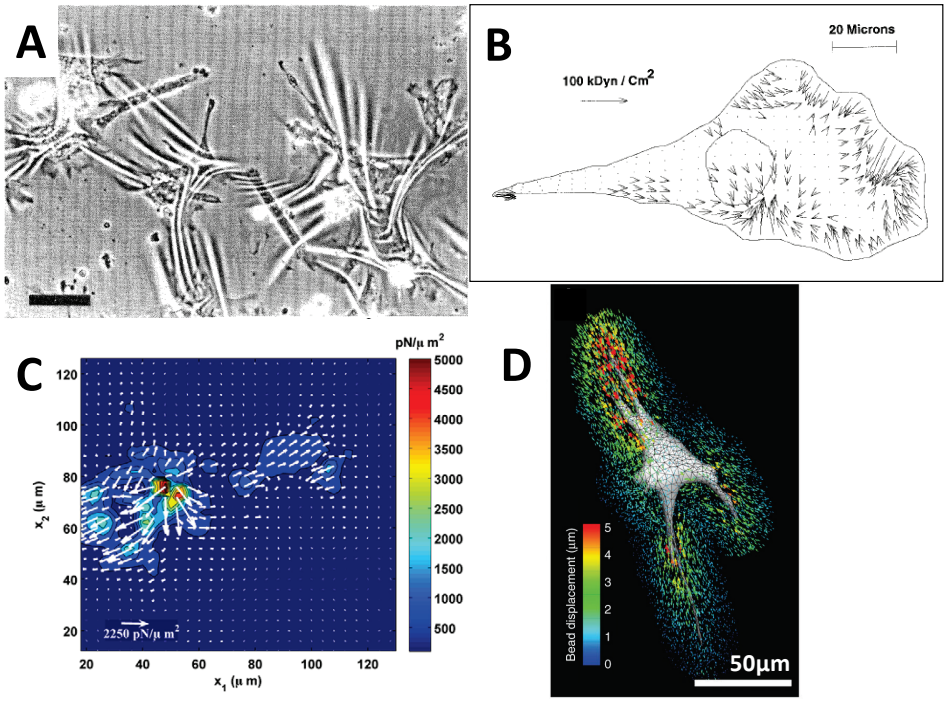

Figure 4: Evolution of traction force microscopy

A) Harris et al. demonstrated cellular tractions by observing the wrinkling of silicone sheets (26). B) Dembo et al. developed techniques which allowed cell tractions to be measured on 2D substrates (27, 28). Extensions of these studies allowed for 3D forces to be observed below cells (C) on 2D substrates (31) and surrounding encapsulated cells(D) (24). Figures adapted from respective sources.

Peak Stress (pN/μm²)	Duration	Material	Cells	Reference
2,000-10,000	*Relaxation*	2D Polyacrylamide	Fibroblast	Dembo (1999)
2,000-6,000	7 days	PDMS Microposts	MSC	Fu (2010)
1,300-3,600	*Relaxation*	2D Polyacrylamide	Endothelial	Califano (2010)
1,200-5,000	140 min	2½D Polyacrylamide	Fibroblast	Franck (2011)
500-5,000	90 min	3D PEG Hydrogel	Fibroblast	Legant (2010)
40-150	*Relaxation*	3D Collagen Gel	Epithelial	Gjorevski (2012)

Table 1: List of key traction force studies

As previously mentioned, visualizing the result of force propagation through the ECM requires precise observation of displacements generated by cells. An established technique for visualizing displacements in cell culture systems involves embedding microcarrier beads in the ECM. This has been used to capture displacements driven by thermal motion (32), by cells pulling on deformable substrates (33), cells migrating on 2D hydrogels (31), and for cellular extensions in 3D PEG hydrogels (24). These approaches allow forces to be computed and work well for homogenous materials, but fail to capture the more complex behavior of fibrin clots and collagen gels (34, 35). Of note, is the discrepancy shown by Gjorevski et al. in Table 1. Their use of a collagen matrix coupled with a linear elastic material model led to significant errors in the measurement of cellular tractions. The authors attempted to compensate for this by including a correction factor, but this approach is not ideal (36). More accurate measures of matrix deformation are instead observed through fiber displacements (37), but these fiber element-based models do not allow for simple computation of force gradients. Thus, solving the inverse problem of determining the forces that create an observed displacement is complex and often relies on a simplifying mechanical model. However, this model must be appropriate for the material to be of use.

Synthetic ECM for Endothelial Cell Culture

Traditionally, EC are cultured on 2D substrates. This format allows for modeling of the vascular epithelium under fluid shear stresses and has been a fertile avenue of

research into vascular biology (38). Established synthetic hydrogels composed of polydimethylsiloxane (PDMS), polyacrylamide, or polyethylene glycol (PEG) have been shown to be adhesive to stromal cells (39-42) but have not been adhesive to EC to the same degree *in vitro* (43). Of note is the work of Leslie-Barbick et al. (44) where a monolayer of EC are found to spontaneously form capillary-like structures on top of pre-polymerized PEG gels (45). However, translation of these systems to culturing EC has not been as productive. This hurdle may be due to either different ECM binding mechanisms employed between stromal and endothelial cell types (46, 47), or due to inconsistent quantification of ECM binding between hydrogel platforms.

Transitioning to 3D culture of EC has met with difficulties *in vitro*. While PEG hydrogels have been shown to promote vascularization in vivo (48, 49), they have not supported vascular formation in vitro to the same extent. When encapsulated in a 3D matrix, cells must not only respond to the ligand presentation and stiffness of the matrix, but also proteolytically remodel the matrix while maintaining to access sufficient concentrations of nutrients and growth factors (50). Thus, appropriate matrix crosslinking strategies are essential for 3D cell culture.

A common approach to altering the crosslinking of the ECM is to increase the density of the ECM. While this changes the mechanical properties, it also changes the number of ligand binding sites and diffusivity. Synthetic ECM have the advantage of altering the mechanical properties and diffusivity (physical properties) without affecting the number of ligand binding or proteolytic cleavage sites (biochemical properties). Synthetic ECM often consist of inert polymers and adhesive peptide sequences. The extent of polymer

crosslinking controls the physical properties of the gel. However, the biochemical properties of the gel are determined by the peptide sequence and concentration(50).

Hydrogels can now be designed with specific peptide binding motifs, proteolytic degradation sequences, and assembly chemistries (51). This remarkable specificity poses a problem for engineering a new cellular niche. We must know *a priori* which peptide sequences to include into the gel. While there are a litany of 'usual suspects' e.g. RGDS and GFOGER for binding, it is inefficient to test all permutations of binding motif, degradation sequence, and crosslinking chemistry.

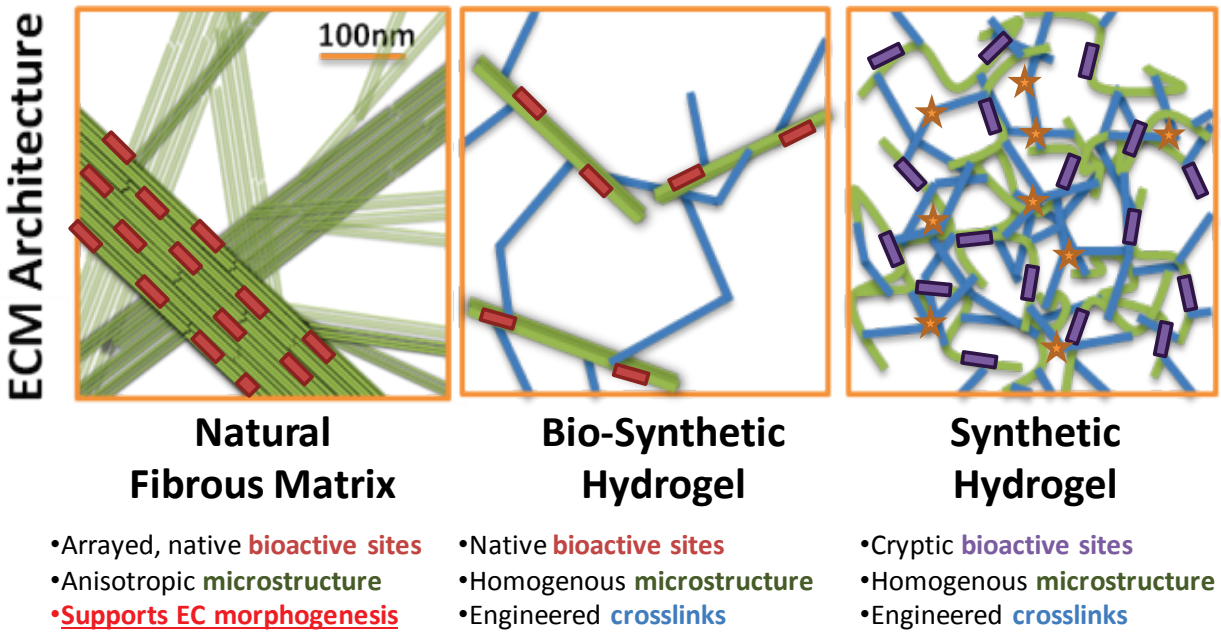

Figure 5: An overview of the approaches to hydrogel design.

Natural hydrogels consist of fibers which have an anisotropic microstructure and support EC morphogenesis. Synthetic hydrogels have a homogenous microstructure, but do not support EC morphogenesis. A hybrid bio-synthetic hydrogel may allow for both a homogenous microstructure and EC morphogenesis.

An alternative to this bottom-up approach is a top-down approach were we begin with a biologically favorable matrix molecule and modify it to have the desired physical properties. These bio-synthetic hydrogels consist of biologically derived components immobilized in a polymer matrix. Conjugation of denatured fibrinogen and collagen for use in 3D cell culture was reported by Seliktar et al. through a number of studies (52-54) while fibrinogen conjugates have been utilized by Peyton et al. (55) for smooth muscle cell culture. Unfortunately, *in vitro* capillary morphogenesis has not been demonstrated in synthetic ECM to the same degree as in fibrin clots (56, 57). This may be due to either inappropriate choice of peptide motifs, non-native conformations of ECM proteins, or a lack of a fibrillar structure.

Objectives & Specific Aims

Following a heart attack or stroke, revascularization of the ischemic scar has been proposed to improve healing. Angiogenic invasion into the scar and maturation into a new capillary network may be affected by the microstructure and the mechanical properties of the scar tissue, in particular, the extracellular matrix (ECM). Traditionally hypoxic, paracrine, and juxtacrine factors have been investigated as mediators of cellular communication; however, the question of how these cells sense their local environment and communicate with non-adjacent cells in order to organize into capillaries and later to anastamose has not been resolved. It is known that endothelial cells (EC) are mechanosensitive and reorient in response to both shear and normal stresses in vessels. Further, they can generate traction forces and displacements in 2D culture. Thus, I hypothesize that in a 3D co-culture model of stromal cells and EC, **the EC utilize the propagation of cell-generated displacements through the ECM to guide the organization of capillary structures**. This will be addressed in the following three aims.

Aim 1: <u>Develop a biosynthetic material platform for endothelial cell (EC) culture</u>. A composite material platform based on the conjugation of polyethylene glycol to type-I collagen, the most abundant ECM protein in the human body, will be developed and characterized. Subsequent cross-linking of the PEG chains into a hydrogel will demonstrate that macromolecular structure and assembly can be controlled via the PEG moieties while the collagen content is held constant. The bulk mechanical

properties, diffusivity, and structure will be assessed. Biocompatibility through 2D adhesion ECs will be assessed on each material.

Aim 2: Determine the influence of matrix crosslinking on EC migration and organization. Viability, elongation, and motility of encapsulated cells will be demonstrated. Maturation of tubules into capillaries will be monitored through ECM remodeling, lumen formation, and permeability, which will be observed using immunofluorescent staining and confocal microscopy in 3D culture.

Aim 3: Investigate the influence of local displacement fields on capillary organization in vitro. Patterned hydrogel constructs will allow *in vitro* live cell-tracking to assess the relationship between capillary invasion and bead displacement. A system will be developed to allow ECM displacements in a 3D co-culture model to be observed through the displacement of embedded beads. The observed bead motions will be correlated with nearby cellular migration and subsequent tubule formation.

Successful completion of these aims will provide new insight into cellular organization and produce a better understanding of the physical principles guiding capillary morphogenesis. Application of this knowledge could lead to improved strategies for revascularization and the treatment of ischemic diseases.

Overview of Methods

Macromolecular Synthesis (Aim 1): Poly(ethylene glycol) diacrylamide and poly(ethylene glycol) diacrylate will be produced from commercial poly(ethylene glycol) using established methods (58). Functionalization efficiency will be assessed via NMR. Conjugation to fibrinogen and collagen will be accomplished using Michael's type and *N*-hydroxysuccinimide mediated addition. Conjugation efficiency will be assessed by biochemical approaches (52, 59).

Physical Characterization (Aim 1): Polymerization rate and shear modulus will be measured by rheology and hydrolysis by bulk release of protein (55, 60). The hydrogels' effective diffusion constant and pore size will be measured using a fluorescent tracer (10). Rheological dynamic mechanical analysis will be used to determine the strain and frequency-dependent behavior of the complex modulus and used to create appropriate viscoelastic constitutive models (61-63).

Tissue Culture (Aim 1 & 2): Bright field and fluorescent images will be collected on an Olympus IX81 inverted microscope with a Hammatsu C10600 CCD digital camera. The viability of stromal and EC cultured on 2D hydrogel constructs and photoencapsulated inside 3D constructs will be assessed using ethidium staining and reported as a percent of the observed population (64). Bulk degradation of hydrogels will be assessed through measurements of the shear modulus, and migration within the constructs will be monitored by live cell tracking (65). Network morphology of co-cultures will be quantified by measuring segment length and total length (66-68).

Microfabrication of Vascular Arrays (Aim 3): Patterned hydrogel constructs will be created by utilizing the UV polymerization of PEG derivatives (69). This

photolithographic approach will be used to create 3D tissue constructs with well-defined cellular niches (70). The ability of EC to invade across boundaries and into varying geometries of ECM will be assessed by confocal microscopy. The physical properties of the ECM will be altered and the effect on EC invasion will be measured.

Software development and analysis (Aim 3): The MATLAB scripting environment will be utilized to automate image processing, statistical analysis, and the computation of physical parameters. Algorithms to track bead displacements will report magnitudes of orthogonal strain components. A continuum model will allow localized displacements to be transformed to stresses. By outlining strain fields, we will correlate those fields will to cellular migration (23, 71).

References

1. World health statistics 2012. Geneva, Switzerland: WHO Press, 2012.

2. Henry TD, Satran D. Therapeutic Angiogenesis: Coronary Artery Disease. In: Barsness GW, Holmes DR, editors.: Springer London; 2012. p. 67-74.

3. Carmeliet P, Jain RK. Molecular mechanisms and clinical applications of angiogenesis. Nature. 2011;473(7347):298-307.

4. Eilken HM, Adams RH. Dynamics of endothelial cell behavior in sprouting angiogenesis. Current Opinion in Cell Biology. 2010;22(5):617-25. doi: 10.1016/j.ceb.2010.08.010.

5. Herbert SP, Stainier DYR. Molecular control of endothelial cell behaviour during blood vessel morphogenesis. Nat Rev Mol Cell Biol. 2011;12(9):551-64.

6. Holderfield MT, Hughes CCW. Crosstalk Between Vascular Endothelial Growth Factor, Notch, and Transforming Growth Factor-β in Vascular Morphogenesis. Circulation Research. 2008;102(6):637-52. doi: 10.1161/circresaha.107.167171.

7. Milde F, Bergdorf M, Koumoutsakos P. Particle Simulations of Growth: Application to Angiogenesis: Modeling Tumor Vasculature. In: Jackson TL, editor.: Springer New York; 2012. p. 305-34.

8. Ghajar CM, Blevins KS, Hughes CCW, George SC, Putnam AJ. Mesenchymal stem cells enhance angiogenesis in mechanically viable prevascularized tissues via early matrix metalloproteinase upregulation. Tissue engineering. 2006;12(10):2875-88.

9. Kniazeva E, Putnam AJ. Endothelial cell traction and ECM density influence both capillary morphogenesis and maintenance in 3-D. American Journal of Physiology - Cell Physiology. 2009;297(1):C179-C87. doi: 10.1152/ajpcell.00018.2009.

10. Ghajar CM, Chen X, Harris JW, Suresh V, Hughes CCW, Jeon NL, et al. The Effect of Matrix Density on the Regulation of 3-D Capillary Morphogenesis. Biophysical Journal. 2008;94(5):1930-41. doi: 10.1529/biophysj.107.120774.

11. Grainger SJ, Putnam AJ. Assessing the Permeability of Engineered Capillary Networks in a 3D Culture. PLoS ONE. 2011;6(7):e22086. doi: 10.1371/journal.pone.0022086.

12. Kachgal S, Carrion B, Janson IA, Putnam AJ. Bone marrow stromal cells stimulate an angiogenic program that requires endothelial MT1-MMP. Journal of Cellular Physiology. 2012:n/a-n/a. doi: 10.1002/jcp.24056.

13. Ghajar CM, Kachgal S, Kniazeva E, Mori H, Costes SV, George SC, et al. Mesenchymal cells stimulate capillary morphogenesis via distinct proteolytic mechanisms. Experimental Cell Research. 2010;316(5):813-25. doi: 10.1016/j.yexcr.2010.01.013.

14. Lamalice L, Le Boeuf F, Huot J. Endothelial Cell Migration During Angiogenesis. Circulation Research. 2007;100(6):782-94. doi: 10.1161/01.RES.0000259593.07661.1e.

15. Holmes JW, Borg TK, Covell JW. Structure and mechanics of healing myocardial infarcts. Annual review of biomedical engineering. 2005;7:223-53.

16. Schugart RC, Friedman A, Zhao R, Sen CK. Wound angiogenesis as a function of tissue oxygen tension: A mathematical model. Proceedings of the National Academy of Sciences. 2008;105(7):2628-33. doi: 10.1073/pnas.0711642105.

17. Vermolen F, Javierre E. A finite-element model for healing of cutaneous wounds combining contraction, angiogenesis and closure. Journal of Mathematical Biology. 2011:1-30. Epub 10 November. doi: 10.1007/s00285-011-0487-4.

18. Xue C, Friedman A, Sen CK. A mathematical model of ischemic cutaneous wounds. Proceedings of the National Academy of Sciences. 2009;106(39):16782-7. doi: 10.1073/pnas.0909115106.

19. Chien S. Mechanotransduction and endothelial cell homeostasis: the wisdom of the cell. American Journal of Physiology - Heart and Circulatory Physiology. 2007;292(3):H1209-H24. doi: 10.1152/ajpheart.01047.2006.

20. Clark ER. Studies on the growth of blood-vessels in the tail of the frog larva — by observation and experiment on the living animal. Am J Anat. 1918;23(1):37-88.

21. Korff T, Augustin HG. Tensional forces in fibrillar extracellular matrices control directional capillary sprouting. Journal of Cell Science. 1999;112(19):3249-58.

22. Winer JP, Oake S, Janmey PA. Non-Linear Elasticity of Extracellular Matrices Enables Contractile Cells to Communicate Local Position and Orientation. PLoS ONE. 2009;4(7):e6382. doi: 10.1371/journal.pone.0006382.

23. Reinhart-King CA, Dembo M, Hammer DA. Cell-Cell Mechanical Communication through Compliant Substrates. Biophysical Journal. 2008;95(12):6044-51. doi: 10.1529/biophysj.107.127662.

24. Legant WR, Miller JS, Blakely BL, Cohen DM, Genin GM, Chen CS. Measurement of mechanical tractions exerted by cells in three-dimensional matrices. Nat Meth. 2010;7(12):969-71. doi: http://www.nature.com/nmeth/journal/v7/n12/abs/nmeth.1531.html#supplementary-information.

25. Kniazeva E, Weidling JW, Singh R, Botvinick EL, Digman MA, Gratton E, et al. Quantification of local matrix deformations and mechanical properties during capillary morphogenesis in 3D. Integrative Biology. 2012;4(4):431-9.

26. Harris AK, Wild P, Stopak D. Silicone rubber substrata: a new wrinkle in the study of cell locomotion. Science. 1980;208(4440):177-9. Epub 1980/04/11. PubMed PMID: 6987736.

27. Dembo M, Oliver T, Ishihara A, Jacobson K. Imaging the traction stresses exerted by locomoting cells with the elastic substratum method. Biophysical journal. 1996;70(4):2008-22. PubMed PMID: PMC1225170.

28. Dembo M, Wang YL. Stresses at the cell-to-substrate interface during locomotion of fibroblasts. Biophysical journal. 1999;76(4):2307-16. PubMed PMID: PMC1300203.

29. Pelham RJ, Wang Y-l. High Resolution Detection of Mechanical Forces Exerted by Locomoting Fibroblasts on the Substrate. Molecular Biology of the Cell. 1999;10(4):935-45. doi: 10.1091/mbc.10.4.935.

30. Pelham RJ, Wang Y-l. Cell locomotion and focal adhesions are regulated by substrate flexibility. Proceedings of the National Academy of Sciences. 1997;94(25):13661-5.

31. Franck C, Maskarinec SA, Tirrell DA, Ravichandran G. Three-Dimensional Traction Force Microscopy: A New Tool for Quantifying Cell-Matrix Interactions. PLoS ONE. 2011;6(3):e17833. doi: 10.1371/journal.pone.0017833.

32. Yamada S, Wirtz D, Kuo SC. Mechanics of Living Cells Measured by Laser Tracking Microrheology. Biophysical Journal. 2000;78(4):1736-47. doi: 10.1016/s0006-3495(00)76725-7.

33. Beningo KA, Wang Y-L. Flexible substrata for the detection of cellular traction forces. Trends in Cell Biology. 2002;12(2):79-84. doi: 10.1016/s0962-8924(01)02205-x.

34. Qi W, Anindita B, Jessamine PW, Arjun Y, Paul AJ. Local and global deformations in a strain-stiffening fibrin gel. New Journal of Physics. 2007;9(11):428.

35. Stein AM, Vader DA, Weitz DA, Sander LM. The micromechanics of three-dimensional collagen-I gels. Complexity. 2011;16(4):22-8. doi: 10.1002/cplx.20332.

36. Gjorevski N, Nelson CM. Mapping of mechanical strains and stresses around quiescent engineered three-dimensional epithelial tissues. Biophysical journal. 2012;103(1):152-62. Epub 2012/07/26. doi: 10.1016/j.bpj.2012.05.048. PubMed PMID: 22828342; PubMed Central PMCID: PMC3388222.

37. Kotlarchyk MA, Shreim SG, Alvarez-Elizondo MB, Estrada LC, Singh R, Valdevit L, et al. Concentration Independent Modulation of Local Micromechanics in a Fibrin Gel. PLoS ONE. 2011;6(5):e20201. doi: 10.1371/journal.pone.0020201.

38. Hahn C, Schwartz MA. Mechanotransduction in vascular physiology and atherogenesis. Nat Rev Mol Cell Biol. 2009;10(1):53-62.

39. Yang F, Williams CG, Wang D-a, Lee H, Manson PN, Elisseeff J. The effect of incorporating RGD adhesive peptide in polyethylene glycol diacrylate hydrogel on

osteogenesis of bone marrow stromal cells. Biomaterials. 2005;26(30):5991-8. doi: 10.1016/j.biomaterials.2005.03.018.

40. Mann BK, West JL. Cell adhesion peptides alter smooth muscle cell adhesion, proliferation, migration, and matrix protein synthesis on modified surfaces and in polymer scaffolds. Journal of Biomedical Materials Research. 2002;60(1):86-93. doi: 10.1002/jbm.10042.

41. Hern DL, Hubbell JA. Incorporation of adhesion peptides into nonadhesive hydrogels useful for tissue resurfacing. Journal of Biomedical Materials Research. 1998;39(2):266-76. doi: 10.1002/(sici)1097-4636(199802)39:2<266::aid-jbm14>3.0.co;2-b.

42. Patel PN, Gobin AS, West JL, Patrick CW. Poly (ethylene glycol) hydrogel system supports preadipocyte viability, adhesion, and proliferation. Tissue engineering. 2005;11(9-10):1498-505.

43. Almany L, Seliktar D. Biosynthetic hydrogel scaffolds made from fibrinogen and polyethylene glycol for 3D cell cultures. Biomaterials. 2005;26(15):2467-77. doi: 10.1016/j.biomaterials.2004.06.047.

44. Leslie-Barbick JE, Saik JE, Gould DJ, Dickinson ME, West JL. The promotion of microvasculature formation in poly(ethylene glycol) diacrylate hydrogels by an

immobilized VEGF-mimetic peptide. Biomaterials. 2011;32(25):5782-9. doi: 10.1016/j.biomaterials.2011.04.060.

45. Arnaoutova I, George J, Kleinman H, Benton G. The endothelial cell tube formation assay on basement membrane turns 20: state of the science and the art. Angiogenesis. 2009;12(3):267-74. doi: 10.1007/s10456-009-9146-4.

46. Odrljin TM, Francis CW, Sporn LA, Bunce LA, Marder VJ, Simpson-Haidaris PJ. Heparin-Binding Domain of Fibrin Mediates Its Binding to Endothelial Cells. Arteriosclerosis, Thrombosis, and Vascular Biology. 1996;16(12):1544-51. doi: 10.1161/01.atv.16.12.1544.

47. Rizzi SC, Ehrbar M, Halstenberg S, Raeber GP, Schmoekel HG, Hagenmüller H, et al. Recombinant Protein-co-PEG Networks as Cell-Adhesive and Proteolytically Degradable Hydrogel Matrixes. Part II: Biofunctional Characteristics. Biomacromolecules. 2006;7(11):3019-29. doi: 10.1021/bm060504a.

48. Phelps EA, Landázuri N, Thulé PM, Taylor WR, García AJ. Bioartificial matrices for therapeutic vascularization. Proceedings of the National Academy of Sciences. 2010;107(8):3323-8. doi: 10.1073/pnas.0905447107.

49. Moon JJ, Saik JE, Poche RA, Leslie-Barbick JE, Lee S-H, Smith AA, et al. Biomimetic hydrogels with pro-angiogenic properties. Biomaterials. 2010;31(14):3840-7. doi: 10.1016/j.biomaterials.2010.01.104. PubMed PMID: PMC2839536.

50. Tibbitt MW, Anseth KS. Hydrogels as extracellular matrix mimics for 3D cell culture. Biotechnology and Bioengineering. 2009;103(4):655-63. doi: 10.1002/bit.22361.

51. Peppas NA, Hilt JZ, Khademhosseini A, Langer R. Hydrogels in Biology and Medicine: From Molecular Principles to Bionanotechnology. Advanced Materials. 2006;18(11):1345-60. doi: 10.1002/adma.200501612.

52. Gonen-Wadmany M, Oss-Ronen L, Seliktar D. Protein–polymer conjugates for forming photopolymerizable biomimetic hydrogels for tissue engineering. Biomaterials. 2007;28(26):3876-86. doi: 10.1016/j.biomaterials.2007.05.005.

53. Almany L, Seliktar D. Biosynthetic hydrogel scaffolds made from fibrinogen and polyethylene glycol for 3D cell cultures. Biomaterials. 2005;26(15):2467-77. Epub 2004/12/09. doi: 10.1016/j.biomaterials.2004.06.047. PubMed PMID: 15585249.

54. Dikovsky D, Bianco-Peled H, Seliktar D. The effect of structural alterations of PEG-fibrinogen hydrogel scaffolds on 3-D cellular morphology and cellular migration. Biomaterials. 2006;27(8):1496-506. Epub 2005/10/26. doi: 10.1016/j.biomaterials.2005.09.038. PubMed PMID: 16243393.

55. Peyton SR, Kim PD, Ghajar CM, Seliktar D, Putnam AJ. The effects of matrix stiffness and RhoA on the phenotypic plasticity of smooth muscle cells in a 3-D biosynthetic hydrogel system. Biomaterials. 2008;29(17):2597-607. doi: 10.1016/j.biomaterials.2008.02.005.

56. Nehls V, Drenckhahn D. A microcarrier-based cocultivation system for the investigation of factors and cells involved in angiogenesis in three-dimensional fibrin matrices in vitro. Histochem Cell Biol. 1995;104(6):459-66. doi: 10.1007/bf01464336.

57. Lutolf MP, Hubbell JA. Synthetic biomaterials as instructive extracellular microenvironments for morphogenesis in tissue engineering. Nat Biotech. 2005;23(1):47-55.

58. Elbert DL, Hubbell JA. Conjugate Addition Reactions Combined with Free-Radical Cross-Linking for the Design of Materials for Tissue Engineering. Biomacromolecules. 2001;2(2):430-41. doi: 10.1021/bm0056299.

59. Lutolf MP, Tirelli N, Cerritelli S, Cavalli L, Hubbell JA. Systematic Modulation of Michael-Type Reactivity of Thiols through the Use of Charged Amino Acids. Bioconjugate Chemistry. 2001;12(6):1051-6. doi: 10.1021/bc015519e.

60. Kim PD, Peyton SR, VanStrien AJ, Putnam AJ. The influence of ascorbic acid, TGF-β1, and cell-mediated remodeling on the bulk mechanical properties of 3-D PEG–fibrinogen constructs. Biomaterials. 2009;30(23–24):3854-64. doi: 10.1016/j.biomaterials.2009.04.013.

61. Yan C, Pochan DJ. Rheological properties of peptide-based hydrogels for biomedical and other applications. Chemical Society Reviews. 2010;39(9):3528-40.

62. Ewoldt RH, Hosoi AE, McKinley GH. New measures for characterizing nonlinear viscoelasticity in large amplitude oscillatory shear. Journal of Rheology. 2008;52(6):1427-58.

63. Holzapfel GA, Ogden RW, editors. Mechanics of Biological Tissue Berlin: Springer-Verlag; 2006.

64. Mironi-Harpaz I, Wang DY, Venkatraman S, Seliktar D. Photopolymerization of cell-encapsulating hydrogels: Crosslinking efficiency versus cytotoxicity. Acta Biomaterialia. 2012;8(5):1838-48. doi: 10.1016/j.actbio.2011.12.034.

65. Dikovsky D, Bianco-Peled H, Seliktar D. Defining the Role of Matrix Compliance and Proteolysis in Three-Dimensional Cell Spreading and Remodeling. Biophysical Journal. 2008;94(7):2914-25.

66. Rao R, Peterson A, Ceccarelli J, Putnam A, Stegemann J. Matrix composition regulates three-dimensional network formation by endothelial cells and mesenchymal stem cells in collagen/fibrin materials. Angiogenesis. 2012:1-12. doi: 10.1007/s10456-012-9257-1.

67. Chang CC, Krishnan L, Nunes SS, Church KH, Edgar LT, Boland ED, et al. Determinants of Microvascular Network Topologies in Implanted Neovasculatures. Arteriosclerosis, Thrombosis, and Vascular Biology. 2012;32(1):5-14. doi: 10.1161/atvbaha.111.238725.

68. Ng CP, Hinz B, Swartz MA. Interstitial fluid flow induces myofibroblast differentiation and collagen alignment in vitro. Journal of Cell Science. 2005;118(20):4731-9. doi: 10.1242/jcs.02605.

69. Billiet T, Vandenhaute M, Schelfhout J, Van Vlierberghe S, Dubruel P. A review of trends and limitations in hydrogel-rapid prototyping for tissue engineering. Biomaterials. 2012;33(26):6020-41. Epub 2012/06/12. doi: 10.1016/j.biomaterials.2012.04.050. PubMed PMID: 22681979.

70. Liu Tsang V, Chen AA, Cho LM, Jadin KD, Sah RL, DeLong S, et al. Fabrication of 3D hepatic tissues by additive photopatterning of cellular hydrogels. FASEB journal : official publication of the Federation of American Societies for Experimental Biology. 2007;21(3):790-801. Epub 2007/01/02. doi: 10.1096/fj.06-7117com. PubMed PMID: 17197384.

71. Bloom RJ, George JP, Celedon A, Sun SX, Wirtz D. Mapping Local Matrix Remodeling Induced by a Migrating Tumor Cell Using Three-Dimensional Multiple-Particle Tracking. Biophysical Journal. 2008;95(8):4077-88. doi: 10.1529/biophysj.108.132738.

Chapter 2:

Development of a biosynthetic material platform for endothelial cell culture

Introduction

A number of pathologic conditions are characterized by a lack of vascularization and inadequate blood supply to the tissue, often leading to necrosis (1). Tissue engineering approaches attempt to address this problem by providing a replacement for the diseased tissue and aiding re-vascularization. One such approach combines cells with a suitable extracellular matrix (ECM) in an attempt to recapitulate the native tissue (2, 3). Previous work has established that natural ECMs of fibrinogen (4) and collagen (5) readily support vascularization, but these protein hydrogels are limited in their range of physical properties. These properties are commonly modulated by changing the concentration of the protein, which simultaneously changes the number of ligands available for cell adhesion, the protease sensitivity, and the matrix architecture (6). Conversely, synthetic ECM can theoretically provide a range of physical properties with independent control over bulk ligand concentration and matrix architecture. However, only a handful of papers have demonstrated the formation of vascular networks within a synthetic gel *in vitro* (7-12). Thus, deconstructing the ECM's multivariable instructive role in the process of capillary morphogenesis continues to be a challenge (13).

Prior studies in the literature have demonstrated the migration of cells in PEG hydrogels from EC spheroids (14), EC and FB aggregates (12), and aortic arches (7). In most cases, these hydrogels were functionalized with RGD, the minimal cell-adhesive binding domain found in fibronectin (7, 9), and included a mechanism for cell-mediated degradation through the incorporation of peptide cross-links sensitive to proteases (7, 12). These limited instructive cues (combined with the correct soluble factors) have been sufficient to support formation of vessel-like networks *in vitro*, but have performed even better at supporting vascularization *in vivo* when combined with protease-mediated release of pro-angiogenic growth factors (14-16). Adding in additional peptide motifs may further improve the vasculogenic potential of these synthetic platforms, but the high cost of purchasing or synthesizing purified peptides can be prohibitive. As a complement to these peptide-functionalized materials, hybrid approaches that utilize conjugate chemistry to covalently link synthetic polymers with biologic macromolecules have also been developed. This approach enables the creation of biosynthetic ECMs with the biological properties defined by the protein and microarchitectures by the synthetic polymer. Previous studies have produced biosynthetic hydrogels utilizing synthetic polymers linked to portions of collagen and fibrinogen (17-19), gelatin (10, 20), heparin (21), or hyaluronic acid (11).

We utilized a biosynthetic hydrogel approach in order to investigate the influence of hydrogel physical properties on the formation of capillary networks *in vitro*. The benefit of the biosynthetic approach in this context is that the bulk concentration of native ECM molecules can be held constant while the physical properties can be controlled

orthogonally through synthetic crosslinking. Our approach was to conjugate non-denatured collagen to poly(ethylene glycol) diacrylamide (PEGDAm) to produce a macromolecule. We then photopolymerized these macromolecules with varying amounts of exogenous PEGDAm to produce cross-linked amorphous hydrogels, and characterized their bulk mechanical and transport properties.

Methods

Synthesis of PEG-diacrylamide

Poly(ethylene glycol) was functionalized as described elsewhere (22). Briefly, poly(ethylene glycol) (20 kDa MW, 100 g, 10 mM -OH) (Fluka, Buchs, Germany) was dried azeotropically against benzene and reacted with triethylamine (4.1 mL, 30 mmol, Acros, Fair Lawn, NJ) and mesyl chloride (2.3 mL, 30 mmol, Acros) overnight under nitrogen at 20°C. The product was precipitated in cold ether (Fisher, Waltham, MA), dried under vacuum and reacted against 25% aqueous ammonia (Acros) for 4 days. After evaporating the ammonia, the pH was adjusted to 13 with 1 N NaOH, and the solution was extracted with dichloromethane (Fisher), concentrated, precipitated, and dried. The resulting poly(ethylene glycol)-di-amine was dialyzed against water and stored at -80°C. For acrylation, 20 mg of the PEG-diamine intermediate was lyophilized and dried azeotropically before addition of dichloromethane, triethylamine (0.41 mL, 3 mmol), and acroyl chloride (0.23 mL, 3 mmol, Aldrich, St. Louis, MO). The reaction proceeded overnight under nitrogen and the product was precipitated and dried. The resulting poly(ethylene glycol)-di-acrylamide (PEGDAm) was dissolved in water, lyophilized and kept at -20°C. Conversion of diols to diacrylamides was confirmed via

^{1}H NMR: (DCCl3) 3.6 ppm (1816 H, PEG), 5.6 ppm (dd, 2 H, CH2=C*H*-CON-), 6.1 ppm, 6.2ppm (dd, 4 H, C*H*2=CH-CON-).

Conjugation of PEGDAm to Collagen & SDS-PAGE

To conjugate PEGDAm to type-I collagen, a modification of a protocol developed by Gonen-Wadmany et al. (17) was used. All steps were performed at 4°C in PBS to prevent denaturing the collagen. Bovine type I collagen (Nutragen, Advanced BioMatrix, San Diego, CA) was diluted to 3 mg/mL in PBS. SATA (N-succinimidyl S-acetylthioacetate, Thermo Scientific, Rockford, IL) was added at 0.075 mg/mg collagen and the reaction proceeded for 24 hours with agitation then purified by dialysis. Thiols were exposed by reaction with 1.8 M hydroxylamine (Acros) and reduced by *tris*(2-carboxyethyl)phosphine, (TCEP, Sigma) then purified by dialysis. Utilizing a Michael's type addition, the product was conjugated to 20 kDa PEGDAm at 4 mg/mg collagen in PBS with 0.15 M triethanolamine and 0.27 mM TCEP at pH 8.3 overnight with agitation then purified by dialysis against PBS through a 50 kDa membrane (Spectrum Labs Rancho Dominguez, CA). The product was aseptically collected and stored at -20°C. Thiols were quantified prior to PEGylation by Ellman's assay and the PEGDAm content determined by dry weight of the final product.

The reaction between PEGDAm and collagen was sampled at 0, 1, 3, 6, 18 hours and the product was reduced in Laemmli buffer before being run in a 10% Tris-Gly polyacrylamide gel (Invitrogen, Carlsbad, CA). Bands were visualized by staining with 0.1% w/v Coomassie blue G250 (Amresco, Solon, OH) and the gel was photographed with an Epson V300 photo scanner.

Rheological Measurements & Hydrogel Degradation

Hydrogels were formulated with PEG-collagen diluted to 2.5 mg/mL with varying amounts of PBS and PEGDAm to achieve the final weight percent of exogenous PEGDAm denoted PC+n%PEG; the photoinitiator Irgacure 2959 (Ciba, Basel Switzerland) was added at a final concentration of 0.6% w/v to form a precursor solution. To assess the kinetics of hydrogel formation, solutions were cured on a 20 mm UV stage in an AR-G2 rheometer (TA Instruments, New Castle, DE) with an oscillation of 1% strain at 1 rad/s with 5 minutes of exposure to 365nm UV light at 2 mW/cm^2.

For bulk mechanical testing, 200 µL of precursor solution was aseptically cast into 8 mm cylinders in a Teflon mold by exposure to UV light at 365 nm, 2 mW/cm^2 for 5 minutes. Hydrogels were transferred to 24-well plates and incubated in PBS + 0.1% Azide at 37°C for 1, 3, 7, or 14 days. Rheological measurements were taken with an 8 mm parallel plate on a Peltier stage at 37°C under PBS; both surfaces were coated with P800 wet or dry sandpaper (3M, St. Paul, Minnesota) to prevent slip. Gaps were adjusted to accommodate the swollen height of the hydrogels. The storage and loss moduli were averaged from mechanical spectra from 0.1 to 10 rad/s at 1% strain. The wet and dry weights of each gel were recorded, and the supernatant was assayed for total protein with Bradford's Assay. The mass swelling ratio was calculated from the wet (W_w) and dry (W_D) weights of the gels, excluding the mass of PBS salts (W_S), as $(W_w-W_S)/(W_D-W_S)$. Bulk mechanical testing of cellularized hydrogels were conducted in a similar manner, but were cultured in EGM-2 instead of PBS.

Dextran Release

The bulk transport properties of the hydrogels were assessed using dextran to simulate the diffusion of macromolecular species (6). Acellular 100 μL hydrogels were aseptically cast containing 10 μg of 70 kDa Texas red-conjugated dextran (Life Technologies, Carlsbad, CA). Hydrogels of each formulation were placed in 24-well plates with sterile PBS and incubated at 37°C. The supernatant was aseptically collected after 1, 3, 6, 9, 12, 24 and 72 hours and replaced with fresh PBS each time. After 72 hours, gels were digested overnight with 40 IU collagenase (Worthington Biochemical, Lakewood, NJ) in PBS to release any remaining dextran. The supernatants from each time point and from the digested gels were assayed in a Fluoroskan Ascent FL (Thermo Scientific) plate reader at Ex:595/Em:615. Masses were determined by comparison to a standard curve of dextran and appropriate buffer.

Collagenase Digestion

To detect the release of cleaved PEG-collagen, conjugates were labeled with ATTO-390 NHS-ester (Fluka) at 21 μg per 3 mg collagen at 4°C overnight at pH 7.4. The labeled conjugate was used to produce hydrogels of each formulation. Unreacted ATTO-390 was removed by washing the gels for 3 days in PBS. Samples were then transferred to a 1 mL solution of 20 IU collagenase and incubated at 37°C in the dark. Samples of supernatant (0.3 mL) were taken after 0.25, 1, 3, 6, 9, and 24 hours and replaced with fresh collagenase solution. The fluorescence intensity of the samples was measured at Ex: 355 Em: 485. The concentration of dye was determined through the dilution factor and molar extinction coefficient of ATTO-390: 24000 mol^{-1} cm^{-1}.

Endothelial Cell Adhesion

To determine if endothelial cells would adhere and spread on PEG-collagen substrates, cells were seeded on prefabricated 2D substrates or photoencapsulated in 3D matrices. 2D substrates were prepared by combining PEG-collagen with photoinitiaor and PBS as previously described, then exposing the solution to UV in a 8 mm teflon mold. For this set of experiments, PEG-collagen wwas prepared at 6 mg/mL by titrting Nutragen without dilution in PBS. This PEG-collagen was used as is (6 mg/mL) diluted 1:1 (3 mg/mL), or diluted 1:2 (1.5 mg/mL) with PBS. For 3D culture 3 mg/mL PEG-collagen solutions were polymerized with either 0% or 5% exogenous PEGdiacrylamide. Cells were cultured overnight then stained with a LIVE/DEAD kit (Invitrogen) and photographed in an inverted position.

Results

Synthesis of PEG-Collagen

Conversion of PEG diols to diacrylamides was performed with 95% efficiency. Of the unreacted groups, >93% were amines with minimal acrylate formation. For the conjugation (Figure 6), incorporation of thiols was measured at 0.23 ± 0.01 mM or 35 thiols per collagen molecule. The final mass of PEGDAm was determined to be 2.52 ± 0.02 mg per mg collagen for a stoichometric ratio of 57:1; the stoichometric difference between thiols and PEGDAm suggests that some unconjugated PEGDAm remains in the final product.

Figure 6: Reaction scheme for conjugation of PEGDAm to collagen

Collagen was modified utilizing SATA to incorporate free thiols, which then reacted with PEGDAm via Michael's type addition to form a PEG-collagen conjugate.

To confirm conjugation, the product was resolved by a polyacrylamide gel electrophoresis, with Coomassie staining revealing ~150 kDa bands that correspond to the α_1 and α_2 chains of collagen (Figure 7) (23). Conjugation of PEGDAm to collagen was evident by disappearance of these 150 kDa bands over time coupled with

appearance of higher molecular weight aggregates, with the mobility shift evident within 18 hours.

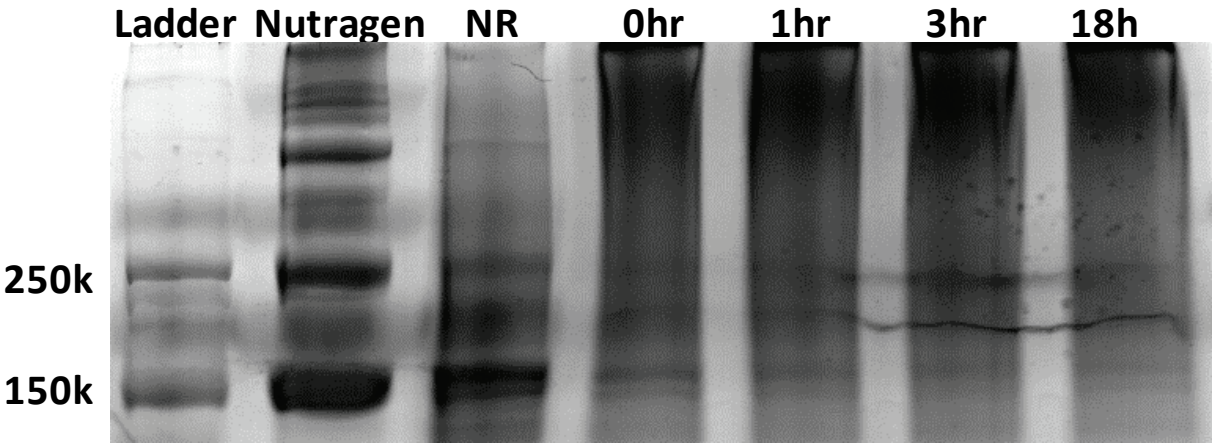

Figure 7: PEG-collagen conjugation reaction progress was monitored by gel electrophoresis

Formation of this conjugate was evident from the mobility shift during the reaction. The Nutragen and thiolated collagen product (NR) displayed bands near 150 kDa, while under alkaline conditions (0h) the bands disappeared and a high molecular weight smear appeared corresponding to PEGDAm-collagen adducts (18h).

Gel Formation

Exposure of all three formulations of PEG-collagen to UV light was accompanied by an increase in the shear storage modulus (G') indicative of gel formation (Figure 8A). The complex shear modulus (G', G'') of the PEG-collagen was increased by addition of exogenous PEGDAm, both prior to and following UV photopolymerization. Nevertheless, the increased storage modulus resulting from the photopolymerization were much pronounced in these samples. The rapid increase in storage modulus of PC+0%PEG solutions following photopolymerization was followed by a volume relaxation (24), making the apparent pre-UV and post-UV moduli not significantly

different (Figure 8B). By contrast, the increase in storage modulus was more gradual for the other two formulations, likely owing to an increase in viscosity, and was significantly increased after UV cross-linking in both cases. Following UV cross-linking, each of the three gel formulations' shear storage moduli were significantly different from one another, spanning two orders of magnitude (Figure 8B). The shear loss moduli did not show any significant trends, but were an order lower than the corresponding storage moduli indicating extensive crosslinking of the material.

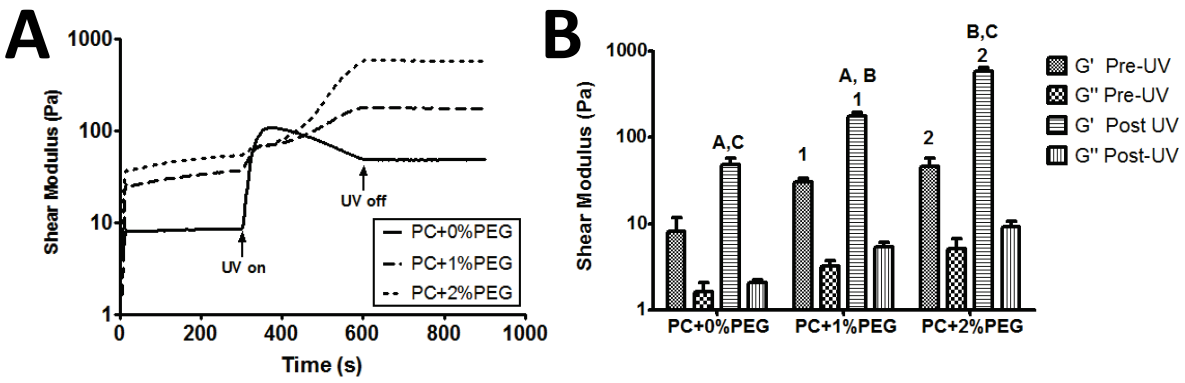

Figure 8: Hydrogels were prepared from PEGylated collagen and subsequent photopolymerization.

A) Subsequent exposure of conjugates (with photoinitiator and varying wt% PEGDAm) to UV light in a parallel plate rheometer led to rapid increases in shear modulus and gel formation. While the crosslinking rate slowed with addition of exogenous PEGDAm, all formulations set within the 5 minutes of UV exposure. B) Comparisons of the shear moduli before and after UV exposure revealed that the final shear storage modulus (G') of each formulation was significantly different from each other; the loss moduli (G'') did not differ significantly. Matched symbols denote $P < 0.01$ (n=3).

Assessment of Hydrolytic Stability

Hydrogels were stable in buffer without significant changes over time in the wet mass of the gel (Figure 9A) or the mass swelling ratio (Figure 9B). The wet masses were

significantly different between formulations (P<0.01), with increased water content observed with higher PEGDAm content. However, the mass swelling ratios were not significantly different between formulations. Adopting a published approach (25), the mesh size was estimated to be 61 ± 2 nm at day 1 for the three formulations, and no noteworthy changes were observed thereafter.

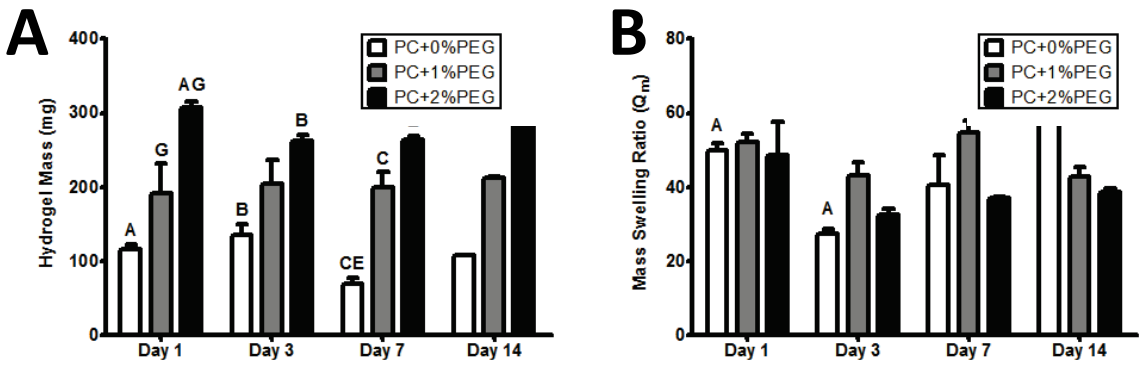

Figure 9: PEG-collagen hydrogel swelling ratio

A) Wet masses of swollen hydrogels of each formulation demonstrated a significantly increased degree of swelling with increasing PEG content. The masses of the gels were stable and did not significantly change over time. B) The mass swelling ratio was also stable and did not show any significant trends with neither the gel formulation nor time in buffer significantly contributing to the variance. Significance was determined by 2-way ANOVA and Bonferroni post-tests with $p < 0.05$ and denoted by matched symbols on the graphs.

Additionally, the shear storage modulus of the hydrogels (Figure 10) were not significantly changed over 14 days for PC+0%PEG and PC+1%PEG, but the modulus of the PC+2%PEG decreased slightly between days 1 and 3 and remained unchanged thereafter. At each day, the shear modulus of the PC+2%PEG gels was significantly larger than the moduli of the PC+0%PEG and PC+1%PEG gels, but the moduli of the swollen PC+0%PEG and PC+1%PEG gels were not significantly different from each other.

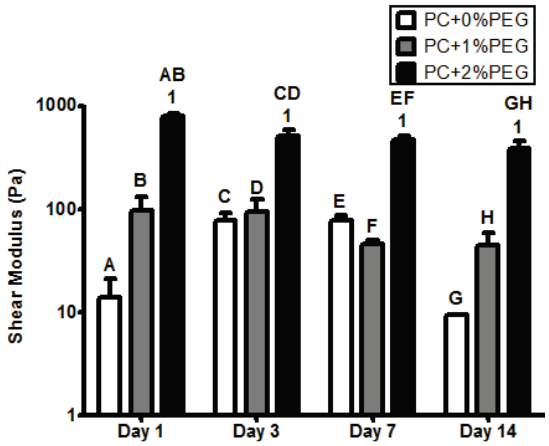

Figure 10: Mechanical properties of acellular PEG-collagen hydrogels

The shear moduli of the PC+0% & 1% PEG gels did not change over time while the PC+2%PEG showed a slight decrease after day 1. At each day, the shear modulus of the PC+2%PEG gels was significantly different from the PC+0% & 1% PEG gels. Significance was determined by 2-way ANOVA and Bonferroni post-tests with $p < 0.05$ and denoted by matched symbols on the graphs.

The protein content of the buffer increased a small yet significant amount ($P < 0.01$) at day 14 (Figure 12Figure 11), indicating a loss of protein from the gels over time; however, the total amount released accounts for only 0.01% of the hydrogel's original protein content. Collectively, these data suggest the PEG-collagen hydrogels are hydrolytically stable in an inert aqueous environment.

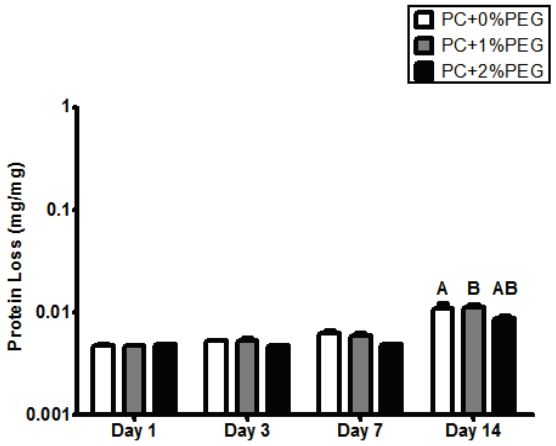

Figure 11: Hydrogel release of conjugated protein

Protein release from the hydrogels was not significant until day 14 when a negligible amount (0.01% w/w) was detected form all gel formulations. Significance was determined by 2-way ANOVA and Bonferroni post-tests with $p < 0.05$ and denoted by matched symbols on the graphs.

Dextran Release

To characterize the differential ability of the PEG-collagen hydrogel formulations to limit diffusive transport, the cumulative release profiles of fluorescent dextran was assessed for each hydrogel. Data were normalized to the total mass of dextran entrapped, which includes the mass after collagenase digestion. The best-fit lines are first-order exponential approximations of diffusive processes in high porosity hydrogels (Eqn. 1) (26).

Eqn. 1: $$M = M_0 + \left(M_f - M_0\right)[1 - \exp(-K \cdot t)]$$

The equation correlated with the data for PC+ 0%, 1%, and 2% PEG with 70 kDa dextran release (Figure 12A) R^2: (0.9988, 0.9882, 0.9902) respectively. The rate constant, K, was also calculated for all release profiles and a sum-of-squares F-test suggested significant ($P < 0.05$) differences in the release rates (Figure 12B). Pair-wise

Bonferoni comparisons showed that the release rate of 70 kDa dextran from PC+0%PEG gels was significantly greater than the other conditions.

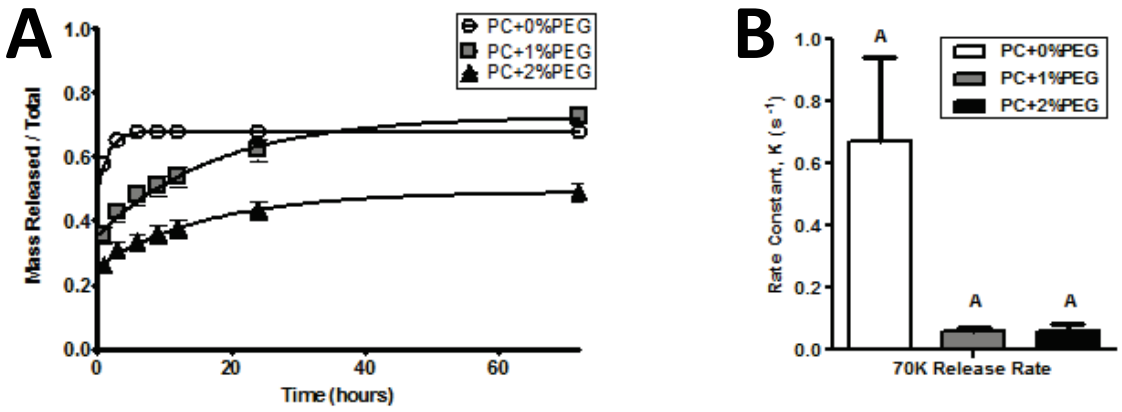

Figure 12: Release of encapsulated dextrans.

To assess the bulk transport properties of the gels, release of encapsulated 70 kDa dextran (A) was monitored and the rate constants were compared (B) with a significantly higher rate for PC+0%PEG and comparable between the other two formulations.

Collagenase Digestion

To characterize the collagenase sensitivity of our new materials, fluorescently labeled hydrogels were prepared with ATTO-390 tagged PEG-collagen. Unreacted ATTO-390 was thoroughly removed by PBS washes with negligible fluorescence of the final PBS wash. All formulations were completely digested by collagenase within 24 hours. The cumulative release of ATTO-390 was assumed to be correlated to the amount of released PEG-collagen with a theoretical labeling ratio of 2.7 fluorophore per collagen molecule. The release profiles (Figure 13Figure 13) followed an exponential (Eqn. 1) with R^2 equal to 0.9544, 0.9478, 0.8098 for PC + 0, 1, & 2% PEG respectively. The rate

constant for the release of tagged collagen fragments, K, was also determined and, a sum-of-squares F-test suggested significant ($P < 0.01$) differences in the release rates of fluorophore. Subsequent Bonferoni pair-wise comparisons showed that all three rates were significantly different from each other.

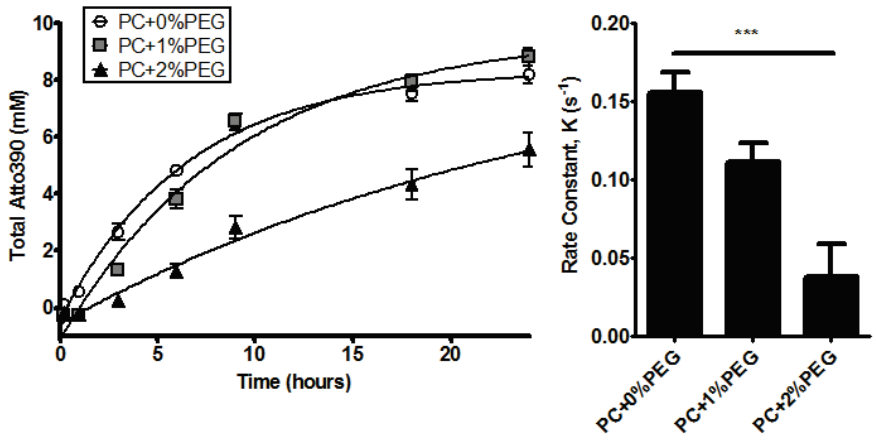

Figure 13: Enzymatic remodeling of hydrogels proceeds in vitro.

Fluorescently labeled hydrogels were digested in a collagenase solution and release of the fluorophore followed an exponential with the release rate being significantly ($P < 0.01$) different across all conditions.

Endothelial Cell Adhesion

PEG-collagen densities supported cell adhesion to varying degrees. On gels with varying PEG-collagen concentrations, the 1.5 mg/mL condition did not support EC spreading while EC on 6 mg/mL substrates were well spread. Cells on the intermediate 3.0 mg/mL substrate adhered and also formed cell-cell junctions and multicellular structures (Figure 14).

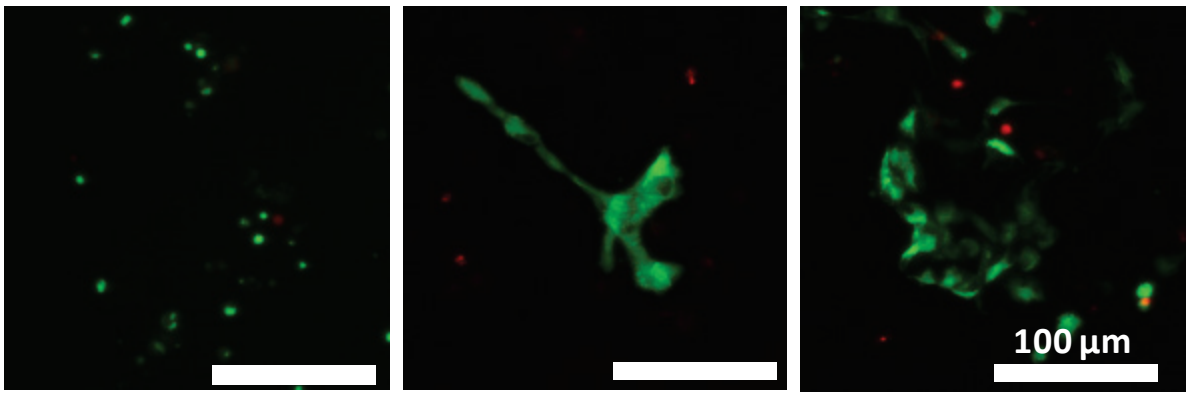

Figure 14: EC viability on gels of varied PEG-Collagen content

Endothelial cells were cultured on 2D PEG-collagen hydrogels of varying PEG-collagen concentration. Cells were viable, but spread poorly on 1.5 mg/mL hydrogels; they adhered to the substrate and formed multicellular structures on 3 mg/mL hydrogels; and spread extensively on 6 mg/mL hydrogels. LIVE/DEAD staining shows dead cells ad red and live cells as green.

Inclusion of exogenous PEG slightly modulated 2D adhesion of EC to the hydrogels. A preference for cell-cell junctions was seen by formation of multicellular structures in the presence of 5% PEG condition (Figure 15). However, 3D encapsulation in 5% exogenous PEG had a detrimental effect on cell survival (Figure 15).

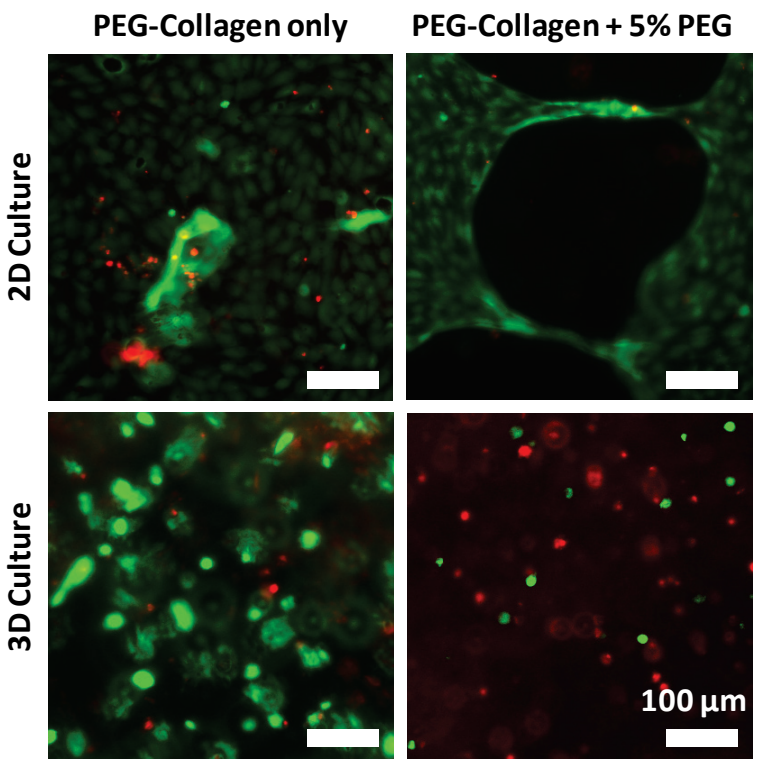

Figure 15: EC viability to gels of varying PEG content

Addition of exogenous PEGdiacrylaime to 3.0 mg/mL hydrogels slightly altered adhesion and spreading on 2D substrates, but had a detrimental effect on 3D culture. LIVE/DEAD staining shows dead cells ad red and live cells as green.

Discussion

At the heart of our approach is a conjugate of PEGdiacrylamide and collagen, which rapidly photopolymerizes into a hydrogel that is hydrolytically stable. The resistance to hydrolysis arises from the amide having a less detrimental effect on the thioether of the Michael's adduct than an ester that results from the more typical linkage to PEGdiacrylate (22, 27). An earlier approach of making a similar conjugate relied on denaturing buffers to solubilize collagen (17). We found that the reaction could be accomplished under conditions that preserve the native conformation of the collagen macromolecules. We hypothesize that maintaining the triple-helical structure of the collagen macromolecules provides a native presentation of peptide sequences preserving binding sites for integrins, growth factors, and enzymes (28). The synthetic modification allows for hydrogels to form by brief exposure to low-power long-wave UV light, forming gels much faster than unmodified collagen. Further, the rapid dissolution of the gels in collagenase demonstrates that the collagen macromolecules play a central role in stabilizing the structure. Thus, the microstructure of the gel is expected to be similar to that of other PEG-based hydrogels; wherein, it is composed of randomly dispersed collagen macromolecules immobilized by PEGDAm crosslinks with increasing amounts of PEGDAm predominantly producing longer crosslinks. This amorphous PEG-collagen material is in direct contrast to the fibrillar nature of unmodified collagen gels (29).

While the swelling ratios provide rough approximations of mesh size, they could not discriminate between the three formulations owing to their low polymer content.

Instead, we utilized dextran release since it provides a more direct assessment of the transport properties than mesh size estimates. The 70 kDa dextran released rapidly in the PC+0%PEG formulation but more slowly in the others, thus indicating that the larger molecules could be entrapped in the PEG-Collagen network as the cross-linking density is increased. Because both the PC+0%PEG and PC+1%PEG gels were comparably able to support capillary formation despite significant differences in their abilities to support diffusive transport, the transport of large molecules appears not to be the factor limiting capillary formation in this system. Preliminary biocompatibility studies showed adhesion and spreading of ECs to hydrogels. Further, photoencapsulation in formulations of PEG-collagen with exogenous PEG also outlined a range of formulations which could be investigated further as a platform for 3D EC culture. Thus, this material may provide an effective platform for the study of EC behavior *in vitro*.

Conclusions

We developed a novel biosynthetic hydrogel material by conjugating PEGdiacrylamide to macromolecular type I collagen. This was shown to photopolymerize into a hydrogel. Wherein the material properties could be modulated by the addition of exogenous PEGdiacrylamide. The shear modulus ranged two orders of magnitude offering a wide range to investigate cellular behavior. While more crosslinked gels engorged greater quantities of water, the swelling ratio was consistent showing that the entire volume is solvent accessible, thereby favoring diffusion of nutrients and growth factors to embedded cells.

Importantly, this material displayed hydrolytic stability while maintaining proteolytic susceptibility. Thus, we expect remodeling of the material to be solely attributable to cellular mechanisms. This formulation provides a major advantage over previous acrylate-based systems which allowed for passive hydrolysis of the material, rendering it difficult to attribute bulk remodeling to cellular factors.

Further, this material shows promise as a substrate for EC culture. ECs were found to attach to the surface, and to remain viable when encapsulated in 3D. These findings suggest that this material could a suitable matrix to generate vascularized structures *ex vivo*. This would have applications in the creation of engineered tissues for regenerative medicine and biological studies.

References

1. Simons M, Ware JA. Therapeutic angiogenesis in cardiovascular disease. Nat Rev Drug Discov. 2003;2(11):863-72.

2. Losordo DW, Dimmeler S. Therapeutic angiogenesis and vasculogenesis for ischemic disease: part II: cell-based therapies. Circulation. 2004;109(22):2692-7. doi: 10.1161/01.cir.0000128596.49339.05.

3. Phelps EA, Garcia AJ. Update on therapeutic vascularization strategies. Regen Med. 2008;4(1):65-80. doi: 10.2217/17460751.4.1.65.

4. Tonnesen MG, Feng X, Clark RAF. Angiogenesis in wound healing. J Investig Dermatol Symp Proc. 2000;5(1):40-6.

5. Koh W, Stratman AN, Sacharidou A, Davis GE. In vtro three dimensional collagen matrix models of endothelial lumen formation during vasculogenesis and angiogenesis. In: David AC, editor. Methods in Enzymology: Academic Press; 2008. p. 83-101.

6. Ghajar CM, Chen X, Harris JW, Suresh V, Hughes CC, Jeon NL, et al. The effect of matrix density on the regulation of 3-D capillary morphogenesis. Biophysical journal. 2008;94(5):1930-41. Epub 2007/11/13. doi: 10.1529/biophysj.107.120774. PubMed PMID: 17993494; PubMed Central PMCID: PMC2242748.

7. Miller JS, Shen CJ, Legant WR, Baranski JD, Blakely BL, Chen CS. Bioactive hydrogels made from step-growth derived PEG–peptide macromers. Biomaterials. 2010;31(13):3736-43. doi: http://dx.doi.org/10.1016/j.biomaterials.2010.01.058.

8. Miller JS, Stevens KR, Yang MT, Baker BM, Nguyen D-HT, Cohen DM, et al. Rapid casting of patterned vascular networks for perfusable engineered three-dimensional tissues. Nat Mater. 2012;11(9):768-74. doi: http://www.nature.com/nmat/journal/v11/n9/abs/nmat3357.html#supplementary-information.

9. Moon JJ, Saik JE, Poche RA, Leslie-Barbick JE, Lee S-H, Smith AA, et al. Biomimetic hydrogels with pro-angiogenic properties. Biomaterials. 2010;31(14):3840-7. doi: 10.1016/j.biomaterials.2010.01.104. PubMed PMID: PMC2839536.

10. Chen Y-C, Lin R-Z, Qi H, Yang Y, Bae H, Melero-Martin JM, et al. Functional human vascular network generated in photocrosslinkable gelatin methacrylate hydrogels. Adv Funct Mater. 2012;22(10):2027-39. doi: 10.1002/adfm.201101662.

11. Hanjaya-Putra D, Wong KT, Hirotsu K, Khetan S, Burdick JA, Gerecht S. Spatial control of cell-mediated degradation to regulate vasculogenesis and angiogenesis in hyaluronan hydrogels. Biomaterials. 2012;33(26):6123-31. doi: http://dx.doi.org/10.1016/j.biomaterials.2012.05.027.

12. Turturro MV, Christenson MC, Larson JC, Young DA, Brey EM, Papavasiliou G. MMP-sensitive PEG diacrylate hydrogels with spatial variations in matrix properties stimulate directional vascular sprout formation. PLoS ONE. 2013;8(3):e58897. doi: 10.1371/journal.pone.0058897.

13. Lutolf MP, Hubbell JA. Synthetic biomaterials as instructive extracellular microenvironments for morphogenesis in tissue engineering. Nat Biotechnol. 2005;23(1):47-55.

14. Zisch AH, Lutolf MP, Ehrbar M, Raeber GP, Rizzi SC, Davies N, et al. Cell-demanded release of VEGF from synthetic, biointeractive cell-ingrowth matrices for vascularized tissue growth. FASEB J. 2003. doi: 10.1096/fj.02-1041fje.

15. Chwalek K, Levental KR, Tsurkan MV, Zieris A, Freudenberg U, Werner C. Two-tier hydrogel degradation to boost endothelial cell morphogenesis. Biomaterials. 2011;32(36):9649-57. Epub 2011/09/23. doi: 10.1016/j.biomaterials.2011.08.078. PubMed PMID: 21937106.

16. Phelps EA, Landázuri N, Thulé PM, Taylor WR, García AJ. Bioartificial matrices for therapeutic vascularization. Proc Natl Acad Sci U S A. 2009. doi: 10.1073/pnas.0905447107.

17. Gonen-Wadmany M, Oss-Ronen L, Seliktar D. Protein–polymer conjugates for forming photopolymerizable biomimetic hydrogels for tissue engineering. Biomaterials. 2007;28(26):3876-86. doi: http://dx.doi.org/10.1016/j.biomaterials.2007.05.005.

18. Martino MM, Briquez PS, Ranga A, Lutolf MP, Hubbell JA. Heparin-binding domain of fibrin(ogen) binds growth factors and promotes tissue repair when incorporated within a synthetic matrix. Proc Natl Acad Sci U S A. 2013;110(12):4563-8. doi: 10.1073/pnas.1221602110.

19. Lee HJ, Lee J-S, Chansakul T, Yu C, Elisseeff JH, Yu SM. Collagen mimetic peptide-conjugated photopolymerizable PEG hydrogel. Biomaterials. 2006;27(30):5268-76. doi: http://dx.doi.org/10.1016/j.biomaterials.2006.06.001.

20. Fu Y, Xu K, Zheng X, Giacomin AJ, Mix AW, Kao WJ. 3D cell entrapment in crosslinked thiolated gelatin-poly(ethylene glycol) diacrylate hydrogels. Biomaterials. 2012;33(1):48-58. doi: http://dx.doi.org/10.1016/j.biomaterials.2011.09.031.

21. Benoit DSW, Durney AR, Anseth KS. The effect of heparin-functionalized PEG hydrogels on three-dimensional human mesenchymal stem cell osteogenic differentiation. Biomaterials. 2007;28(1):66-77. doi: http://dx.doi.org/10.1016/j.biomaterials.2006.08.033.

22. Elbert DL, Hubbell JA. Conjugate addition reactions combined with free-radical cross-lnking for the design of materials for tissue engineering. Biomacromolecules. 2001;2(2):430-41. doi: 10.1021/bm0056299.

23. Furthmayr H, Timpl R. Characterization of collagen peptides by sodium dodecylsulfate-polyacrylamide electrophoresis. Analytical Biochemistry. 1971;41(2):510-6. doi: http://dx.doi.org/10.1016/0003-2697(71)90173-4.

24. Anseth KS, Bowman CN, Peppas NA. Polymerization kinetics and volume relaxation behavior of photopolymerized multifunctional monomers producing highly crosslinked networks. J Polym Sci A Polym Chem. 1994;32(1):139-47. doi: 10.1002/pola.1994.080320116.

25. Canal T, Peppas NA. Correlation between mesh size and equilibrium degree of swelling of polymeric networks. J Biomed Mater Res. 1989;23(10):1183-93. doi: 10.1002/jbm.820231007.

26. Patil NS, Dordick JS, Rethwisch DG. Macroporous poly(sucrose acrylate) hydrogel for controlled release of macromolecules. Biomaterials. 1996;17(24):2343-50. doi: http://dx.doi.org/10.1016/S0142-9612(96)00089-0.

27. Browning MB, Cosgriff-Hernandez E. Development of a biostable replacement for PEGDA hydrogels. Biomacromolecules. 2012;13(3):779-86. doi: 10.1021/bm201707z.

28. Brodsky B, Persikov AV. Molecular structure of the collagen triple helix. In: David ADP, John MS, editors. Adv Protein Chem: Academic Press; 2005. p. 301-39.

29. Seliktar D. Designing cell-compatible hydrogels for biomedical applications. Science. 2012;336(6085):1124-8. doi: 10.1126/science.1214804.

Chapter 3:

The influence of matrix crosslinking on EC migration and organization

Introduction

The extracellular matrix provides a multitude of cues to direct cell fate. The molecules of the ECM provide biological factors such as binding sites for integrins, growth factors, and proteolytic enzymes. Further, it can modulate the diffusion of paracrine factors and provide mechanical resistance to cell-generated forces (1, 2). This mechanical resistance is can be described by the material's mechanical properties, or commonly stiffness. Much attention has been brought to this field through the work of Engler et al. where they found that substrate stiffness could control the lineage commitment of stem cells (3). Moreover, it had been shown that cell motility could be modulated by substrate stiffness in a process dubbed 'durotaxis' (4). This has been observed with mesechymal stem cells (5), breast cancer cells (6), smooth muscle cells (7), fibroblasts (8), and others. Of note is the work of Reinhart-King who studied endothelial cells cultured on compliant 2D polyacrylamide substrates derivatized with type I collagen. They found EC network formation was favored on soft substrates with high ligand concentration or stiff substrates with sparse ligand concentrations (9). In a 3D ECM composed of collagen, ligand concentration and stiffness are intrinsically coupled. Thus it is difficult to create a stiff collagenous matrix with sparse ligands. Further, in collagen,

ligands and degradation motifs are presented on the same molecule, so a stiff matrix is harder to degrade and will inhibit cell motility. So in order to present a suitably degradable matrix, we chose to design ECM that are compliant and have a high ligand concentration.

The role of matrix compliance in 3D cell migration has been well-studied and is reviewed elsewhere (10, 11). However, less work has been focused on capillary formation in matrices of varying stiffness. Previous studies by our group have shown that capillary invasion was attenuated by matrix density, but could be recovered by inclusion of fibroblasts (12) and the matrix density modulates angiogenesis in a manner that requires cell-generated tractional forces (13). However, it is important to note that increasing the densiy of the fibrin matrix increased both the stiffness and ligand concentration. In a PEG-based system, we could independently control these factors. Indeed, our group has used these systems to study smooth muscle cells (14, 15). However, transitioning to culturing EC required development of a new biosynthetic material which was outlined in Aim 1. This system allows us to alter matrix crosslinking without changing ligand concentration. We further characterized the effects of crosslinking on key physical properties of stiffness, mesh size (via swelling), and degradation. Thus, we sought to determine if a co-culture of stromal and endothelial cells would form vasculature and respond to matrix crosslinking with a constant ligand concentration.

Methods

Cell Culture

Human umbilical vein endothelial cells (EC) were isolated as described previously (16), and cultured in endothelial growth medium (EGM-2, Lonza, Walkersville, MD) at 37°C, 5% CO_2 and used at passage 2. Normal human lung fibroblasts (FB, Lonza) were cultured in DMEM (Invitrogen) supplemented with 10% fetal bovine serum (FBS, Life Technologies) at 37°C, 5% CO_2 and used between passages 9 and 12. Cell types were chosen that had previously been shown to support robust capillary formation *in vitro* (12, 17). This allows us to control for variability between endothelial and stromal types and to evaluate the performance of our material. For routine culture, medium was changed every other day and cells were harvested at 80% confluence with 0.05% Trypsin EDTA (Life Technologies).

Cell Encapsulation & Culture

Cells were encapsulated at either 1e6 EC/mL or 1e6 FB/mL for monoculture, or 1e6 EC and 1e6 FB per mL for co-culture conditions. Cells were resuspended in 1 mL of hydrogel precursor solution, divided into 100 µL aliquots, and photopolymerized in 4.7 mm diameter syringe top (18). To prevent constructs from adhering to the culture surface, 24-well plates were coated with 1% agarose (Denville, Metuchen, NJ). Media were changed after 3 hours and then every other day thereafter. For a subset of experiments, constructs were cultured in EGM-2 containing either 1 µM or 5 µM GM6001 (EMD Chemicals, San Diego, CA) dissolved in DMSO to inhibit MMPs; as a

control, constructs were treated with the vehicle alone. GM6001 was replenished with each media change.

Control constructs were prepared with unmodified collagen diluted to 2.5 mg/mL with sterile water and 10x PBS before raising the pH to 7.2 with 0.1 N NaOH. Cell pellets were suspended in the solution and pipetted in 100 µL drops on non-treated tissue culture 24-well plates and cured for 1 hour before addition of media. After two days of culture, collagen hydrogels were transferred to agarose-coated plates.

Cell Viability

Cell viability was assessed after 1 and 3 days in 4.7 mm constructs with a LIVE/DEAD kit (Invitrogen). Fluorescent images were taken with an Olympus IX81 microscope equipped with a 100 W high pressure mercury lamp (Olympus, Center Valley, PA) and Hammamatsu camera (Bridgewater, NJ) and stained cells were counted using the Count Nuclei module of MetaMorph (Molecular Devices, Sunnyvale, CA).

Hydrogel Compaction

After 14 days of co-culture, 4.7 mm hydrogel plugs were transferred to untreated 24-well plates and suspended in PBS before photography with an EPSON perfection V300 photo scanner (Suwa, Japan). The diameters were measured from the digital images using NIH Image J (National Institutes of Health, Bethesda, Maryland). Separately, gels were placed on a glass slide and photographed with a Casio Exilm digital camera (Tokyo, Japan) to illustrate the 3D shape of the gels.

Time-Lapse Imaging of EC Organization

ECs were fluorescently labeled by transduction with a gene encoding mCherry. Phoenix Ampho cells (Orbigen, San Diego, CA) were transfected with a pBMN-mCherry plasmid using Lipofecamine 2000 (Invitrogen). Retroviral containing supernatant was collected, passed through a 0.45 μm filter, and supplemented with 5 μg/mL Polybrene (EMD Millipore, Billerica, MA) before incubation with EC for 12 hours. The media was changed to EGM-2 and cells were cultured for 2 days, passaged once, and frozen until use. Constructs were prepared with mCherry-labeled EC and wild-type FB and allowed to float freely in agarose coated wells and photographed with an Olympus Microscope (Ex:558/Em:583) *in situ* daily for 14 days. A custom MATLAB script was used to quantify the total network length from the fluorescent images.

Immunofluorescent Staining

Constructs were washed 3x with PBS then fixed overnight in 4% formaldehyde (Sigma) in PBS at 4°C then washed again. Cells were permeablized with TBS + 1% Triton X-100 (TBS-T), rinsed with TBS-T and blocked with 2% bovine serum albumin (Sigma) in TBS-T (AbDil) overnight at 4°C. Constructs were incubated overnight at 4°C in a monoclonal mouse anti-human CD31 antibody (Dako, Glostrup, Denmark) diluted 1:200 in AbDil. After multiple washes, samples were then incubated overnight at 4°C in AlexaFluor 594 goat anti-mouse antibody (Invitrogen) diluted 1:450 in AbDil. Further washing was performed before counter-staining with DAPI (1:10,000; Sigma) and Oregon Green 488 phalloidin (1:200; Invitrogen) For α-SMA staining, a similar protocol was utilized with a primary mouse monoclonal anti-α-smooth muscle actin antibody

(1:200; AbCam, Cambridge, MA). Fluorescent images of the constructs were taken and the network lengths were quantified using the angiogenesis module in Metamorph.

Results

Cellular Viability

More than 60% of encapsulated cells were found to be viable in all constructs after 24 hours (Figure 16A). Quantification and comparisons between the conditions (Figure 16B) revealed viability was highest in PC+0%PEG and similar in the others. Both monocultures and the co-culture showed similar trends with the cell type not being a significant ($P > 0.05$) source of variation by 2-way analysis of variance (ANOVA); pairwise comparisons were determined by Bonferroni post-tests. By day three (Figure 16C), both the cell type and material had a significant influence on viability. The viability of FB was still close to 60%, while the viability of EC had dropped across all conditions with the lowest viability observed in PC+2%PEG. Viability was retained best in co-cultures, which were still comparable to their viability after one day. The individual viability of each cell type in the co-culture is unknown.

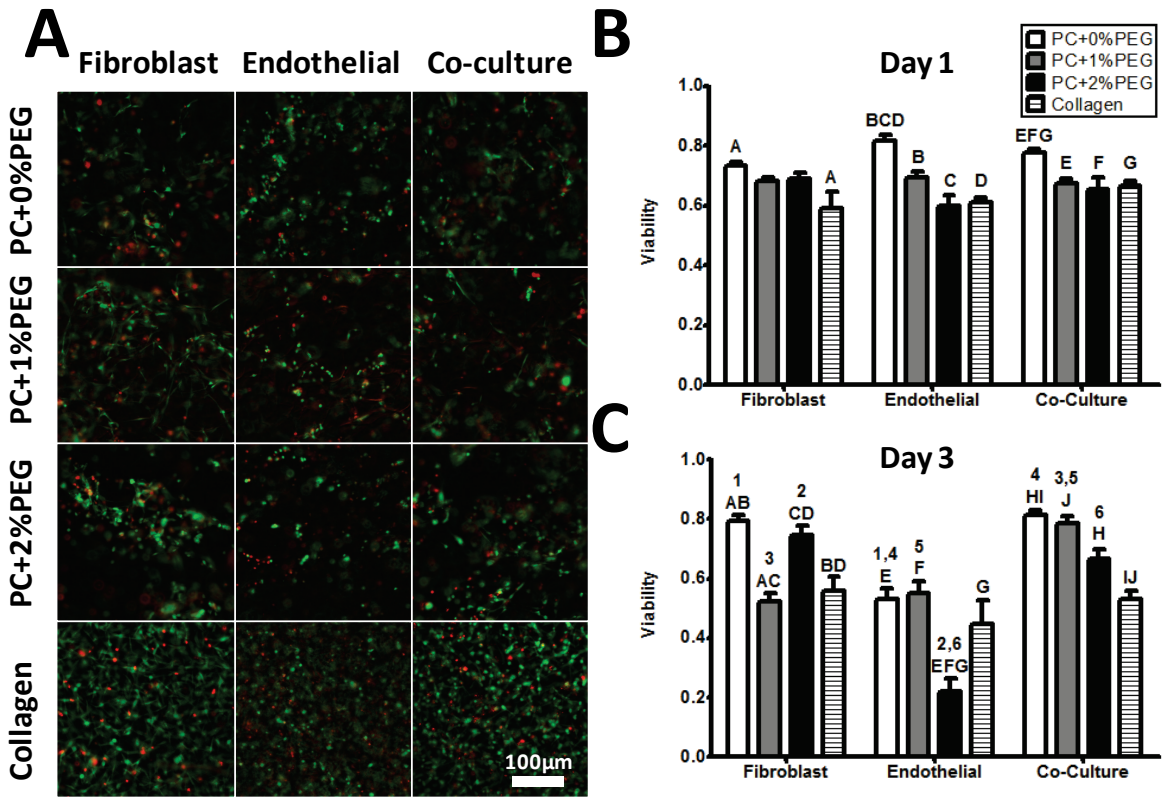

Figure 16: Viability of cells encapsulated in PEG-collagen

A) A fluorescent assay for 3D viability (green cells are live and red cells are dead) revealed that > 60% of cells are viable after 24 hours in culture (B) with similar viability for all cell types, and only the PC+0%PEG being significantly higher. C) By 72 hours, the viability was influenced by cell type and material with EC-only being the worst. Viability of co-cultures were comparable to the earlier time point. Significant comparisons are indicated on the graphs with matched symbols ($P < 0.05$).

Bulk Cellular Remodeling & Hydrogel Compaction

Shear storage moduli of the cell-seeded constructs (Figure 17) were similar to the acellular constructs. Significant ($P < 0.05$) differences between formulations at each time point were observed. Linear regression revealed no significant trends over time in the PC+0%PEG and PC+2%PEG gels, but for the PC+1%PEG gels, a significant negative trend ($P < 0.05$) was observed over time.

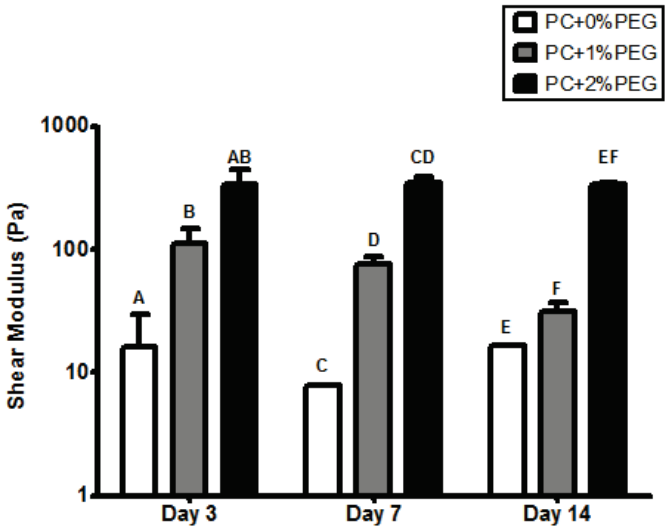

Figure 17: Bulk mechanical properties of PEG-collagen gels seeded with co-cultures of cells remain unchanged over time.

Shear moduli of the hydrogels were significantly different for each formulation at each time point. There were no significant trends over time in the shear moduli of the PC+0%PEG or the PC+2%PEG conditions, but a slight downward trend was observed in the shear modulus of the PC+1%PEG condition. Significant comparisons are indicated on the graphs with matched symbols ($P < 0.05$).

The constructs, which were initially cast as 4.7 mm plugs, all decreased in diameter over the 14 day culture period with the PC hydrogels retaining a cylindrical shape with discernible edges (Figure 18). The PC+2% PEG compacted the least to ~4mm. The

PC+0%PEG and PC+1%PEG gels compacted to a diameter of ~2 mm with no significant difference between them, but were significantly smaller than the PC+2%PEG condition. The collagen gel compacted to a spherule less than 1 mm in diameter which was significantly smaller than the other conditions. Significance ($P < 0.01$) was determined by one-way ANOVA and Tukey's post-tests.

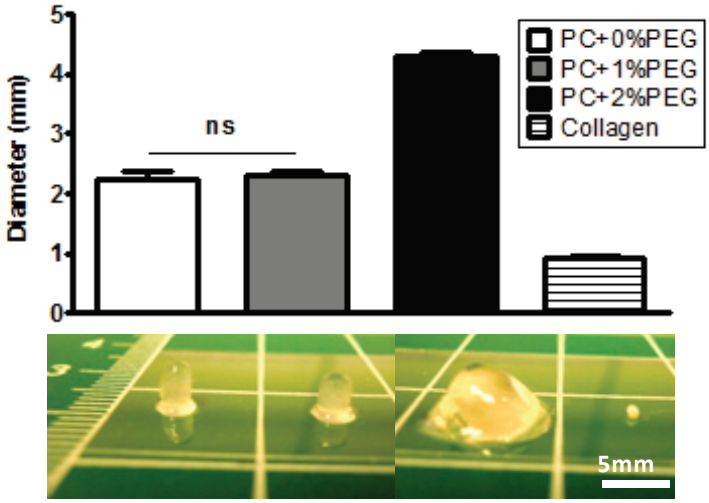

Figure 18: Compaction of hydrogel constructs

Constructs were cast as plugs with an initial diameter of 4.7 mm and measured again after 14 days of culture. The diameters significantly decreased with all being different ($P < 0.01$) unless otherwise noted (ns).

Capillary Morphogenesis in PEG-Collagen Hydrogels

When ECs and FBs were co-encapsulated within PEG-collagen hydrogels, the labeled EC elongated within the first 3 days of culture (Figure 19), leading to the formation of capillary-like networks by day 10 in PC+0%PEG and day 14 in PC+1%PEG. EC in the PC+2%PEG constructs failed to elongate or form multicellular structures. The collagen constructs rapidly formed networks in one day, but the EC structures began to regress after the construct was detached from the substrate (to mimic the PC conditions) while significant cell-mediated compaction occurred in the remaining 13 days.

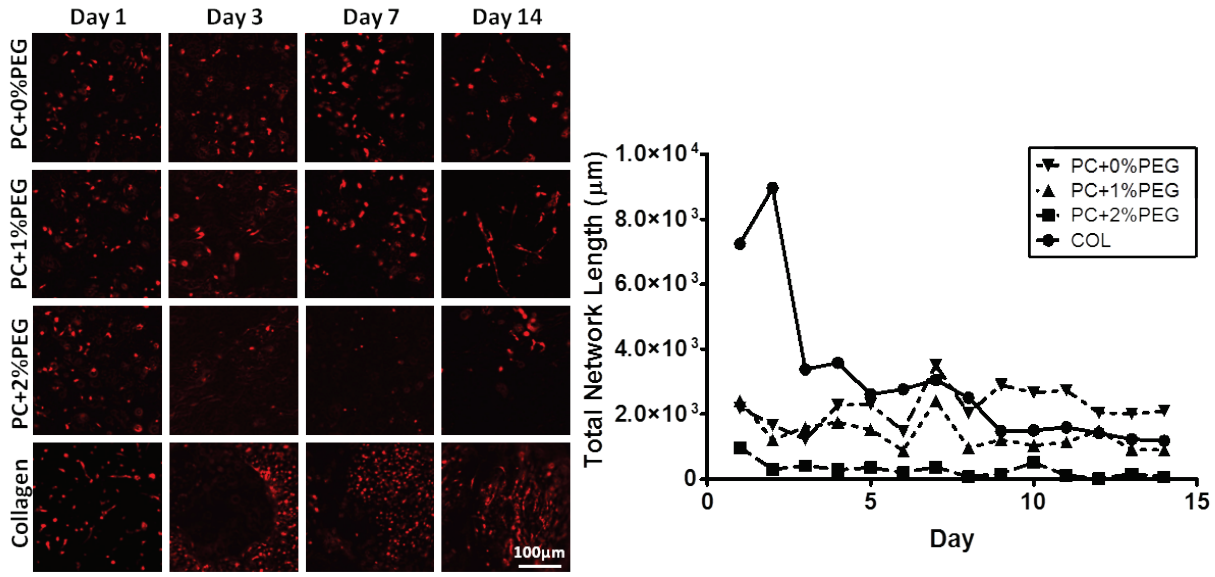

Figure 19: Time-lapse monitoring of EC organization in PEG-collagen hydrogels.

Constructs prepared with mCherry labeled EC reveled the kinetics of morphogenesis in PC+0%PEG and PC+1%PEG gels. There was little evidence of network formation in PC+2%PEG gels due to the limited survival of EC in those gels. While EC formed networks in 1 day in anchored collagen constructs, detachment of the constructs from the culture surface led to rapid compaction and regression of EC networks. Quantification of the total network lengths reflected the rapid deterioration in the Collagen gels, and the gradual formation of networks in the PC+0%PEG and PC+1%PEG conditions.

To confirm the formation of capillary structures, staining was conducted for a vascular EC cell-surface maker CD31 and a pericyte marker αSMA. Staining of co-cultures in PC+0%PEG and PC+1%PEG revealed organization of CD31+ ECs into tube-like structures by day 14 (Figure 21Figure 20A). While very few EC were observed in the PC+2%PEG condition, elongated FB were found throughout the constructs. Further, staining for α-SMA revealed stromal cells positive for the pericytic marker across all three conditions (Figure 20B).

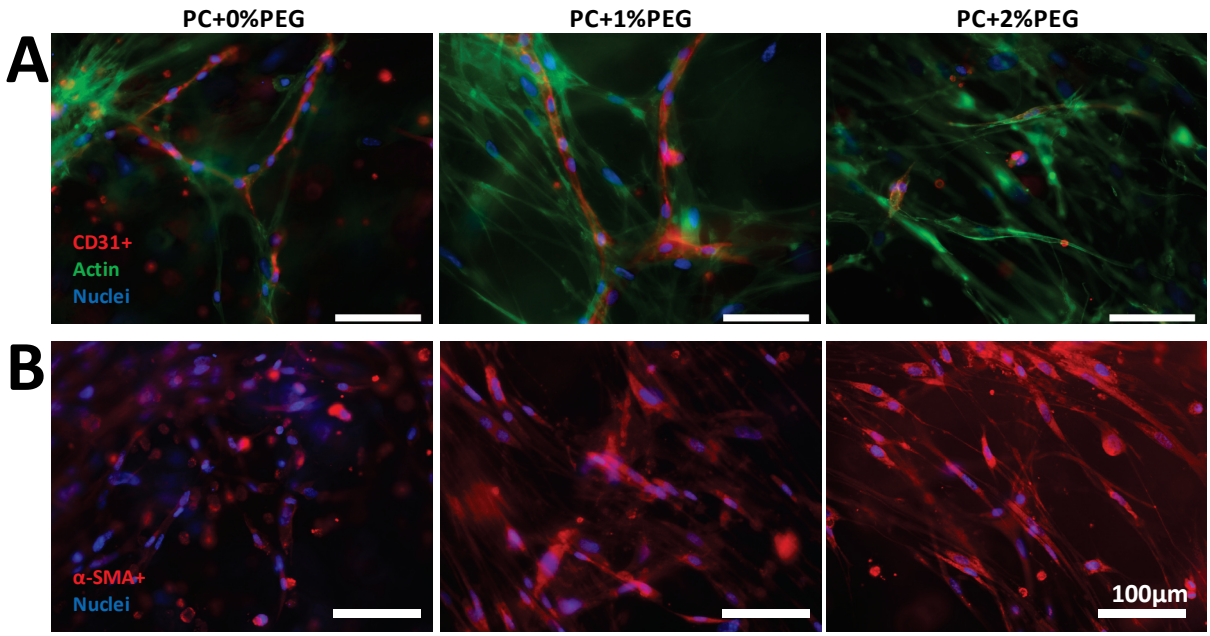

Figure 20: Cellular staining of co-cultures revels expression of vascular and pericyte markers.

A) Immunofluorescent staining of constructs prepared with wild type EC on day 14 revealed capillary networks in PC+0%PEG and PC+1% PEG (red are CD31+ cells, green is actin, and blue are nuclei). B) Fibroblasts were found to express α-SMA in all three formulations and adopted an elongated morphology in the more crosslinked gels (red are α-SMA+ and blue are nuclei).

Quantification of network lengths (Figure 21A) were found to be significantly ($P < 0.05$) lower in the PC+2%PEG condition, but not significantly different between the PC+0%PEG and PC+1%PEG by a one way ANOVA with Bonferroni post-tests. Confocal z-stacks taken at higher magnification revealed that the CD31+ capillary-like structures possess hollow lumens in the PC+1%PEG condition (Figure 21B).

MMP Inhibition

Supplementation of culture medium with a broad-spectrum MMP inhibitor, GM6001 (19), prevented endothelial invasion and subsequent organization within the material

(Figure 22A). Quantification of total network lengths revealed significant increases in total network length in cultures treated with 1 μM GM6001 (relative to those treated with DMSO vehicle) treatment across all PC material formulations (Figure 22B). Further assessment of the mean segment length revealed a dose-dependent decrease across the PC conditions (Figure 22C). Thus, low doses of GM6001 caused the EC to produce more numerous, yet, shorter tubes in PC+0%PEG and PC+1%PEG hydrogels. EC organization was not observed in the PC+2%PEG gels to an appreciable extent. In all conditions, 5μM doses of GM6001 abrogated the formation of capillary networks as determined by both total network or mean segment length.

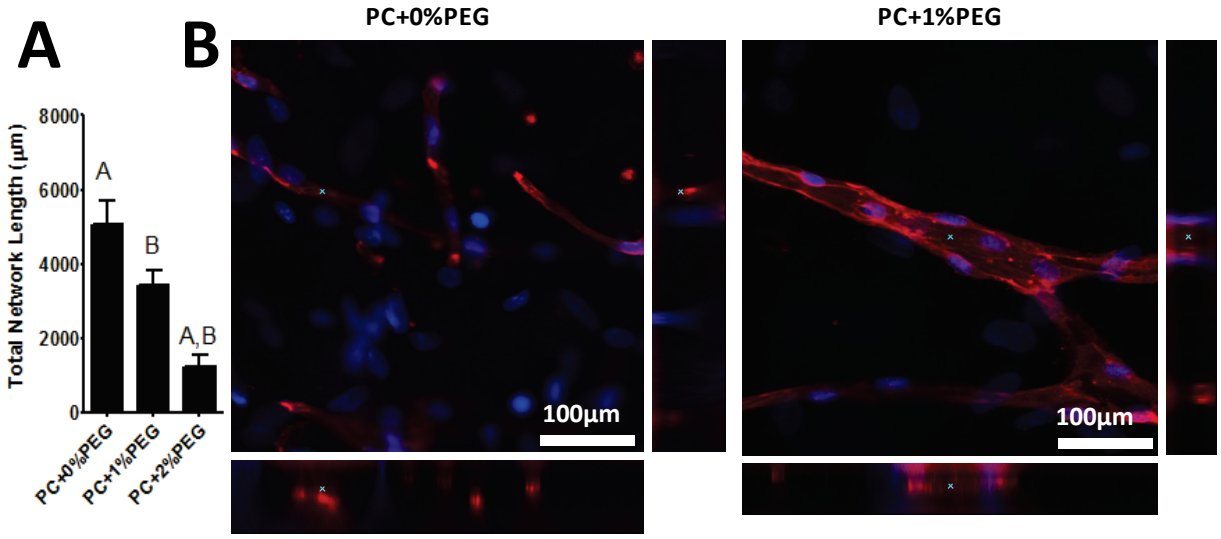

Figure 21: Capillary formation was observed in PEG-collagen hydrogels.

A) Quantification of total network lengths in the stained images reveled significantly reduced network formation in PC+2%PEG gels with no significant differences between the lengths of PC+0%PEG and PC+1%PEG gels observed. Matched symbols denote significance ($P < 0.01$). B) Confocal stacks of the EC structures in PC+0%PEG (left) and PC+1%PEG (right) revealed lumenal expansion in the PC+1%PEG material (red are α-SMA+ and blue are nuclei). Asterisks (*) on the xy, xz (bottom), and yz (right) panels of each image denote the same region of interest.

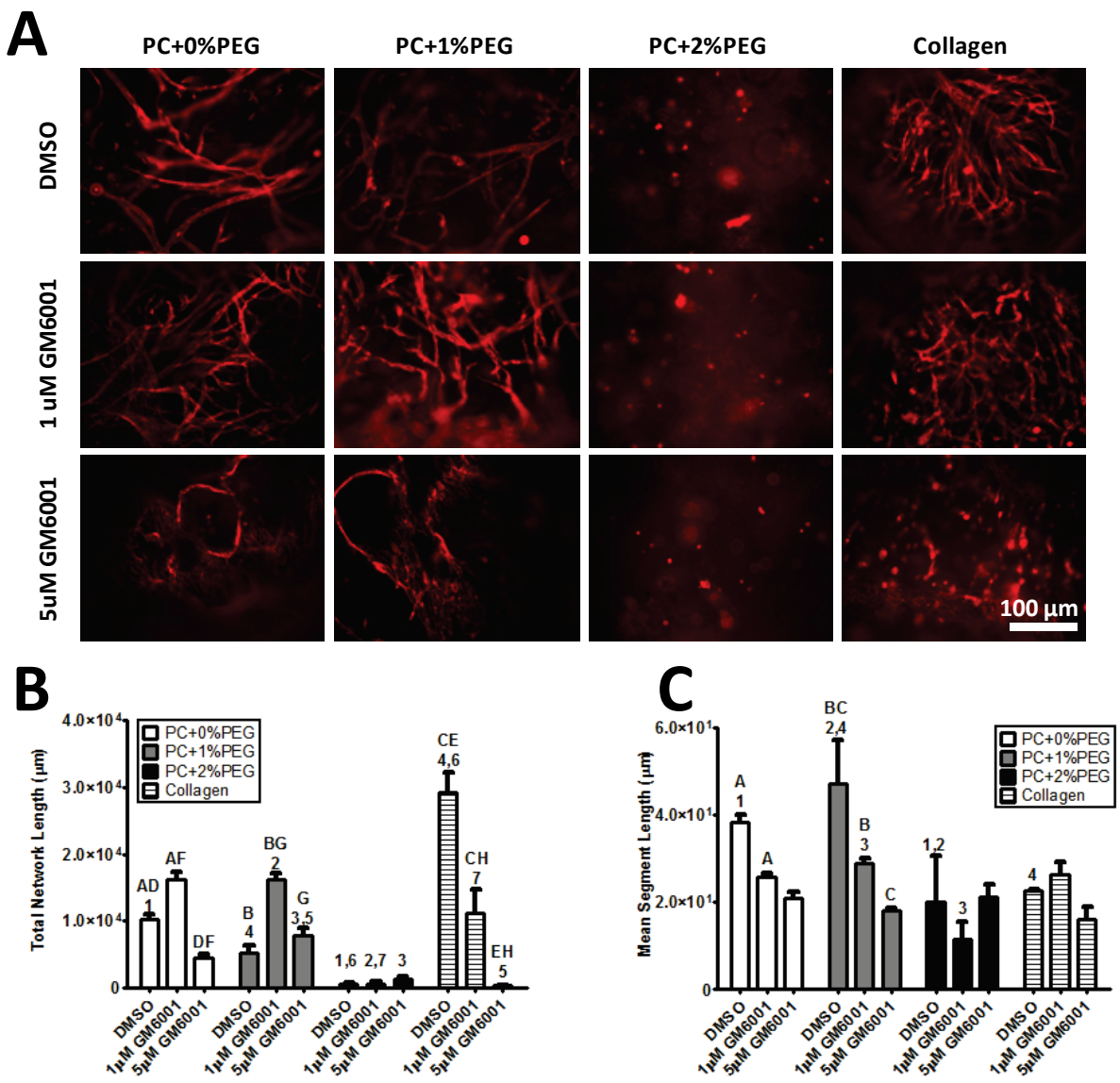

Figure 22: MMP inhibition prevents EC organization in PEG-collagen hydrogels.

A) EC invasion and organization were inhibited by addition of 5 µM GM6001 in the PC+0%PEG and PC+1%PEG materials. EC survival in the PC+2%PEG condition was limited. Red staining is for CD31+ cells. B) Quantification of network morphology revealed significant increases in total network lengths in the presence of low dose GM6001 (1 µM) in PC+0%PEG and PC+1%PEG owing to a larger number of EC structures. Higher doses (5 µM) significantly reduced network lengths in PC+0%PEG. Both doses reduced total network lengths in collagen gel controls. C) Quantification of mean segment lengths showed reductions in PC+0%PEG and PC+1%PEG gels with both doses of inhibitor. Matched symbols denote statistical significance ($P < 0.01$).

Discussion

In this study, we have demonstrated that capillary morphogenesis can be recapitulated *in vitro* in a PEG-based hydrogel by adopting a biosynthetic approach that presents native collagen macromolecules and has permissive mechanical and transport properties. Endothelial cell organization within this biosynthetic hydrogel system was dependent on the degree of crosslinking. By utilizing inert PEGDAm crosslinks, the physical properties of the gels were independently changed without altering the concentration of bioactive sites. Large numbers of immature capillaries formed in the weakly crosslinked gels, while fewer, more mature capillaries formed in the intermediate gels; no capillaries were observed in the most highly crosslinked gels.

Viability of encapsulated cells after 24 hours revealed that most cells survive the photoencapsulation process with monocultures and co-cultures being similarly viable. Cellular responses to the material and culture environment were more apparent after 72 hours. The EC monocultures exhibited the lowest viability, but viability increased in FB and co-cultures. The higher viability of some co-cultures may be due to FB aiding EC survival, as reported by others (20). Interestingly, the PC+2%PEG gels showed the lowest EC viability, but the viability of FB was not affected. This differential response of the two cell types may reflect preferences for different ECM stiffness ranges. Compared to the high viabilities (>80%) typically published in cell encapsulation studies (21), the viabilities here are fairly low, even in the pure collagen hydrogels. We attribute

these differences to the high cell densities and the fact that constructs were formed in the presence of PBS rather than culture medium.

In the presence of cells, the PEG-collagen gels partially retained their different mechanical properties over extended culture periods, with the shear storage moduli of the PC+2%PEG gels being significantly different than the other two material formulations at all time points tested. However, the differences between the PC+0%PEG and the PC+1%PEG gels were not significant and were in fact quite similar after 14 days of culture, suggesting that the cells remodel both materials to generate similar mechanical properties. Minimal compaction of the PC+2%PEG hydrogels was observed, but the compaction of the PC+0%PEG and PC+1%PEG formulations was similar. In contrast, the shear storage modulus of collagen gels (22) is similar to that of the PC+0% PEG, but the collagen gels undergo the highest degree of compaction. These observations suggest that the degree of compaction may be governed by some other criteria than gel's bulk modulus. Other studies have demonstrated that endothelins secreted by EC in collagen gels are responsible for inducing a contractile phenotype in FB (23). The PC+2%PEG gels do not support EC culture; it follows that the FB are not receiving cues to compact the gels. Interestingly, when constructs are cultured on tissue-culture treated plates, instead of agarose, EC colonize the culture surface. In these conditions, all gel formulations compact and support capillary formation (data not shown). This suggests that the PC+2%PEG gels are not too stiff to be compacted by fibroblasts, rather, it is the EC which modulate FB compaction of the gels.

Endothelial cells organized into networks in both PC+0%PEG and PC+1%PEG formulations. Confocal imaging of the EC networks in PC+0%PEG gels revealed multinucleated EC tube structures. In the PC+1%PEG gels, these tubes were more pronounced and displayed clear lumenal expansion to form capillaries. Networks in PC+0%PEG networks consisted of a larger number of short structures, while the ECs in the PC+1%PEG gels formed fewer but longer structures. These qualitative differences suggest that increased matrix crosslinking affects capillary morphogenesis. This finding is consistent with a recent study showing that lumen formation in EC-FB co-cultures requires crosslinking of cell-secreted ECM components (20), and suggests the existence of an optimal matrix mechanical environment to support endothelial morphogenesis and maturation. Furthermore, we showed that inhibition of MMPs prevented capillary formation in the PEG-collagen gels, recapitulating the requirement for enzymatic remodeling for the formation of vascular networks in natural materials (24).

In the PC+0%PEG and PC+1%PEG hydrogels, discernible multicellular networks formed on day 10, in contrast to the formation of networks in mechanically anchored collagen gels within one day. However, these EC networks rapidly regressed after the collagen gels were detached from their substrate and placed on agarose. In the PC gels, the large number of PEGDAm crosslinked per collagen molecule stabilize the hydrogels against compaction by slowing the rate of network formation. Relative to unmodified collagen hydrogels and their fibrillar architecture, the amorphous structure and highly-crosslinked nature of the PC gels requires cleavage of a larger number of collagen molecules to create the physical space in the matrix necessary for

tubulogenesis. Despite the slower rate of morphogenesis *in vitro*, the benefit of increased mechanical stability may translate to capillary stability *in vivo,* since constructs may not be immediately anchored to the surrounding tissue upon injection or implantation.

Conclusions

We developed a biosynthetic hydrogel that exhibited proteolytic susceptibility coupled with hydrolytic stability, and demonstrated the ability of this material to support and sustain capillary morphogenesis *in vitro*. The physical properties of these hydrogels could be altered by increasing the cross-linking using exogenous PEGDAm, and our data showed that co-encapsulation of EC and FB within these hydrogels yielded mature capillaries with well-defined lumens in hydrogel formulations with up to 1% exogenous PEGDAm. Organization of EC in these hydrogels could be prevented by inhibition of MMP activity, recapitulating the necessity of these proteases for capillary formation observed in native collagen hydrogels. Collectively, these findings demonstrate the utility of this tractable material platform for the assembly of vascularized tissue constructs *in vitro*. Further application of this material platform as a tool to dissect the mechanisms by which the ECM governs vascularization may inspire new therapeutic approaches for the treatment of various ischemic diseases.

References

1. Frantz C, Stewart KM, Weaver VM. The extracellular matrix at a glance. Journal of Cell Science. 2010;123(24):4195-200. doi: 10.1242/jcs.023820.

2. Discher DE, Mooney DJ, Zandstra PW. Growth Factors, Matrices, and Forces Combine and Control Stem Cells. Science. 2009;324(5935):1673-7. doi: 10.1126/science.1171643.

3. Engler AJ, Sen S, Sweeney HL, Discher DE. Matrix Elasticity Directs Stem Cell Lineage Specification. Cell. 2006;126(4):677-89. doi: http://dx.doi.org/10.1016/j.cell.2006.06.044.

4. Lo CM, Wang HB, Dembo M, Wang YL. Cell movement is guided by the rigidity of the substrate. Biophysical journal. 2000;79(1):144-52. Epub 2000/06/27. doi: 10.1016/s0006-3495(00)76279-5. PubMed PMID: 10866943; PubMed Central PMCID: PMC1300921.

5. Vincent LG, Choi YS, Alonso-Latorre B, del Álamo JC, Engler AJ. Mesenchymal Stem Cell Durotaxis Depends on Substrate Stiffness Gradient Strength. Biotechnology journal. 2013;8(4):472-84. doi: 10.1002/biot.201200205. PubMed PMID: PMC3749305.

6. Kumar S, Weaver V. Mechanics, malignancy, and metastasis: The force journey of a tumor cell. Cancer Metastasis Rev. 2009;28(1-2):113-27. doi: 10.1007/s10555-008-9173-4.

7. Isenberg BC, DiMilla PA, Walker M, Kim S, Wong JY. Vascular Smooth Muscle Cell Durotaxis Depends on Substrate Stiffness Gradient Strength. Biophysical journal. 2009;97(5):1313-22. doi: http://dx.doi.org/10.1016/j.bpj.2009.06.021.

8. Dokukina IV, Gracheva ME. A Model of Fibroblast Motility on Substrates with Different Rigidities. Biophysical journal. 2010;98(12):2794-803. doi: http://dx.doi.org/10.1016/j.bpj.2010.03.026.

9. Califano J, Reinhart-King C. A Balance of Substrate Mechanics and Matrix Chemistry Regulates Endothelial Cell Network Assembly. Cel Mol Bioeng. 2008;1(2-3):122-32. doi: 10.1007/s12195-008-0022-x.

10. Grinnell F, Petroll WM. Cell Motility and Mechanics in Three-Dimensional Collagen Matrices. Annual Review of Cell and Developmental Biology. 2010;26(1):335-61. doi: doi:10.1146/annurev.cellbio.042308.113318. PubMed PMID: 19575667.

11. Janmey PA, Winer JP, Murray ME, Wen Q. The hard life of soft cells. Cell Motility and the Cytoskeleton. 2009;66(8):597-605. doi: 10.1002/cm.20382.

12. Ghajar CM, Chen X, Harris JW, Suresh V, Hughes CC, Jeon NL, et al. The effect of matrix density on the regulation of 3-D capillary morphogenesis. Biophysical journal. 2008;94(5):1930-41. Epub 2007/11/13. doi: 10.1529/biophysj.107.120774. PubMed PMID: 17993494; PubMed Central PMCID: PMC2242748.

13. Kniazeva E, Putnam AJ. Endothelial cell traction and ECM density influence both capillary morphogenesis and maintenance in 3-D. American journal of physiology Cell physiology. 2009;297(1):C179-87. Epub 2009/05/15. doi: 10.1152/ajpcell.00018.2009. PubMed PMID: 19439531.

14. Peyton SR, Kim PD, Ghajar CM, Seliktar D, Putnam AJ. The effects of matrix stiffness and RhoA on the phenotypic plasticity of smooth muscle cells in a 3-D biosynthetic hydrogel system. Biomaterials. 2008;29(17):2597-607. Epub 2008/03/18. doi: 10.1016/j.biomaterials.2008.02.005. PubMed PMID: 18342366; PubMed Central PMCID: PMC2855209.

15. Kim PD, Peyton SR, VanStrien AJ, Putnam AJ. The influence of ascorbic acid, TGF-beta1, and cell-mediated remodeling on the bulk mechanical properties of 3-D PEG-fibrinogen constructs. Biomaterials. 2009;30(23-24):3854-64. Epub 2009/05/16. doi: 10.1016/j.biomaterials.2009.04.013. PubMed PMID: 19443026.

16. Griffith CK, Miller C, Sainson RC, Calvert JW, Jeon NL, Hughes CC, et al. Diffusion limits of an in vitro thick prevascularized tissue. Tissue Eng. 2005;11(1-2):257-66.

17. Kniazeva E, Putnam AJ. Endothelial cell traction and ECM density influence both capillary morphogenesis and maintenance in 3-D. Am J Physiol Cell Physiol. 2009;297(1):C179-C87. doi: 10.1152/ajpcell.00018.2009.

18. Khetan S, Burdick J. Cellular encapsulation in 3D hydrogels for tissue engineering. J Vis Exp. 2009(32):e1590. doi: doi:10.3791/1590.

19. Grobelny D, Poncz L, Galardy RE. Inhibition of human skin fibroblast collagenase, thermolysin, and Pseudomonas aeruginosa elastase by peptide hydroxamic acids. Biochemistry. 1992;31(31):7152-4. Epub 1992/08/11. PubMed PMID: 1322694.

20. Newman AC, Nakatsu MN, Chou W, Gershon PD, Hughes CCW. The requirement for fibroblasts in angiogenesis: fibroblast-derived matrix proteins are essential for endothelial cell lumen formation. Mol Biol Cell. 2011;22(20):3791-800. doi: 10.1091/mbc.E11-05-0393.

21. Moon JJ, Saik JE, Poche RA, Leslie-Barbick JE, Lee S-H, Smith AA, et al. Biomimetic hydrogels with pro-angiogenic properties. Biomaterials. 2010;31(14):3840-7. doi: 10.1016/j.biomaterials.2010.01.104. PubMed PMID: PMC2839536.

22. Raub CB, Suresh V, Krasieva T, Lyubovitsky J, Mih JD, Putnam AJ, et al. Noninvasive assessment of collagen gel microstructure and mechanics using multiphoton microscopy. Biophys J. 2007;92(6):2212-22. doi: http://dx.doi.org/10.1529/biophysj.106.097998.

23. Guidry C, Hook M. Endothelins produced by endothelial cells promote collagen gel contraction by fibroblasts. J Cell Biol. 1991;115(3):873-80. doi: 10.1083/jcb.115.3.873.

24. Chun T-H, Sabeh F, Ota I, Murphy H, McDonagh KT, Holmbeck K, et al. MT1-MMP–dependent neovessel formation within the confines of the three-dimensional extracellular matrix. J Cell Biol. 2004;167(4):757-67. doi: 10.1083/jcb.200405001.

Chapter 4:

Investigation of the influence of local displacement fields on capillary organization in vitro

Introduction

The formation of vasculature is a key step in development and misregulation of vasculature is associated with a multitude of diseases such as cancer, myocardial infarction, stroke, diabetes, macular degeneration, and ulcerative disorders to name a few (1, 2). Devising treatments for these conditions relies on understanding the underlying factors which govern the formation of vasculature. Traditionally, research has focused on the growth factors (3). These can be manipulated, isolated, an quantified using established techniques ultimately leading to new classes of drugs (4). Much less attention has been focused on the mechanical cues which are more difficult to accurately measure. Systems have been developed to analyze mechanical and fluid forces in arteogenesis (5) and at the other extreme, single-cell system to study endothelial cell homeostasis (6). However, we lack a means of studying the mechanical cues involved at the scale of capillary growth and angiogenesis.

An early framework of capillary growth was put forth by Thoma in 1893 (7). Of note is his second postulate: "Increase or decrease in the length of a vessel is governed by the

tension exerted on the vessel wall in a longitudinal direction by tissues and organs outside of the vessel." (8). Demonstration of mechanical tension guiding capillary sprouting was shown by Korff & Augustin (9) and in capillary translocation by Kilarski et al. (10). Efforts to quantify these forces *in vitro* have been confounded by the complex structural and mechanical properties of the ECM (11) used to support the formation of neovasculature. However, these limitations can be overcome by utilizing synthetic ECM analogues. These have recently been shown to support angiogenesis *in vitro* by ourselves (12, 13) and others (14-17).

In the preceding chapters, a new material platform has been characterized an validated for endothelial cell culture and capillary morphogenesis. The material consists of polyethylene glycol diacrylamide conjugated to macromolecular type-I collagen (Figure 6). It was photopolymerized into a hydrogel which exhibited hydrolytic stability (Figure 10, Figure 11, Figure 12), but was susceptible to enzymatic remodeling (Figure 13). Crucially, the mechanical properties are suitable for continuum modeling. The material is linearly elastic with a modulus which, for the PC+2%PEG formulation, is not significantly altered by cell culture (Figure 17). While cells were viable in all formulations (Figure 16), only the PC+0%PEG and PC+1%PEG formulation supported capillary morphogenesis (Figure 21). One approach to resolving this discrepancy would be to combine both formulations into a composite structure to allow both capillary formation and accurate material modeling. An assay could be developed wherein ECs form capillaries in pre-defined islands of PC+1%PEG and the resulting capillaries invade a surrounding phase of PC+2%PEG which could be utilized as a mechanical sensor. We hypothesize, that in such an arrangement that the capillaries would invade

the surrounding matrix and the forges generated during this process could be measured.

By utilizing such an approach, we have developed a method to quantify the forces produced by capillaries during the formation of an anastamoses. Indeed, our observations show that tension propagates through the matrix and correlates with longitudinal growth of capillary sprouts. These measurements elucidate the quantitative framework governing this critical biologic process, and will unlock a new avenues for investigating the behavior of multicellular structures.

Methods

Cell Culture & Staining

Endothelial cells were isolated as described previously (18) cultured in fully-supplemented EGM-2 (Lonza) at 37°C, 5% CO_2 and used at passage 2. Stromal cells (NHLFs; ATCC, Manassas, VA) were cultured in DMEM (Life Technologies, Carlsbad, CA) supplemented with 10% fetal bovine serum (Life Technologies at 37°C, 5% CO2, and used up to passage 12. Medium was replaced every other day and cells were harvested at 80% confluence via trypsin-EDTA (Life Technologies, Carlsbad, CA) treatment. Endothelial cells were labeled with SP-DiOC18(3) (3,3'-Dioctadecyl-5,5'-Di(4-Sulfophenyl) Oxacarbocyanine, Sodium Salt) (Life Technologies, Carlsbad, CA) at 1:800 dye to media concentration according to the manufacturer's protocol immediately before use in assays.

After 14 days of culture, constructs were immunofluorescently stained as previously described (12). Briefly, constructs were fixed with 10% formalin in Phosphate buffered saline, permeabilized with Triton X-100 in Tris-buffered saline, and blocked with 2% albumin. The constructs were probed with a mouse anti-human CD31 (Dako, Carpinteria, CA) primary antibody and Alexa-flour 488 goat anti-mouse IgG secondary antibody (Life Technologies, Carlsbad, CA).

Array Fabrication

Cells were encapsulated in a 3D PEG-collagen matrix. The material was prepared as previously described (12). Photolithography of the material utilized a photomask, a hydrophobic well, and an acrylated coverslip. Photomasks were designed in AUTOCAD 2013 and submitted to CAD Art Services Inc. (Bandon, Oregon) for printing.

Hydrophobic PDMS wells were prepared by polymerizing PDMS (SYLGARD® 184, Dow Corning, Midland, MI) between clean glass slides and a glass plate separated by a 0.6mm spacer. The PDMS was partially cured at 60°C for 30 minutes before separating the slides from the glass plate. A 20 mm punch was used to create wells in the PDMS. Wells were then fully cured overnight at 60°C. Wells were then cleaned with Piranha solution (1:3 Hydrogen peroxide to sulfuric acid) washed with distilled water and dried at 110°C before treatment with 1 mM (Heptadecafluoro – 1,1,2,2 – Tetrahydrodecyl) Trichlorosilane (Gelest, Inc. Morrisville, PA) in dry tetrahydrofuran under nitrogen for 2 hours. Slides were baked again at 110°C for 15 minutes to cure and stored under vacuum.

Acrylated coverslips were prepared from 22 mm square, No. 1 cover glass (VWR International, Radnor, PA). Coverslips were cleaned in Piranha solution, washed with distilled water, then ethanol, and dried under nitrogen. Coverslips were then treated with a 0.1% v/v solution of (3-Acryloxypropyl) Methyl Dichlorosilane in dry n-Heptane for 15 minutes at 20°C then baked at 70°C for 20 minutes. Coverslips were stored under vacuum and protected from light.

Photolithography of the PEG-Collagen gels was performed under sterile conditions. A 365 nm UV hand lamp (Spectroline® EN-280L, Spectronics Corp., Westbury, NY) was adjusted to 0.5 mw/cm2 with 9 mil (0.2 mm) polystyrene filters, as measured with a dosimeter (Chomaline® UV minder, Apprise Technologies, Inc., Duluth, MN) at 3 cm. The hexagonal lattice phase was cast by combining PEG-collagen with 2% w/v exogenous 20kDa PEG-diacrylamide, 0.6% w/v Irgacure 2959 (Ciba, Basel, Switzerland), and 0.1 % v/v fluorescent beads (FluoSpheres® Sulfate Microspheres, 1.0 µm, red fluorescent (580/605), 2% solids, Life Technologies). This pre-polymer solution was placed in the coated PDMS well, an acrylated cover slip was placed on top, and the photo mask was placed on top of the cover slip. The assembly was placed 2 cm away from the UV light and exposed for 5 minutes. The lattice subsequently bound to the cover slip and was transferred to PBS to wash away unpolymerized PEG-collagen. The lattices were removed from PBS and dried with a sterile cotton tip applicator (ThermoFisher Scientific, Waltham, MA). In a subset of experiments, lattices were fabricated from PEG-collagen solutions containing 1.0, 1.5, 2.5, and 3.0% w/v exogenous PEG diacryalmide.

A second phase of PEG collagen was used to fill the lattice. PEG-collagen was combined with 1% w/v exogenous 20kDa PEG-diacrylamide, 0.6% w/v Irgacure 2959 (Ciba, Basel, Switzerland), and PBS. This solution was used to suspend labeled endothelial cell pellets at 1 million cells per milliliter. For a subset of experiments the cell concentrations were adjusted to $2x10^6$, $5x10^6$, and $10x10^6$ cells per milliliter. The cell-laden solution was dropped onto the dried lattice and further exposed to UV light for 5 minutes. The assembled construct was then placed in a 6-well plate that had

previously been coated with 1% agarose (Denville, Metuchen, NJ). Media (EGM-2, Lonza, Basel, Switzerland) was added to the well along with a suspension of 100,000 stromal cells. Media was replaced the next day and every other day thereafter.

Angiogenic invasion into the lattice was assessed at day 14 by immunofluorescent staining. Capillary invasion distances were measured manually using ImageJ (NIH, Bethesda, MD). The length of a capillary inside the lattice was determined by the length of the capillary that overlaps with the red channel of the image.

Imaging and Image Processing

Constructs we photographed both during the culture period and after fixation and staining. For live cell imaging, constructs remained in the agarose-coated wells and were photographed with an Olympus IX81 microscope equipped with a 100-W high pressure mercury lamp (Olympus, Center Valley, PA) and Hamamatsu ORCA-R2 C10600 camera (Bridgewater, NJ) with red (Ex:562/Em:641), green (Ex:473/Em:520), and blue (Ex:377/Em:447) filters. Constructs were photographed *in situ* daily from days 7 to 14. The z-plane was manually adjusted to be consistent from day-to-day. The microscope's automated stage and Metamorph's (Molecular Devices, Sunnyvale, CA) scan slide setting were used to capture multiple 4x exposures and to stitch a composite panorama that spanned the entire construct.

Unlabeled collagen and PEG-collagen hydrogels were visualized using confocal reflectance microscopy. Confocal reflectance images were taken on a Zeiss LSM 510-

META Laser Scanning Confocal microscope using a 63x water immersion objective (C-Aprochromat, Carl Zeiss, Thornwood, NY). Gels were illuminated using a 488 nm Argon laser through an 80/20 filter.

Image processing was performed in MATLAB (Mathworks, Natick, MA). To correct for uneven illumination from the microscope's optics, 'blank' images (n=10) were taken of fluorescent beads on coverglass. The images were normalized to [0, 1] then used to fit a polynomial

$$f(x,y) = p_{00} + p_{10}x + p_{01}y + p_{20}x^2 + p_{11}xy + p_{02}y^2 + p_{21}x^2y + p_{12}xy^2 + p_{03}y^3$$

to represent the background illumination. The background was tiled to match the size of the slide scans and the tiled background was used to adjust the image intensity:

$$\mathbf{A_c} = 2\mathbf{A} - \mathbf{A} \circ \mathbf{B}$$

where Ac is the corrected image, A is the original image, I is the identity matrix, and B is the tiled background function f(x,y) and ◦ is the Hadamard product.

Image registration was performed on the tiled red channel which corresponds to the fluorescent beads. Exposures from subsequent days were aligned using a modified MATLAB implementation of Fourier-Mellin image registration (19, 20). Images were windowed to 4096 px^2 and pre-processed to outline edges. The images were scaled then morphologically opened with a disk element of 10, 50, 100, 200 pixels before

passing through a Sobel edge detector. This produced outlined gradients of the image at various levels. The resulting edges were expanded based on the iteration (desired resolution) of the alignment algorithm before being summed to produce a "topographic projection" of the intensity profile of the image.

The outlined images were iteratively shifted. Initial shifts could be seeded based on manual estimates of the shift in the x-y plane and the rotation angle. This helped prevent aliasing and sped convergence of the algorithm. The images were then aligned with Fourier-Mellin image registration. Briefly, the spatial 2D Fourier transform of the image was taken then convolved with a high-pass filter. The spectra was then subjected to a log-polar transform to produce the Mellin transform of the original image. The cross-power spectra of the two Mellin transforms were taken and the global maxima was taken to be the rotation angle, θ. One of the original images were rotated by $-\theta$ before computing the cross-power spectrum of the original image pair. The global maximum yielded the shifts of Δx & Δy.

This processes was repeated with successively narrower expansions of the edge detector. Next, the shifts were applied to the original (un-windowed) image pair and further Fourier Mellin registration was performed to determine the accuracy of the solution. An optimal solution was returned when transforms of the original image no longer produced shifts. Finally a region of interest was manually outlined and passed to PIV Lab, a MATLAB implementation of a time-resolved particle tracking algorithm (21, 22). The aligned image pairs were analyzed in PIVLab with first pass window of 120 px and step of 128 px, second pass with size of 64 px and third pass with step of 32 px.

The PIVLab algorithm proceeds to perform direct cross correlation (DCC) in the image and Fourier domains to compute window shifts. This produced displacement vector fields corresponding to a mesh of 50 μm^2 and a time step of one day. The strains at each element were assumed to be small ($\varepsilon << 1$) and the Cauchy's (infinitesimal) strain tensor was computed:

$$\varepsilon_{ij} = {}^{1}/_{2}\left(u_{i,j} + u_{j,i}\right)$$

Which reduced to the following 2D equations with a square mesh in x and y.

$$\varepsilon_{xx} = \frac{du_x}{dx}, \qquad \varepsilon_{yy} = \frac{du_y}{dy}, \qquad \varepsilon_{xy} = \frac{1}{2}\left(\frac{du_x}{dy} + \frac{du_y}{dx}\right) = \varepsilon_{yx}$$

The derivatives were numerically evaluated using the second order central difference formula over the mesh.

In order to compute the stresses in the beams, the shear modulus, G was previously measured to be 334 Pa in the presence of cells at day 14 (12). Further it has been established that the Poisson's ratio of a swollen hydrogel is 0.5 (23). An approximate value of 0.49 was used to avoid creating a singularity in the compliance matrix. Finally, for a linear elastic material the Young's modulus is defined as:

$$E = 2G(1 + \nu)$$

Optical sections used for particle tracking were 50 μm in the z-direction, as set by the microscope's optics (4x, NA=0.13). Sections were taken near the midpoint of the much taller (0.6 mm) lattice. Owing to these length scales, the principal strain in the z-direction is constrained and assumed to be zero. This assumption allows the section to be treated as a 2D body in plane strain (24, 25). Further due to the thin section's location, the boundary conditions were assumed to not have significant effects on the stress. Thus, the following plane-strain compliance matrix was used.

$$\begin{bmatrix}\sigma_{xx}\\ \sigma_{yy}\\ \sigma_{xy}\end{bmatrix} = \frac{E}{(1+\nu)(1-2\nu)}\begin{bmatrix}1-\nu & \nu & 0\\ \nu & 1-\nu & 0\\ 0 & 0 & 1-2\nu\end{bmatrix}\begin{bmatrix}\varepsilon_{xx}\\ \varepsilon_{yy}\\ \varepsilon_{xy}\end{bmatrix}$$

Finally, the stress invariants were calculated using coordinate transforms to yield Cauchy's first and second principal stresses. The angle of the normal stress θ_p relative to the reference frame could likewise be computed.

$$\sigma_1, \sigma_2 = \frac{\sigma_{xx}+\sigma_{yy}}{2} \pm \sqrt{\left(\frac{\sigma_{xx}-\sigma_{yy}}{2}\right)^2 + \sigma_{xy}^2},$$

$$\theta_p = \frac{1}{2}\tan^{-1}\left(\frac{2\sigma_{xy}}{\sigma_{xx}-\sigma_{yy}}\right)$$

To quantify the degree of correlation between capillary locations and computed fields, the Pearson's correlation coefficient (r) was computed (26, 27). The stained image showing capillary development at day 14 was cropped to the same region of interest as the particle-tracking analysis. The 75th percentile strain or stress fields were overlaid

from each of 7 days to create a composite image of the 'mechanical history' of the material. Both images were truncated to only include the region overlaying the bead-laden lattice. The size of each image was adjusted to 533 px^2 before computation (df = 284,089-2).

$$r = \frac{\sum(A_i - A_{av}) \cdot (B_i - B_{av})}{\sqrt{\sum(A_i - A_{av})^2 \cdot \sum(B_i - B_{av})^2}}$$

Where *A* and *B* are images with *i* pixels and the subscript *av* denotes the average of the image.

Shear Rheology

Hydrogel samples were tested on an AR-G2 rheometer (TA Instruments, New Castle, DE) with a 20mm parallel-plate arrangement. For collagen gels, samples were prepared by neutralizing 2.5 mg/mL solutions of Nutragen (Advanced Biomatrix) with 0.1N NaOH and placing the samples on a 37°C Peltier stage to cure for 30 minutes with a mineral oil solvent trap. For PEG-collagen samples, a solution was prepared with 0% exogenous PEGdiacryalmide and cured on an illuminated stage with exposure to UV light at 365 nm at 2 mW/cm^2 for 5 minutes. The resulting gels were tested *in situ* with a strain sweep from 0.1% to 100% with a fixed frequency of 1 rad/s. The relative modulus is the shear storage modulus G' normalized to the shear storage modulus at 0.1% strain. The phase angle, δ, of the material is the ratio of the shear loss modulus G" to the shear storage modulus.

Statistical Analysis

Where appropriate, statistical analysis was performed using Graphpad Prism software (La Jolla, CA). Experimental groups were compared using a one-way ANOVAs with Bonferroni post-tests and significance set at $p < 0.05$. Graphs are shown with mean and standard error of the mean, unless otherwise noted.

Results

Arrays were fabricated using a hexagonal lattice template (Figure 23) with feature widths of 0.5, 1.0, 2.0 mm.

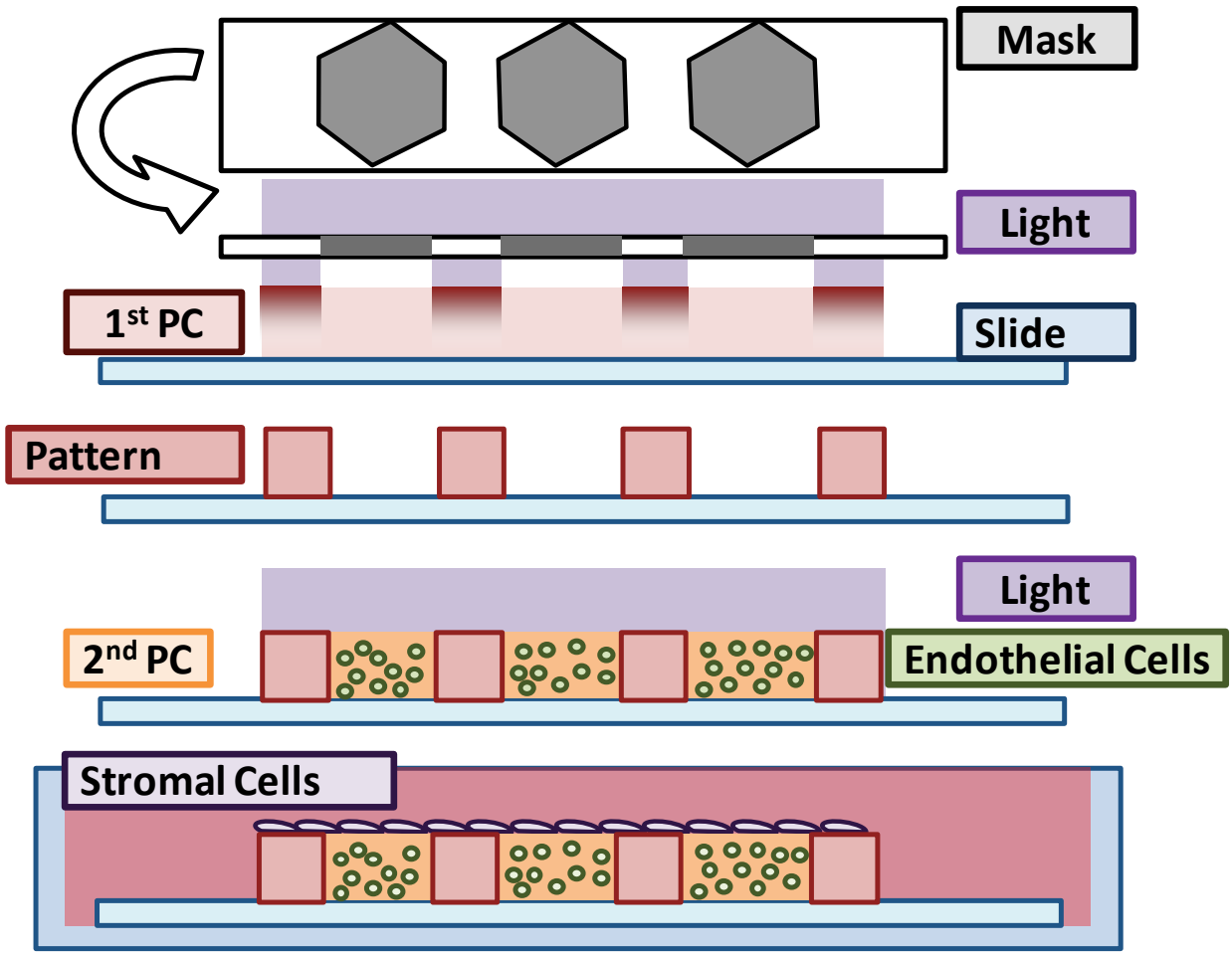

Figure 23: Photolithographic fabrication of lattice assays

Photolithography of PEG-collagen produced hydrogels with distinct compartments. A) A mask printed with the negative of the pattern selectively allowed UV light to polymerize the first phase of PEG-collagen containing 1 micron beads. Unpolymerized material was removed before polymerizing another phase of PEG-collagen containing endothelial cells. The construct was overlaid with stromal cells and cultured 14 days.

These constructs were shown to support vascular formation in the 'wells' with angiogenic invasion of the 'beams' by capillaries. Fluorescent images reveal the relative length scale of these features (Figure 24).

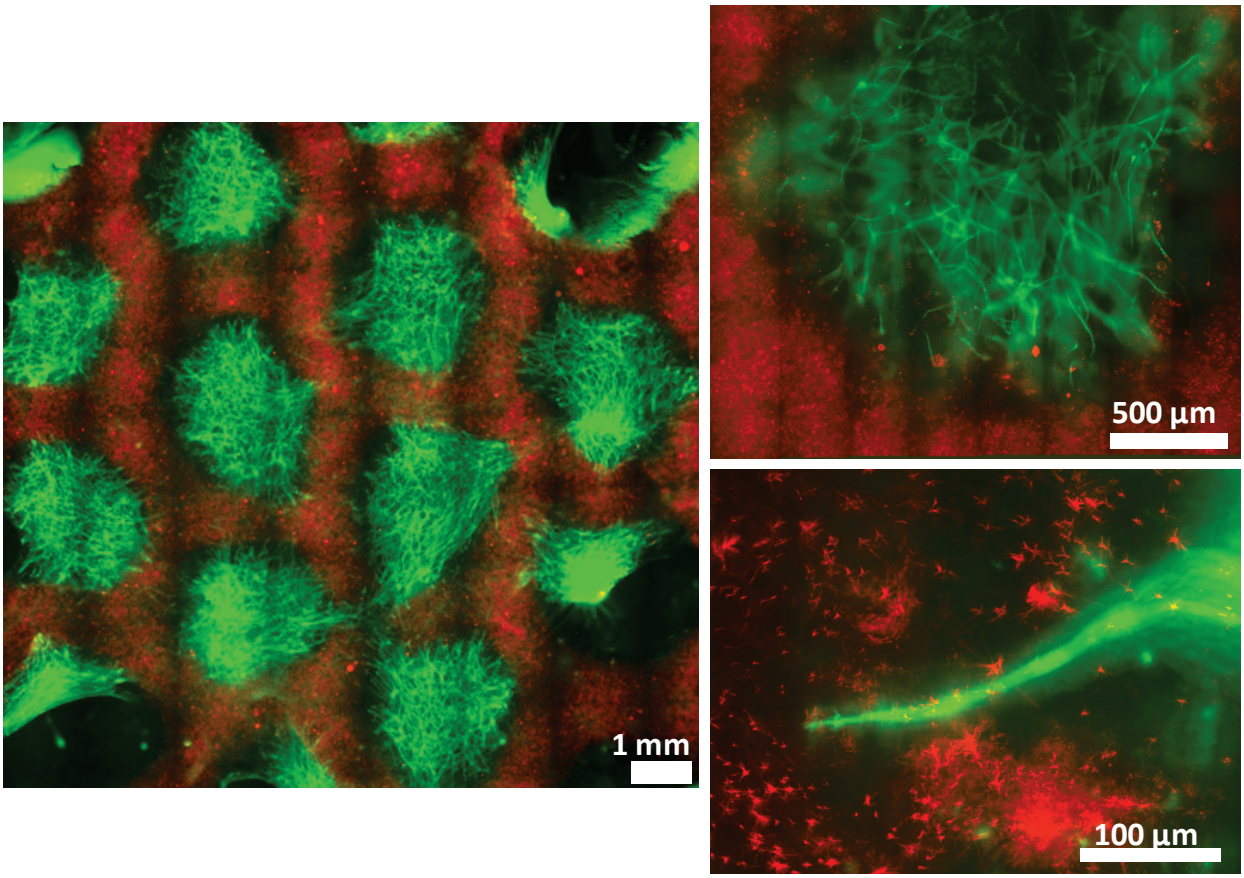

Figure 24: Feature size of vascularized lattice assays

Immunofluorescent staining of EC (green) and micron beads (red) reveals EC organization within phases of PEG-collagen. Cells form capillary beads within 2 mm wells. These capillaries proceed to invade the bead-laden phase of PEG-collagen.

Increased seeding density of the EC had an adverse effect on invasion into the lattice. Using a fixed beam width of 1mm, increasing the EC seeding density to $5x10^6$ or 10

x10^6 cell/mL produced significantly shorter invading capillaries than the 1x10^6 cell/mL condition (Figure 25).

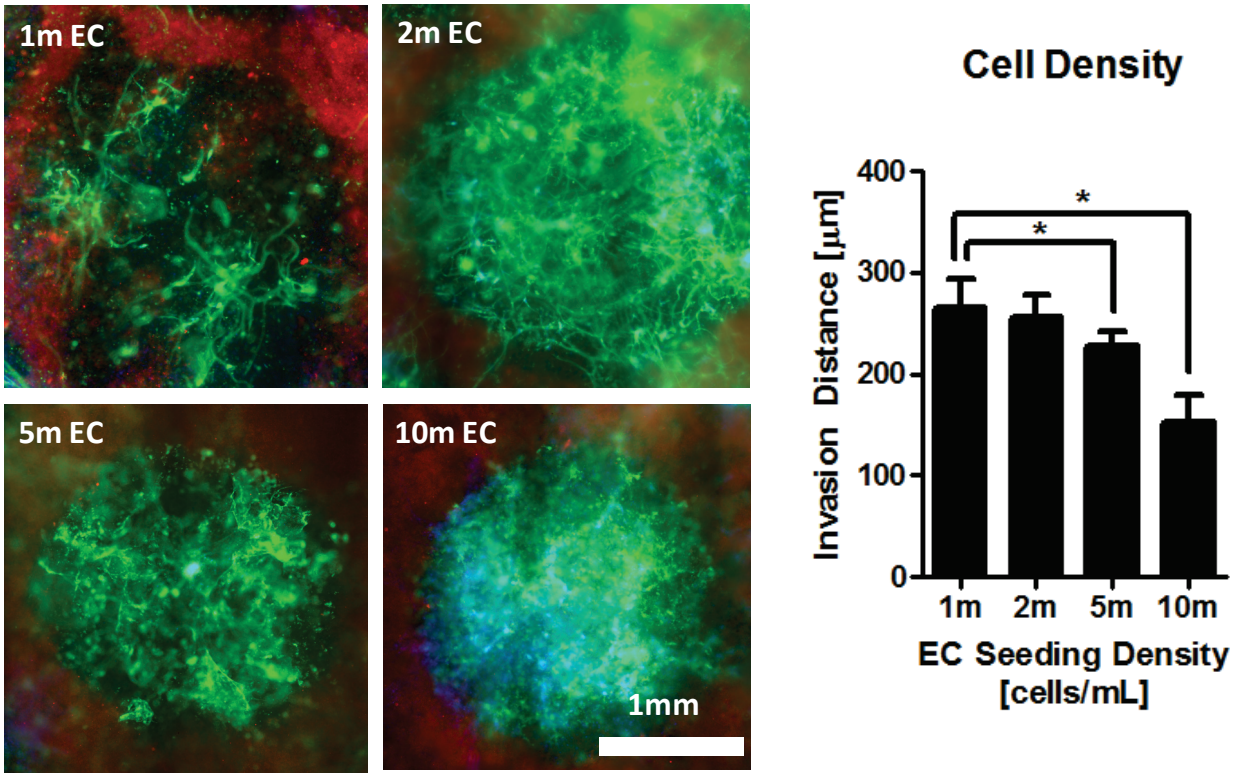

Figure 25: Capillary invasion is attenuated by increased EC seeding.

Increasing EC (green) seeding density reduced the extent of capillary invasion into the lattice (red). Quantification reveled a significant (*) decrease with 5x10^6 and 10x10^6 cells when compared to 1x10^6 cells.

Decreasing the beam width to 0.5 mm significantly increased invasion distance when compared to widths of 1mm and 2mm. While the invasion distance of 2mm beams was decreased, this was not statistically significant compared to the 1mm condition (Figure 26).

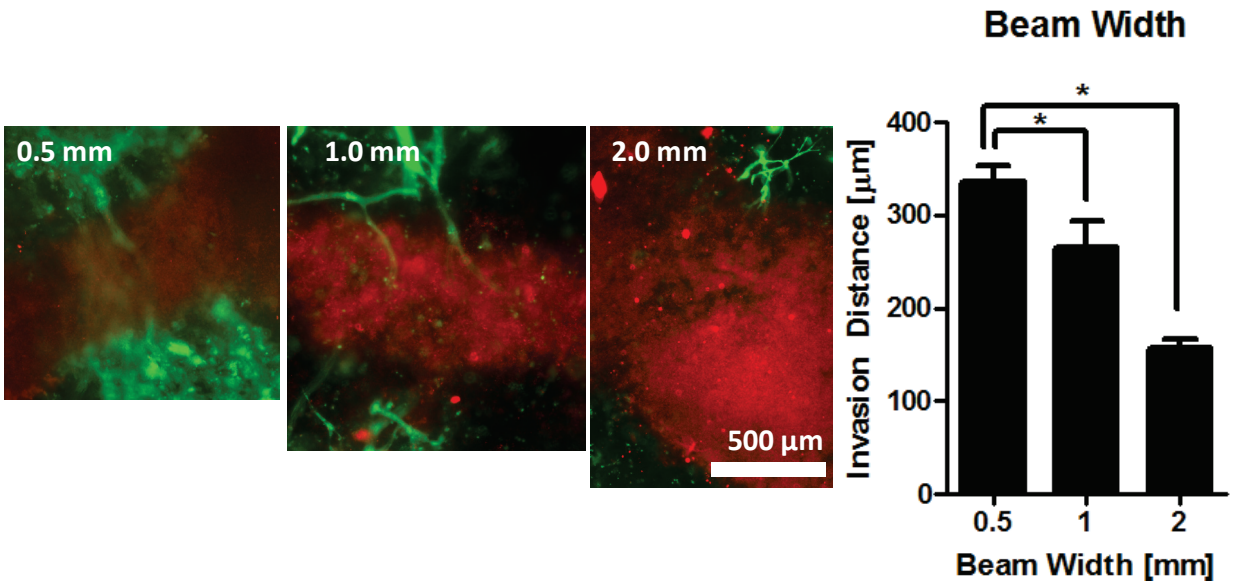

Figure 26: Capillary invasion is attenuated by increased beam width.

Increasing the lattice beam width reduced the extent of capillary invasion. ECs are labeled green while the lattice is red. Quantification revealed that 1 mm and 2 mm beams significantly (*) reduces invasion distance when compared to 0.5 mm beams.

With a fixed beam width of 1mm, increasing the exogenous weight percent of PEG diacrylamide also affected sprouting. Lattices formed with either 2.5% or 3.0% exogenous PEG diacrylamide reduced invasion distance significantly compared to 2% exogenous PEGdiacrylamide (Figure 27). However, lattices fabricated from PEG collagen with 1.0 and 1.5% w/v exogenous PEG diacrylamide failed to form stable constructs.

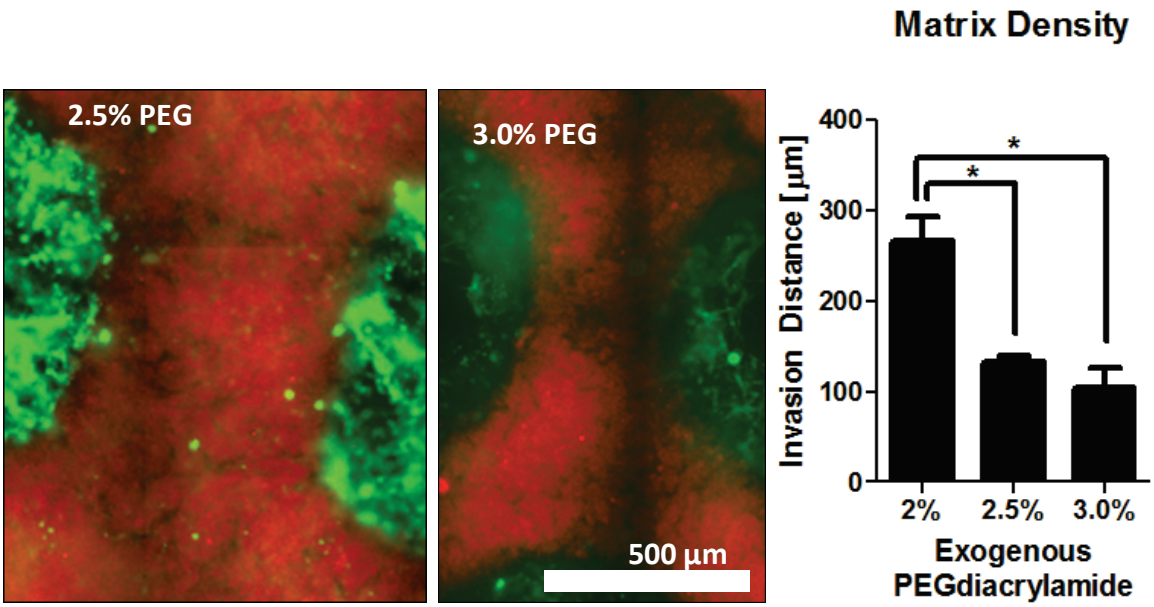

Figure 27: Lattice crosslinking attenuates capillary invasion.

Increasing the lattice crosslinking with exogenous PEG reduced the extent of capillary invasion. ECs are labeled green while the lattice is red. Quantification revealed a significant decrease with 2.5% or 3.0% exogenous PEG when compared to 2.0%.

Image registration (Figure 28) produced aligned image pairs which were analyzed to produce displacement fields which were mapped to strain fields across the beam as previously mentioned. In the subsequent analysis, an anastomosis, was identified forming across a beam. This was confirmed by immunofluorescent staining of the structure at day 14 (Figure 29). A region of the strain field is shown in Figure 30 to highlight the magnitudes and directions of the strain vectors. Further, these images correspond to the eventual location of an anastomosis and two regions of strain can be seen moving towards one another.

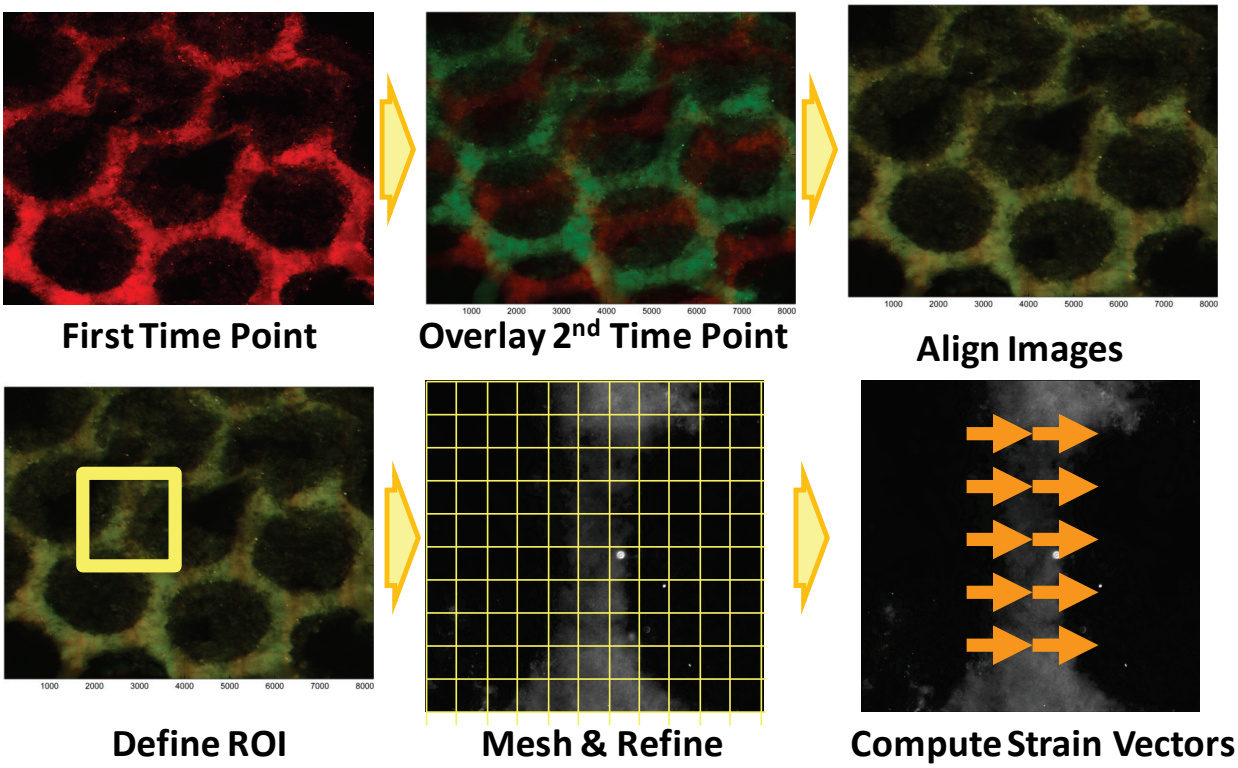

Figure 28: Overview of particle tracking algorithm

Time-lapse images of the assay were utilized to determine strain fields in the lattice during angiogenic invasion. Fluorescent image stacks were registered and pre-processed to remove motion artifacts. Subsequent particle image velocimetry revealed the presence of displacements in the beam.

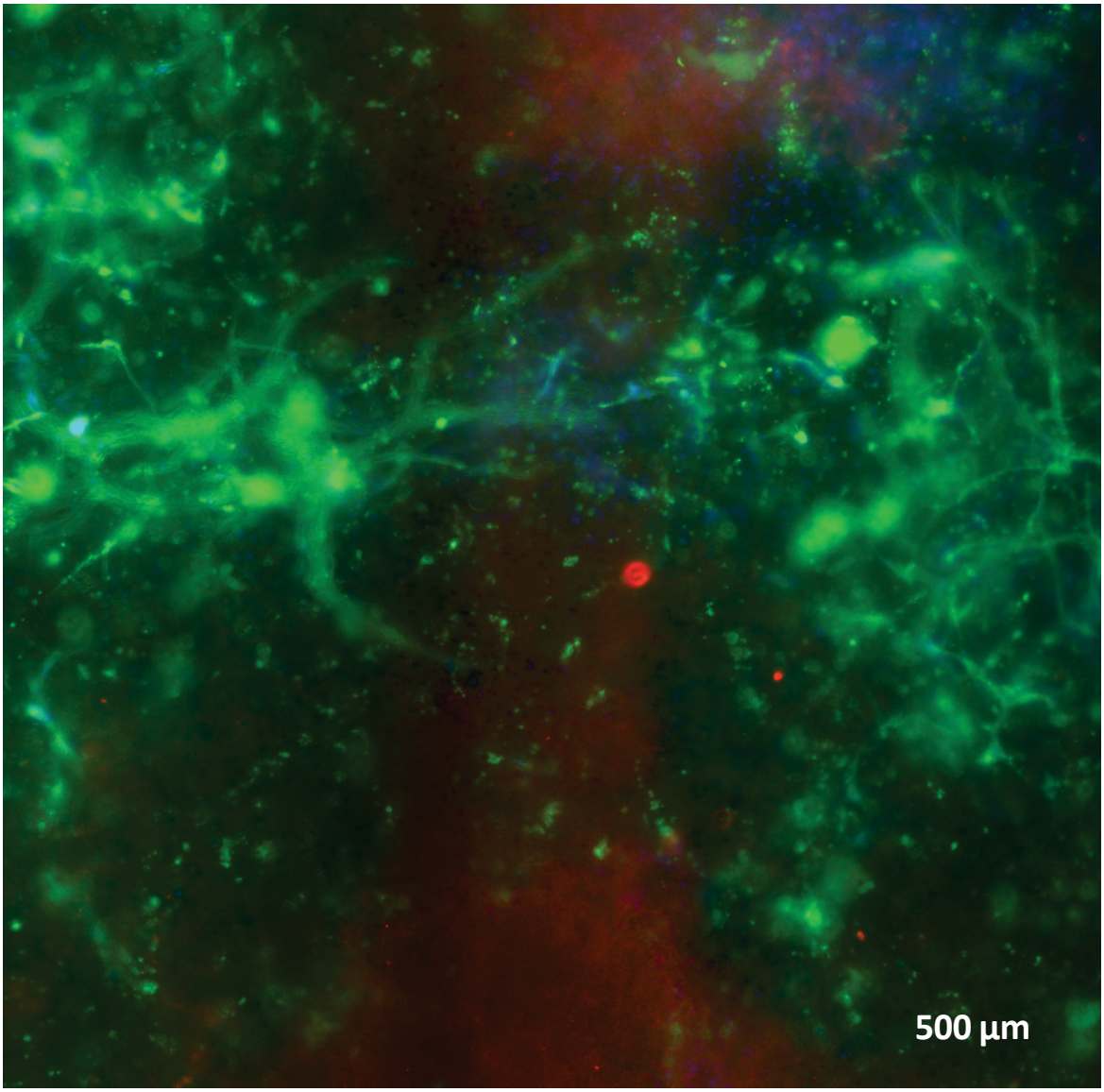

Figure 29: Immunofluorescent image of analyzed anastomosis

An anastomosis was found to be forming through a beam in the lattice. ECs are labeled green, the lattice is labeled red, and cell nuclei are blue. Mechanical modeling was performed on this structure. The analysis of region highlighted in yellow is shown in Figure 30.

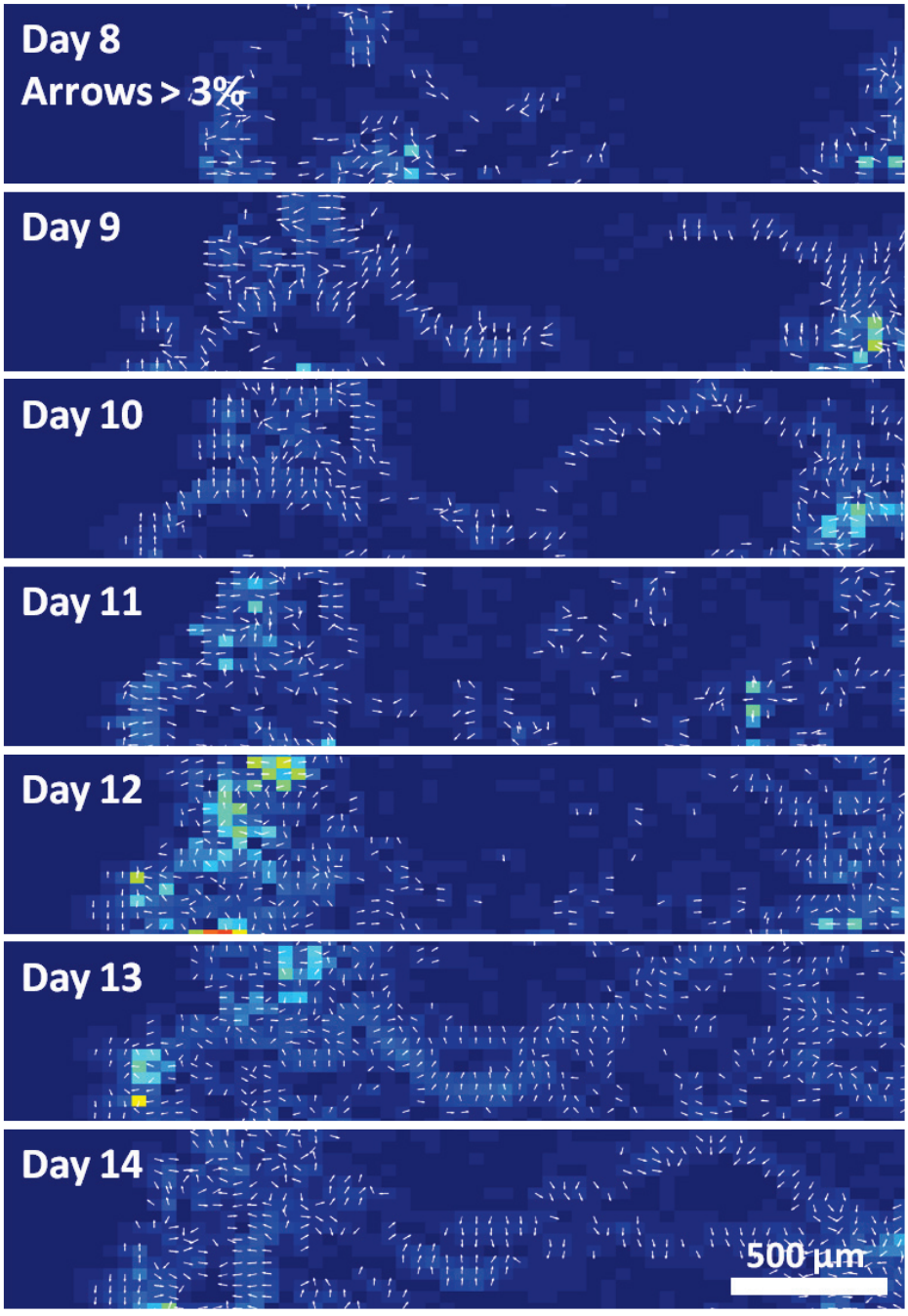

Figure 30: Strain vectors determined by PIV

Strain vectors were computed from coordinate transformations of the displacement fields determined by particle image velocimetry (PIV). Strain magnitudes are shown by colored pixels (50 um^2) and the direction denoted by white arrows. Time resolved analysis revealed the evolution of strain in the eventual location of an anastomosis.

The distribution of strains is highly skewed following a log-normal curve ($R^2 > 0.98$) with infrequent large strains and frequent small strains (Figure 31).

$$Y = amplitude * \exp\left(-\frac{1}{2}\ln\left(\frac{X/center}{width}\right)^2\right)$$

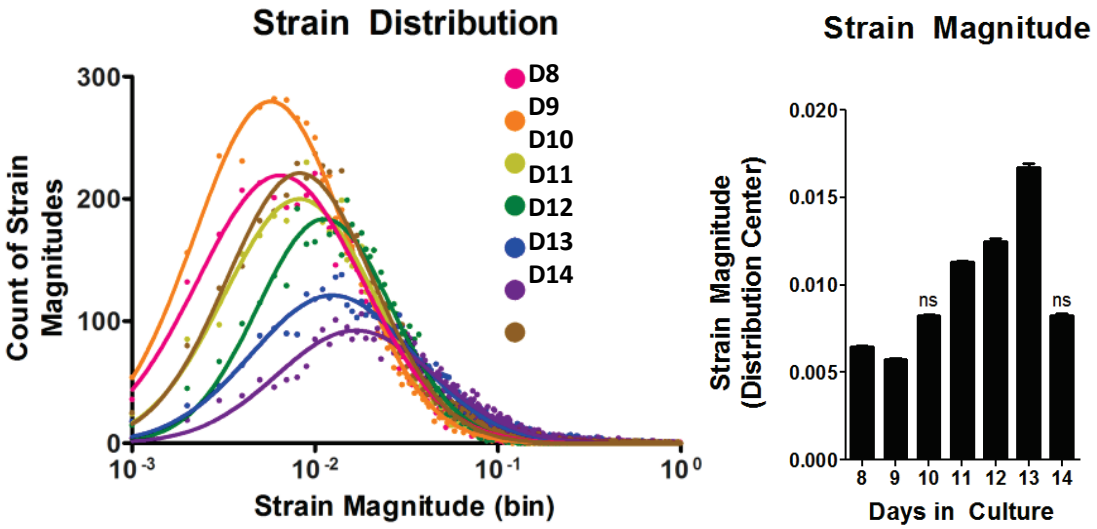

Figure 31: Strain magnitudes across the beam follow a log-normal distribution.

The magnitudes of strain vectors followed a log-normal distribution with rare strain events being 4-fold higher than the distribution center. All comparisons between distribution centers were significant unless denoted otherwise (ns).

These infrequent large strains were observed to be co-localized (Figure 32) with regions of capillary invasion. Further, the background strain field was orders-of magnitude smaller in acellular regions of the lattice. The magnitude of these changed over time following a linear trend with a maximum at day 13 before relaxing at day 14 (Figure 33).

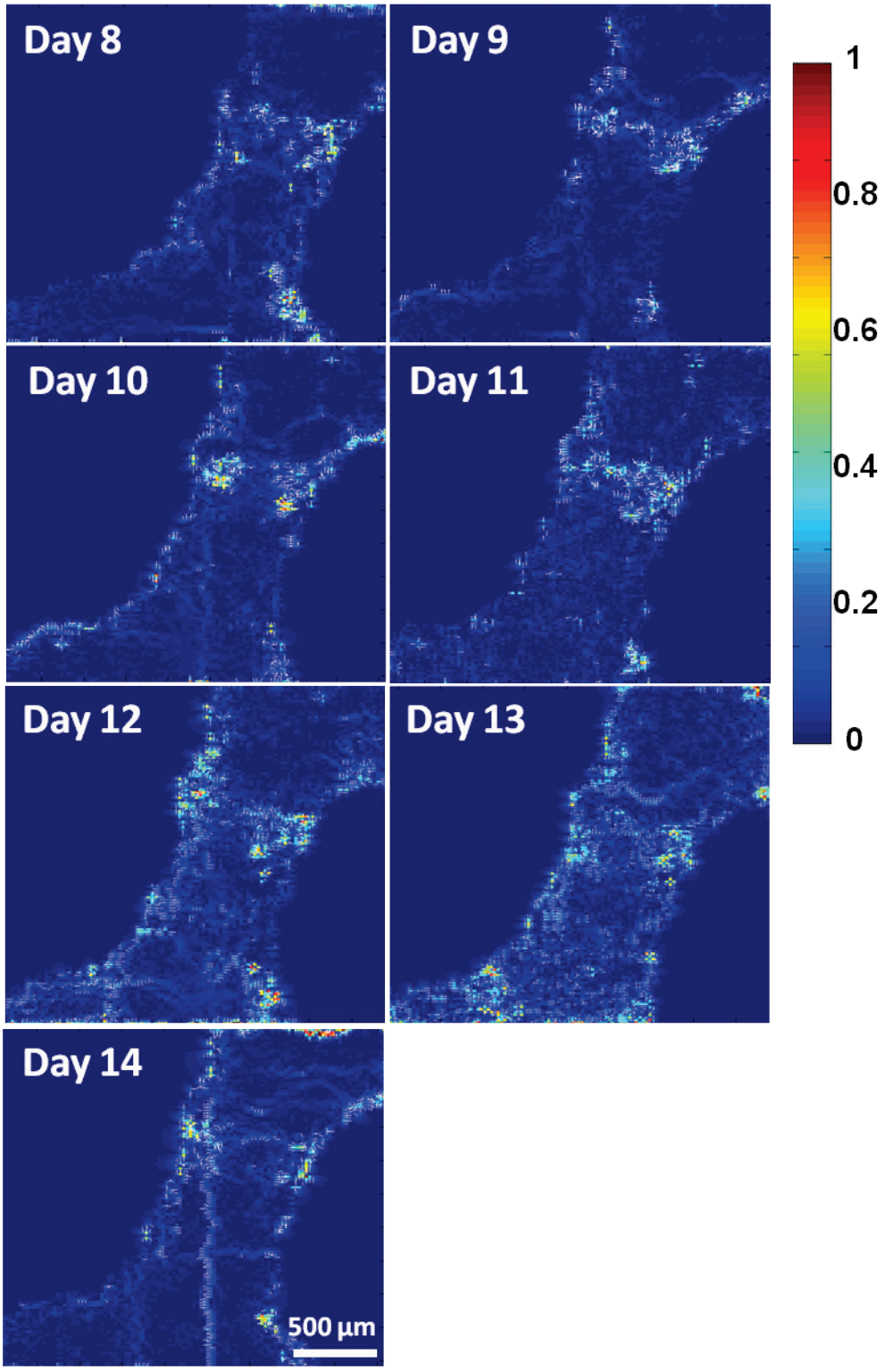

Figure 32: Regions of strain are heterogeneous across a beam.

Strain maps were generated across a 4096 px^2 region of the lattice. The magnitudes are shown in color and directions with white arrows. Regions with eventual capillary formation (see Figure 29) have a higher magnitude than regions that lack capillaries.

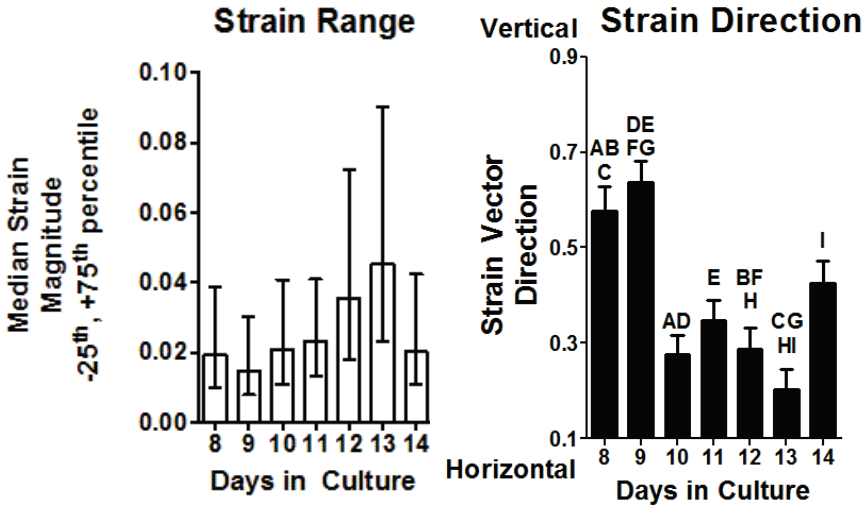

Figure 33: Strain vectors increased in magnitude and aligned over time.

The ranges of strain vector magnitudes increased over time, peaking at day 13. The angle of the strain vectors evolved over time to become more horizontal and parallel to the direction of capillary growth. Statistically significant pairs are denoted with matched letters.

Additionally, the strain vector's angles were mapped to the range of 0° to 90° before taking the tangent. Strain angles have no preferred orientation at day 7, but become more horizontal by day 13 (Figure 33).

$$direction = 1 - \tanh((\theta \bmod \pi - \pi/2)^2)$$

Confocal reflectance images of the collagen and PEG-collagen gels reveals the different microstructures of these materials. Collagen displays the expected fibrillar microstructure while PEG-collagen gels do not have such a microstructure at this length

scale (Figure 34A). The rheological properties of collagen display strain-dependant increases in the shear modulus consistent with strain-stiffening (hyperelastic) behavior while the PEG-collagen gel is constant (Figure 34B).

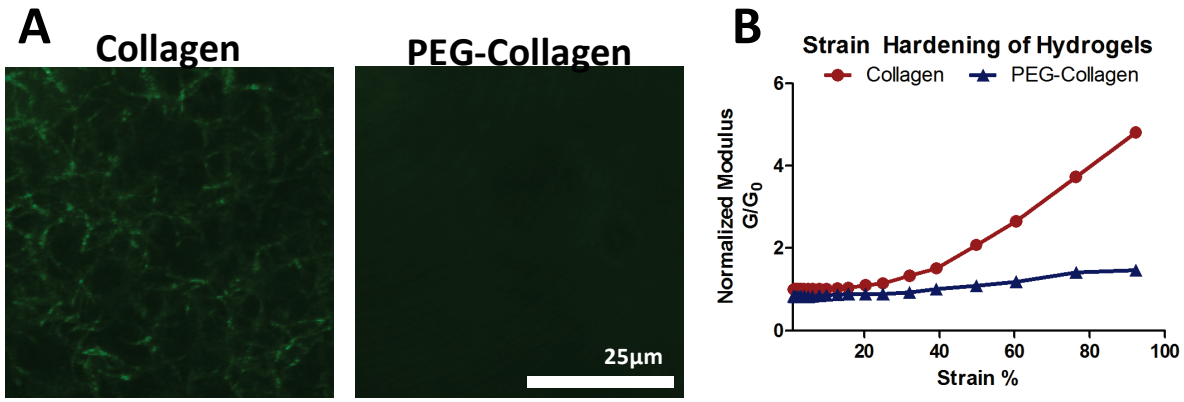

Figure 34: PEG-collagen hydrogels lack a fibriliar structure and posses linear mechanical properties.

Structural characterization of PEG-collagen was used to validate the mechanical model used to compute matrix strain fields. A) Confocal reflectance image s show the fibrillar structure of a collagen gel compared to the homogenous structure of a PEG-collagen gel at the same length scales. B) The shear modulus of collagen gels displays hyperelastic behavior while PEG-collagen is linearly elastic.

Further the phase angle of the collagen gels δ=8.0 is much greater than the phase angle of the PEG-collagen gel δ=1.9. This shows that the PEG-collagen displays more elastic behavior while the collagen is more visco-elastic. Thus, the PEG-collagen has a linear elastic behavior which fits within the assumptions of our mechanical model. This allows transformation of the strain fields into principal stresses (Figure 35).

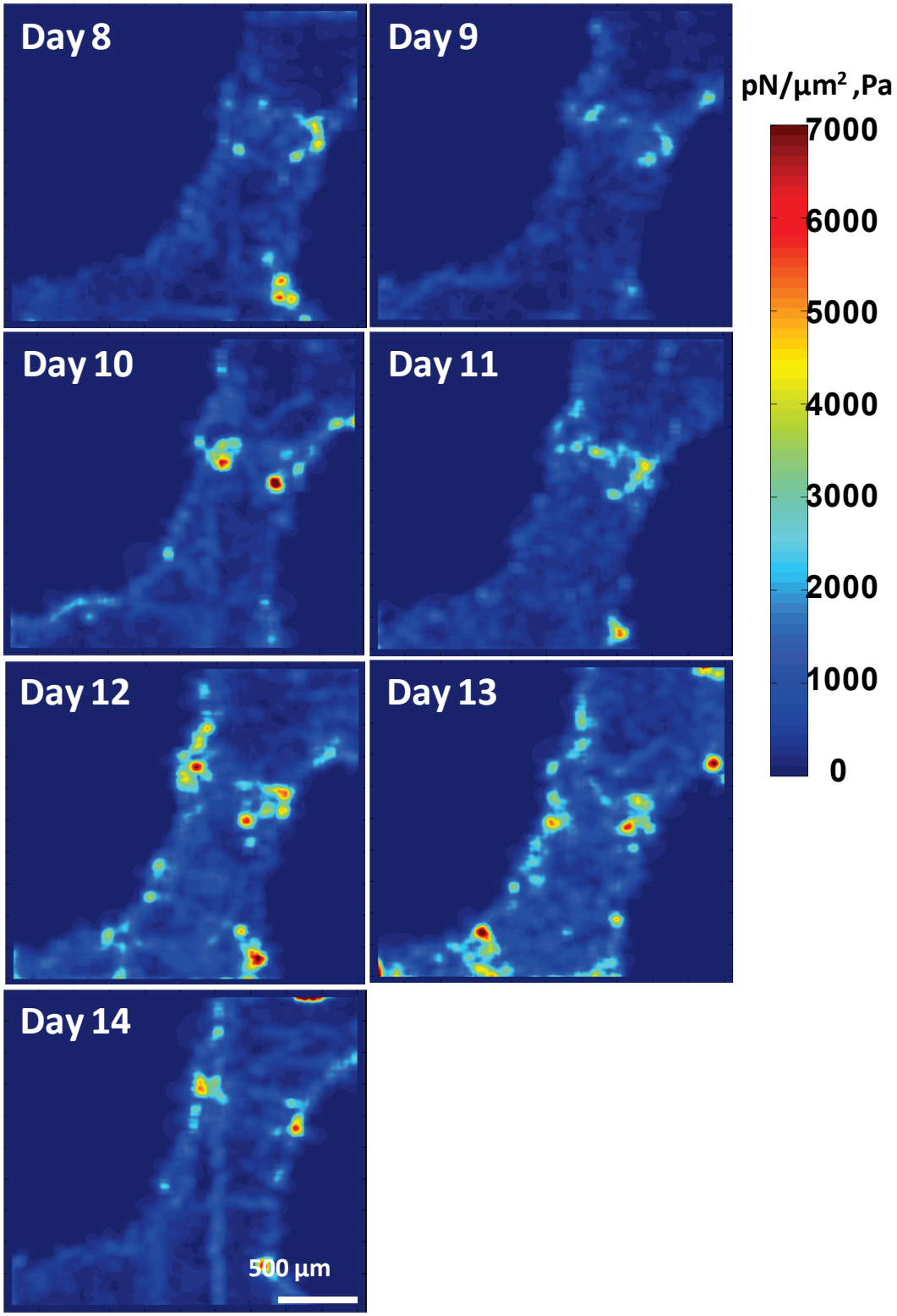

Figure 35: Regions of stress are heterogeneous across the beam.

Stress fields in lattices were localized with background strains across the lattice being small. The first principal stress is shown in color

The element stresses were found to follow similar distributions to the strains. This correspondence is due to the linear transformation provided by the elasticity matrix. Hence, the magnitudes were found to increase over time, peaking on day 13. Further, the distributions were log-normal with a large number of small stresses and a few pronounced stresses (Figure 36).

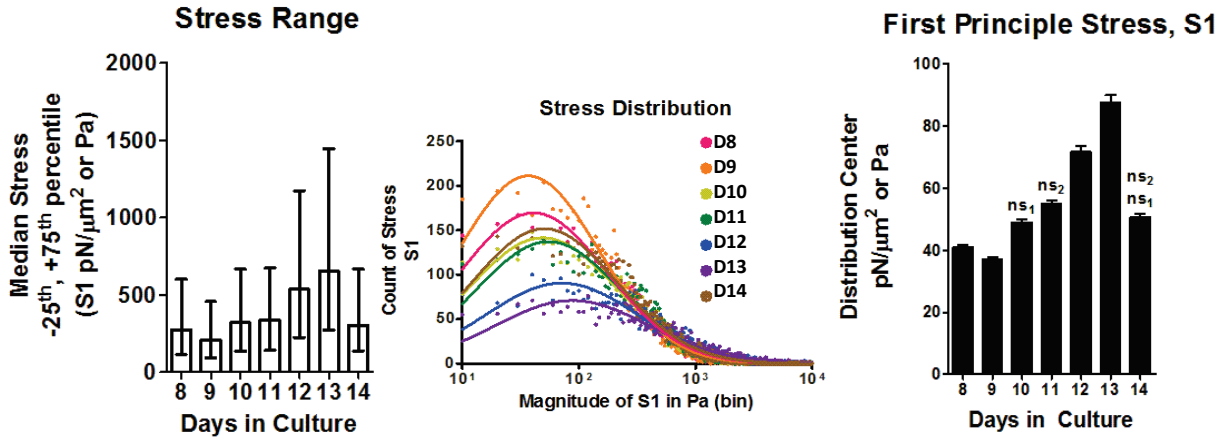

Figure 36: Stress distributions surrounding capillaries

The ranges of first principle stresses increased over time, peaking at day 13. The magnitudes of stresses followed a log-normal distribution with rare stress events being 10-fold higher than the distribution center. All comparisons between distribution centers were significant unless denoted otherwise (ns).

Overlaying these strains and stresses shows co-localization with regions of capillary formation (Figure 37). At a strain level of 9% we found that r=0.44 and at a stress level of 1,500 Pa r = 0.44. Performing a t-test against the null hypothesis (r=0) produces a p-value much less than 0.001. However, this is a result of the high degree-of-freedom of the test, or the assumption that each pixel is independent from neighbors in the same image. This may be true for the strain fields which are computed on a finite mesh, but not so for the fluorescent image which have high autocorrelations. So while the

correlation itself is good and the statistical test is strong, relying solely on the p-value alone would not be appropriate.

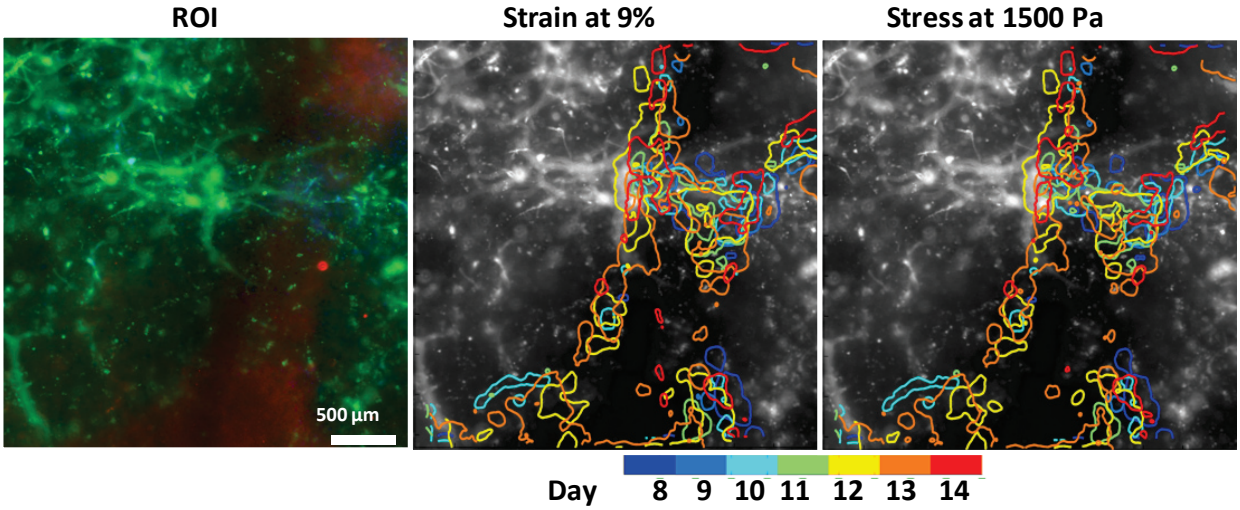

Figure 37: Stress fields localize to capillary sprouting

Overlays of the strain field at 9% and stress field at 1500 Pa (maximum, day 13, 75th percentile) with final stained images of endothelial cells (green, white). Image correlations were good at r=0.44 between the fields and the capillaries.

Discussion

It has been longstanding question as to how cells orient and undergo collective migration to form complex structures Prevailing hypothesis focus on the roles of growth factors in the extracellular environment. Others have suggested that mechanical tension in the extracellular matrix communicates information between cells. However, detection and quantification of these events has been elusive. In this work we presented a method to directly quantify the forces exerted by endothelial cells undergoing capillary morphogenesis.

Previous approached have been limited by the complex structural and mechanical properties of fibrin and collagen gels. Our approach utilizes an engineered biomaterial with well-behaved mechanical properties. Due to its homogenous, linear-elastic behavior transformation of displacements to strains is simple. Furthermore, by controlling the geometry of the system, we are able to compute stresses.

This approach spatially partitioned regions of capillary formation from regions of capillary migration. We were able to study angiogenesis without confounding effects of forces produced by stray EC, or disruptions by regions of digested matrix left behind after EC have migrated. Furthermore, this fabrication technique produced highly regular arrays in which to observe migration events. In these arrays, we found that increasing the seeding density of EC did not produce increased capillary invasion. It would be expected that cells would migrate away from high density regions, similar to what has been shown in spheroid models (28, 29). The increased EC concentration would

produce greater sources of growth factors to induce neighboring cells to migrate towards adjacent wells (30-32). However, at these densities, we observed an opposite trend, i.e. cells remained in the wells and organized into capillary beds without migration into the acellular lattice. We propose that this is due to the mechanical cues from cells within the wells exceeding the mechanical cues coming from adjacent wells.

We proceeded to control the separation between capillary beds and observed a detrimental effect on capillary migration with increased separation. It would be expected that capillary growth rate would be independent of the distance of acellular matrix ahead of it. Instead, we observed that the capillaries could 'sense' the lack of nearby cells. While growth factor gradients would be a plausible explanation, the geometric arrangement of this assays provides uniform distribution of stromal-derived factors orthogonal to the direction of capillary growth. Thus, the capillary growth would be in response to factors from EC in adjacent wells. Others have posed that the nonlinear mechanical properties and fibrous nature of some ECM may facilitate long-range force transmission (33, 34). As these are absent in our system, EC forces may be confounded or diminished as they cross large distances. Finally, this experimental system parallels the avascular gap present in scar tissue and may help to explain why large wounds fail to revascularize.

Increased matrix crosslinking had a detrimental effect on the invasion of capillaries. While a more-crosslinked matrix provides a greater resistance to deformation, previous studies of EC on 2D surfaces have indicated that increased stiffness would lead to increased force generation (35, 36). However, it seems that these effects cannot

overcome the increased proteolytic resistance of the matrix (12). Thus, even if the cells are communicating more efficiently, they cannot act on these signals.

The strain fields were observed to be highly heterogeneous, i.e., they followed a log-normal distribution which is expected for propagation through an elastic network. Notably, these distributions arise from multiplicative processes that are largely influenced by rare events and are highly sensitive to nearest-neighbor correlations (37). While this distribution of strains arises from simple physical relations, it is interesting to think of how it would influence the organization of tissues. Indeed, biological organization has been shown to follow the same distribution in feature sizes for biological structures and populations (38-41). Previous studies imposing external mechanical loading have utilized uniform strain fields to axially direct capillary growth (42, 43). Interestingly, the strains are distributed such that 'rare' events (75th quartile) ranges from 3% to 9% strain (Supplementary Table 1). These values match well with the external fields imposed in those experiments. Our observation of infrequent, localized strains suggest that these events could act as a beacon to direct capillary growth. We hypothesize that capillary path finding could be controlled more precisely by application of localized strain sources by microrheological techniques.

The focus of our work was determining how matrix stresses relate to cellular migration. By overlaying the strain fields on the final capillary network, we computed a good ($r = 0.42$) degree of spatial correlation with capillary network formation. This shows a coupling between the high strain fields and capillary pathfinding. While it does not demonstrate causality, it lends support for our hypothesis.

While we did not compute the cell traction forces, these could be determined from precise identification of the cell boundary and solving the force balance. Doing so would require higher resolution measurements and will be the focus of further work. As a result of the assumptions of the mechanical model, stresses were only determined in the plane of the image. If a capillary is out-of-plane and creating visible displacements, only the projected stress is known. A more thorough analysis would analyze the strain at multiple cross sections of the beam and compute the 3D deformation matrix. While this may more precisely reflect the magnitudes of the stresses, we do not expect the result to be qualitatively different.

The stress being a linear function of strain, preserved the log-normal distribution. Interestingly, our peak matrix stress magnitudes (7,000 pN/μm^2) somewhat exceed the peak values reported by others in single-cell measurements: 2,000 (44), 3,600 (35), 4,000 (45), 5,000 (46) pN/μm^2). We would attribute this to the additive effects of multiple cells exerting traction on the matrix. However, the values we measured for capillary morphogenesis are greater than those reported for mammary morphogenesis (150 pN/μm^2) (47). A factor contributing to this is that our study and the single-cell measurements were performed with linearly elastic materials. However, Gjorevski & Nelson utilized collagen matricies, but failed to account for the material properties in their transformation from displacments to stresses (47).

In summary, we are the first to quantify the stresses produced by cells during the formation of capillary anastomosis. This study not only shows that mechanical guidance cues are present in the formation of complex cellular structures, but that they

may be the predominate form of communication for path finding. Thus, we have precisely measure ad key factor in the formation, repair and remodeling of tissues. Knowledge of the mechanical microenvironment surrounding capillaries will enhance our understanding of this fundamental physiological process. This knowledge will help to guide the treatment of ischemic diseases with new therapies.

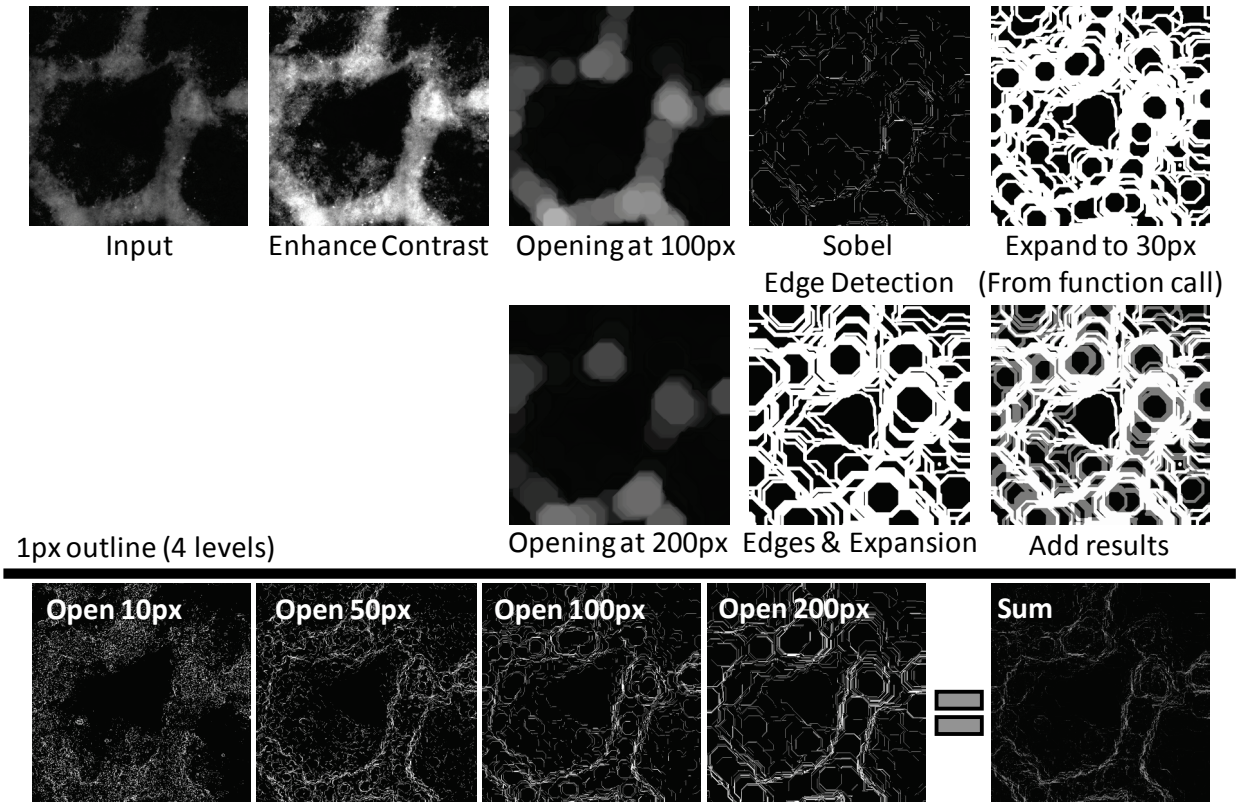

Figure 38: Supplementary figure: Edge detection algorithm

Edge detection was performed by multiple morphological opening, binary edge detection, and edge expansion steps. Grayscale images were contrast enhanced then opened with varying radii to highlight the lattice network. The radii were altered to provide various 'levels' or resolutions of the lattice structure. Next, the edges of these opened structures were detected suing the Sobel algorithm before expansion of the edge widths. The expansion produced correspondingly wider optima in the FFT domain and speeding the solutionconvergence. These images were overlaid to produce an image which was subsequently aligned.

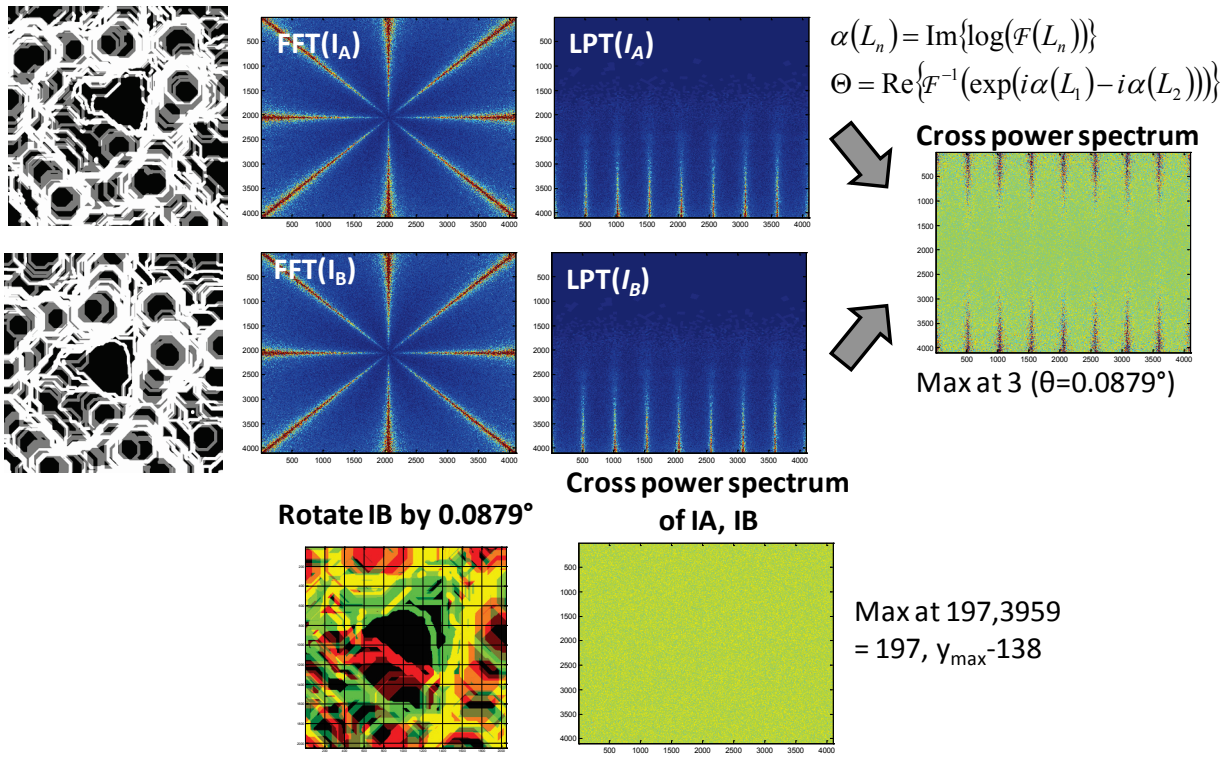

Figure 39: Supplementary figure: Fourier-Mellin Transform and Spectral Analysis Algorithm Overview

Fourier-Mellin transforms were computed with edge detected images to determine the image rotation angle. First, the fast Fourier transform (FFT) of the image is taken. Then the log-polar transform is used to 'unwrap' the spectral response. Finally, the cross power spectrum reveals the maxima corresponding to rotation angles. After reversing the rotation, images were cross-correlated to compute x,y shifts.

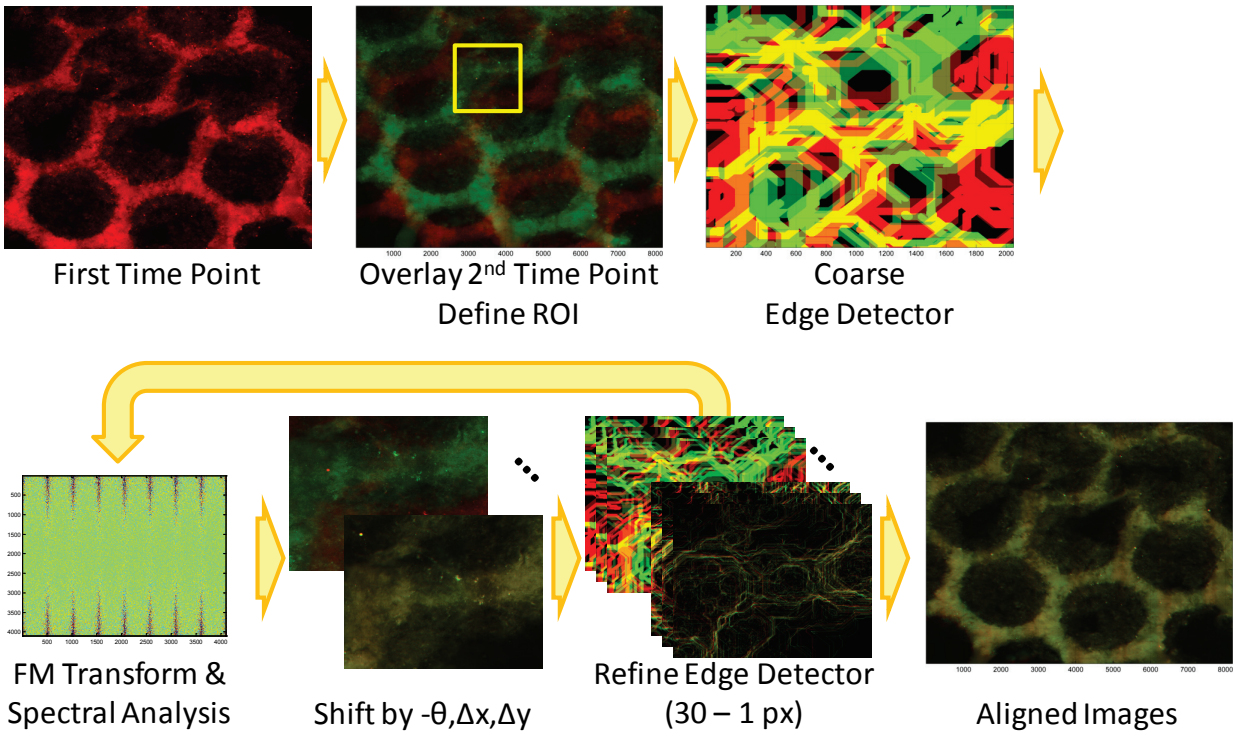

Figure 40: Supplementary figure: Overview of image registration process

Images from subsequent days were overlaid for manual shifting which expedited algorithm convergence. Fine image alignment was performed by first converting the images with edge detection (Figure 38) then passing the images to the FMT algorithm to compute shifts (Figure 39). This process was repeated with successively finer edge detections and ultimately with the 'raw' images. The aligned image pair was passed to PIVlab.

Strain Data - in beam							
Days in Culture	8	9	10	11	12	13	14
Total number of values	6372	6312	6290	6409	6580	6368	6786
Number of excluded values	1	0	0	0	3	2	3
Number of binned values	6371	6312	6290	6409	6577	6366	6783
Minimum	0.001006	0.001006	0.001023	0.001031	0.001044	0.00101	0.001035
25% Percentile	0.009732	0.00774	0.01076	0.013217	0.017901	0.022919	0.010741
Median	0.019136	0.014751	0.020656	0.023079	0.035441	0.045146	0.020085
75% Percentile	0.03856	0.03011	0.040681	0.040883	0.072199	0.09027	0.042235
Maximum	1.027	0.52517	0.97206	0.72655	1.3535	1.5968	1.6643
Best-fit values							
AMPLITUDE	219.2	279.7	199.9	183.6	121.1	92.3	221
CENTER	0.006451	0.005739	0.008241	0.0113	0.01249	0.01672	0.008271
WIDTH	1.039	0.96	0.9461	0.8421	1.016	0.991	0.9179
Std. Error							
AMPLITUDE	1.424	1.135	1.136	1.147	0.8098	0.7564	1.346
CENTER	6.9E-05	3.45E-05	6.82E-05	8.79E-05	0.000134	0.000212	7.04E-05
WIDTH	0.007412	0.00433	0.00601	0.005952	0.007523	0.009032	0.006271
Goodness of Fit							
Degrees of Freedom	497	497	497	497	497	497	497
R^2	0.9859	0.9945	0.9888	0.9861	0.9833	0.9734	0.9871
Absolute Sum of Squares	9518	4902	6930	8431	5807	6582	9410
Sy.x	4.376	3.141	3.734	4.119	3.418	3.639	4.351

Table 2: Strain data summary

Summary and log-normal fit statistics for the strain vectors.

Stress Data - in beam							
Days in Culture	8	9	10	11	12	13	14
Total number of values	6656	6585	6516	6677	6773	6511	6958
Number of excluded values	0	0	0	0	0	0	1
Number of binned values	6656	6585	6516	6677	6773	6511	6957
Minimum	0.036461	0.027217	0.0039	0.035533	0.027358	0.21377	0.06581
25% Percentile	113.537	91.3495	134.825	139.48	223.965	272.37	135.95
Median	272.94	206.19	320.205	336.16	535.55	653.81	302.565
75% Percentile	601.657	455.305	668.083	672.22	1173.2	1445.9	666.935
Maximum	21647	12466	23176	17424	28500	27092	33242
Best-fit values							
AMPLITUDE	169.5	211.2	141.5	137.2	90.63	71.03	151.8
CENTER	40.88	37.02	48.97	54.86	71.61	87.7	50.72
WIDTH	1.453	1.386	1.449	1.427	1.504	1.51	1.429
Std. Error							
AMPLITUDE	1.138	1.47	1.079	1.192	0.8792	0.6809	1.32
CENTER	0.7116	0.6349	0.9542	1.19	1.837	2.232	1.106
WIDTH	0.009869	0.01004	0.01108	0.01247	0.01428	0.01419	0.01253
Goodness of Fit							
Degrees of Freedom	997	997	997	997	997	997	997
R^2	0.9768	0.9744	0.9697	0.9602	0.9502	0.9496	0.9604
Absolute Sum of Squares	11156	16120	12033	16220	12103	8921	18400
Sy.x	3.345	4.021	3.474	4.033	3.484	2.991	4.296

Table 3: Stress data table

Summary and log-normal fit statistics for the stress vectors.

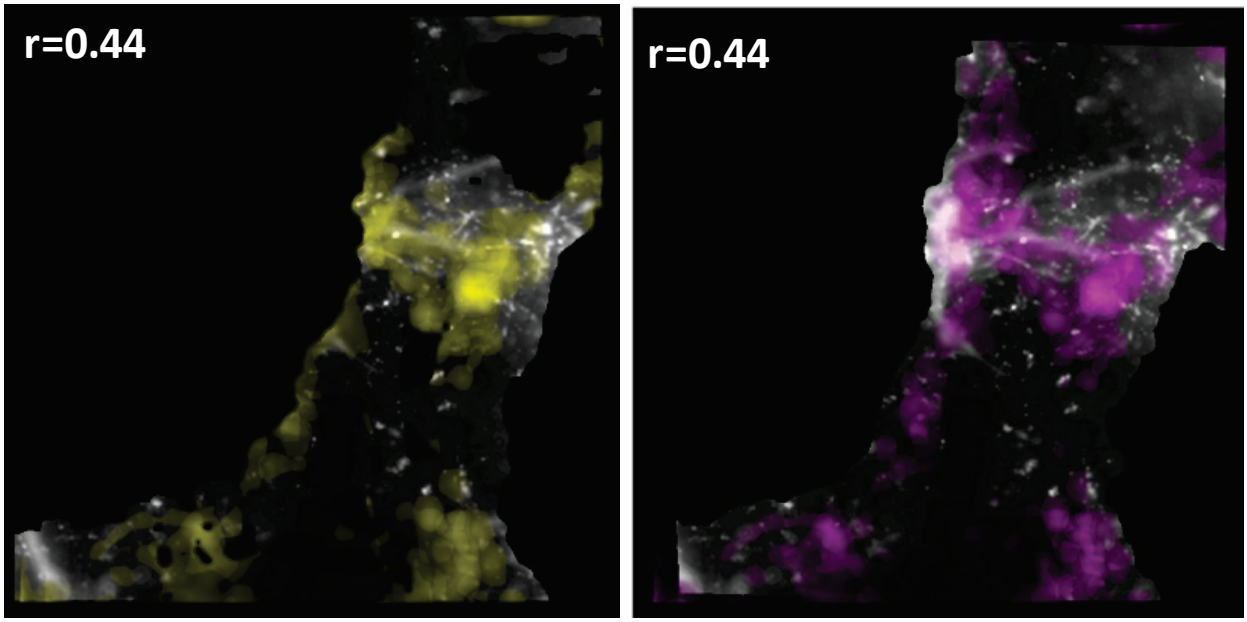

Figure 41: Supplementary figure: Image correlations with strain and stress fields.

The grayscale images of EC staining at day 14 were correlated to the measured strain and stress fields. The time-lapse fields were flattened by summation and normalized. Both images were re-sampled to 4096x4096 and cropped to only include pixels where both images had values greater than zero. The resulting strain (yellow, left) and stress (magenta, right) images are shown above. Linear correlation was performed to yield correlation coefficients of 0.44 for both stress and strain.

References

1. Carmeliet P, Jain RK. Molecular mechanisms and clinical applications of angiogenesis. Nature. 2011;473(7347):298-307.

2. Folkman J. Angiogenesis: an organizing principle for drug discovery? Nat Rev Drug Discov. 2007;6(4):273-86.

3. Yancopoulos GD, Davis S, Gale NW, Rudge JS, Wiegand SJ, Holash J. Vascular-specific growth factors and blood vessel formation. Nature. 2000;407(6801):242-8.

4. Ferrara N, Hillan KJ, Gerber H-P, Novotny W. Discovery and development of bevacizumab, an anti-VEGF antibody for treating cancer. Nat Rev Drug Discov. 2004;3(5):391-400.

5. Hahn C, Schwartz MA. Mechanotransduction in vascular physiology and atherogenesis. Nat Rev Mol Cell Biol. 2009;10(1):53-62.

6. Chien S. Mechanotransduction and endothelial cell homeostasis: the wisdom of the cell2007 2007-03-01 00:00:00. H1209-H24 p.

7. Kilarski WW. A New Mechanism of Blood Vessel Growth - Hope for New Treatment Strategies. Discovery Medicine [Internet]. 2009. Available from:

http://www.discoverymedicine.com/Witold-W-Kilarski/2009/09/14/a-new-mechanism-of-blood-vessel-growth-hope-for-new-treatment-strategies/.

8. Clark ER. Studies on the growth of blood-vessels in the tail of the frog larva — by observation and experiment on the living animal. Am J Anat. 1918;23(1):37-88.

9. Korff T, Augustin HG. Tensional forces in fibrillar extracellular matrices control directional capillary sprouting. Journal of Cell Science. 1999;112(19):3249-58.

10. Kilarski WW, Samolov B, Petersson L, Kvanta A, Gerwins P. Biomechanical regulation of blood vessel growth during tissue vascularization. Nat Med. 2009;15(6):657-64. doi: http://www.nature.com/nm/journal/v15/n6/suppinfo/nm.1985_S1.html.

11. Qi W, Anindita B, Jessamine PW, Arjun Y, Paul AJ. Local and global deformations in a strain-stiffening fibrin gel. New Journal of Physics. 2007;9(11):428.

12. Singh RK, Seliktar D, Putnam AJ. Capillary morphogenesis in PEG-collagen hydrogels. Biomaterials. 2013;34(37):9331-40. Epub 2013/09/12. doi: 10.1016/j.biomaterials.2013.08.016. PubMed PMID: 24021759; PubMed Central PMCID: PMC3790856.

13. Vigen M, Ceccarelli J, Putnam AJ. Protease-sensitive PEG hydrogels regulate vascularization in vitro and in vivo. Macromolecular bioscience. 2014;14(10):1368-79.

Epub 2014/06/20. doi: 10.1002/mabi.201400161. PubMed PMID: 24943402; PubMed Central PMCID: PMC4198447.

14. Chen Y-C, Lin R-Z, Qi H, Yang Y, Bae H, Melero-Martin JM, et al. Functional Human Vascular Network Generated in Photocrosslinkable Gelatin Methacrylate Hydrogels. Advanced Functional Materials. 2012;22(10):2027-39. doi: 10.1002/adfm.201101662.

15. Sokic S, Papavasiliou G. Controlled proteolytic cleavage site presentation in biomimetic PEGDA hydrogels enhances neovascularization in vitro. Tissue engineering Part A. 2012;18(23-24):2477-86. Epub 2012/06/26. doi: 10.1089/ten.TEA.2012.0173. PubMed PMID: 22725267; PubMed Central PMCID: PMC3501121.

16. Moon JJ, Saik JE, Poche RA, Leslie-Barbick JE, Lee S-H, Smith AA, et al. Biomimetic hydrogels with pro-angiogenic properties. Biomaterials. 2010;31(14):3840-7. doi: 10.1016/j.biomaterials.2010.01.104. PubMed PMID: PMC2839536.

17. Miller JS, Shen CJ, Legant WR, Baranski JD, Blakely BL, Chen CS. Bioactive hydrogels made from step-growth derived PEG-peptide macromers. Biomaterials. 2010;31(13):3736-43. Epub 2010/02/09. doi: 10.1016/j.biomaterials.2010.01.058. PubMed PMID: 20138664; PubMed Central PMCID: PMC2837100.

18. Ghajar CM, Chen X, Harris JW, Suresh V, Hughes CC, Jeon NL, et al. The effect of matrix density on the regulation of 3-D capillary morphogenesis. Biophysical journal.

2008;94(5):1930-41. Epub 2007/11/13. doi: 10.1529/biophysj.107.120774. PubMed PMID: 17993494; PubMed Central PMCID: PMC2242748.

19. Laundon R. Fourier Mellin Image Registration. Matlab Central; 2008. p. An implementation of Fourier Mellin Phase Correlation for Image Registration.

20. Szeliski R. Image alignment and stitching: a tutorial. Found Trends Comput Graph Vis. 2006;2(1):1-104. doi: 10.1561/0600000009.

21. Thielicke W, Stamhuis EJ. PIVlab - Towards User-friendly, Affordable and Accurate Digital Particle Image Velocimetry in MATLAB. Journal of Open Research Software. 2014;2(1). doi: http://dx.doi.org/10.5334/jors.bl.

22. Thielicke W, Stamhuis EJ. PIVlab - Time-Resolved Digital Particle Image Velocimetry Tool for MATLAB. 1.32 ed2014.

23. Bryant SJ, Anseth KS. Photopolymerization of Hydrogel Scaffolds. In: Ma PX, Elisseeff J, editors. Scaffolding in Tissue Engineering: CRC Press; 2005. p. 82.

24. Ragab A-RA, Bayoumi SEA. Solution of the Elastic Problem. Engineering Solid Mechanics: Fundamentals and Applications: CRC Press; 1998. p. 167-9.

25. Pozrikidis C. Plane Stress-Strain Analysis. Introduction to Finite and Spectral Element Methods Using MATLAB. Boca Ratton: Taylor & Francis; 2005.

26. Dunn KW, Kamocka MM, McDonald JH. A practical guide to evaluating colocalization in biological microscopy. American Journal of Physiology - Cell Physiology. 2011;300(4):C723-C42. doi: 10.1152/ajpcell.00462.2010. PubMed PMID: PMC3074624.

27. Adler J, Parmryd I. Quantifying colocalization by correlation: the Pearson correlation coefficient is superior to the Mander's overlap coefficient. Cytometry Part A : the journal of the International Society for Analytical Cytology. 2010;77(8):733-42. Epub 2010/07/24. doi: 10.1002/cyto.a.20896. PubMed PMID: 20653013.

28. Nehls V, Drenckhahn D. A novel, microcarrier-based in vitro assay for rapid and reliable quantification of three-dimensional cell migration and angiogenesis. Microvascular research. 1995;50(3):311-22. Epub 1995/11/01. doi: 10.1006/mvre.1995.1061. PubMed PMID: 8583947.

29. Friedl P, Gilmour D. Collective cell migration in morphogenesis, regeneration and cancer. Nat Rev Mol Cell Biol. 2009;10(7):445-57.

30. Verbridge SS, Chakrabarti A, Del Nero P, Kwee B, Varner JD, Stroock AD, et al. Physicochemical regulation of endothelial sproutingin a 3-D microfluidic angiogenesis model. Journal of biomedical materials research Part A. 2013;101(10):2948-56. doi: 10.1002/jbm.a.34587. PubMed PMID: PMC3776016.

31. Yeon JH, Ryu HR, Chung M, Hu QP, Jeon NL. In vitro formation and characterization of a perfusable three-dimensional tubular capillary network in microfluidic devices. Lab on a Chip. 2012;12(16):2815-22. doi: 10.1039/c2lc40131b.

32. Guo X, Elliott CG, Li Z, Xu Y, Hamilton DW, Guan J. Creating 3D Angiogenic Growth Factor Gradients in Fibrous Constructs to Guide Fast Angiogenesis. Biomacromolecules. 2012;13(10):3262-71. doi: 10.1021/bm301029a.

33. Wang H, Abhilash AS, Chen Christopher S, Wells Rebecca G, Shenoy Vivek B. Long-Range Force Transmission in Fibrous Matrices Enabled by Tension-Driven Alignment of Fibers. Biophysical journal. 2014;107(11):2592-603. doi: http://dx.doi.org/10.1016/j.bpj.2014.09.044.

34. Ma X, Schickel ME, Stevenson Mark D, Sarang-Sieminski Alisha L, Gooch Keith J, Ghadiali Samir N, et al. Fibers in the Extracellular Matrix Enable Long-Range Stress Transmission between Cells. Biophysical journal. 2013;104(7):1410-8. doi: 10.1016/j.bpj.2013.02.017. PubMed PMID: PMC3617419.

35. Califano JP, Reinhart-King CA. Substrate Stiffness and Cell Area Predict Cellular Traction Stresses in Single Cells and Cells in Contact. Cel Mol Bioeng. 2010;3(1):68-75. doi: 10.1007/s12195-010-0102-6.

36. Han Sangyoon J, Bielawski Kevin S, Ting Lucas H, Rodriguez Marita L, Sniadecki Nathan J. Decoupling Substrate Stiffness, Spread Area, and Micropost

Density: A Close Spatial Relationship between Traction Forces and Focal Adhesions. Biophysical journal. 2012;103(4):640-8. doi: 10.1016/j.bpj.2012.07.023. PubMed PMID: PMC3443781.

37. Redner S. Random Multiplicative Processes and Multifractals. In: Julien R, Peliti L, Rammal R, Boccara N, editors. Universalities in Condensed Matter. Heidelberg: Springer-Verlag; 1988. p. 170-5.

38. Gayon J. History of the Concept of Allometry. American Zoologist. 2000;40(5):748-58. doi: 10.1093/icb/40.5.748.

39. Huxley JS. Problems of Relative Growth. London1932.

40. Buzsaki G, Mizuseki K. The log-dynamic brain: how skewed distributions affect network operations. Nat Rev Neurosci. 2014;15(4):264-78. doi: 10.1038/nrn3687.

41. Husainy AN, Morrow AA, Perkins TJ, Lee JM. Robust patterns in the stochastic organization of filopodia. BMC cell biology. 2010;11:86. Epub 2010/11/19. doi: 10.1186/1471-2121-11-86. PubMed PMID: 21083909; PubMed Central PMCID: PMC2992051.

42. Matsumoto T, Yung YC, Fischbach C, Kong HJ, Nakaoka R, Mooney DJ. Mechanical strain regulates endothelial cell patterning in vitro. Tissue engineering.

2007;13(1):207-17. Epub 2007/05/24. doi: 10.1089/ten.2006.0058. PubMed PMID: 17518594.

43. Ceccarelli J, Cheng A, Putnam AJ. Mechanical strain controls endothelial patterning during angiogenic sprouting. Cel Mol Bioeng. 2012;5(4):463-73. doi: 10.1007/s12195-012-0242-y. PubMed PMID: PMC3760594.

44. Legant WR, Miller JS, Blakely BL, Cohen DM, Genin GM, Chen CS. Measurement of mechanical tractions exerted by cells in three-dimensional matrices. Nat Meth. 2010;7(12):969-71. doi: http://www.nature.com/nmeth/journal/v7/n12/abs/nmeth.1531.html#supplementary-information.

45. Fu J, Wang Y-K, Yang MT, Desai RA, Yu X, Liu Z, et al. Mechanical regulation of cell function with geometrically modulated elastomeric substrates. Nat Meth. 2010;7(9):733-6. doi: http://www.nature.com/nmeth/journal/v7/n9/abs/nmeth.1487.html#supplementary-information.

46. Franck C, Maskarinec SA, Tirrell DA, Ravichandran G. Three-Dimensional Traction Force Microscopy: A New Tool for Quantifying Cell-Matrix Interactions. PLoS ONE. 2011;6(3):e17833. doi: 10.1371/journal.pone.0017833.

47. Gjorevski N, Nelson CM. Mapping of mechanical strains and stresses around quiescent engineered three-dimensional epithelial tissues. Biophysical journal. 2012;103(1):152-62. Epub 2012/07/26. doi: 10.1016/j.bpj.2012.05.048. PubMed PMID: 22828342; PubMed Central PMCID: PMC3388222.

Chapter 5:

Concluding Remarks

Conclusions

In this thesis, I used a 3D co-culture model of stromal cells and EC to address the hypothesis that EC utilize the propagation of cell-generated displacements through the ECM to guide the organization of capillary structures.

The goal of Aim 1 was to develop a biosynthetic material platform for EC culture with tunable features suitable for addressing the aforementioned hypothesis. This goal was achieved by conjugating 20kDa PEGdiacrylamide to macromolecular type I collagen and photopolymerizing it into a hydrogel material. The ability to further modulate the physical properties of this material through the addition of PEG crosslinks was demonstrated. Finally, this material was shown to be a suitable substrate for EC culture in 2D and 3D.

The goal of Aim 2 was to determine the influence of matrix crosslinking on EC migration and organization into capillaries in vitro. The data generated in the context of this aim demonstrated the ability of EC to form capillaries was found to depend on the

crosslinking of the matrix. Further, the organization of EC was shown to be dependent on MMPs, which is consistent with the mechanism within a native collagenous matrix.

Finally, the goal of aim 3 was to investigate the influence of local displacement fields on capillary organization in vitro. An innovative microfabricated culture system produced in this aim enabled capillary pathfinding to be quantified in a setting separate from capillary formation or stromal cell migration. The displacement fields around capillary tips were quantified to a 50 μm resolution. Owing to the mechanical properties of the PEG-collagen material platform, strain and stress fields were computed from the displacements. Finally, these fields showed good spatial correlation with capillary formation.

Successful completion of these three aims produced substantial correlative data to support the hypothesis. While displacements were observed and the cell-generated stresses were quantified, it could not be determined if the stresses were guiding the cells. To complete the approach, a causal relation would need to be demonstrated between stress fields and capillary pathfinding. Further studies sought to modulate stress propagation through alteration of the geometry and stiffness of the matrix, and saw corresponding evidence of altered capillary invasion. Further experiments would be needed in order to demonstrate the guidance of capillaries.

Current Limitations and Future Experiments to Address the Hypothesis

In this thesis a scenario was examined wherein two capillaries migrated towards each other. A natural extension of this case would be to analyze situations when a capillary migrates towards a well containing endothelial cells or even an empty well. In these cases, it would be interesting to note the directionality of the stress fields and if the cells are using a random-walk model to 'search' for a mechanical guidance cue.

Experiments could be conducted to look into the role of mechanotransduction pathways in modulation of the stress fields. Mechanotransduction pathways could be disrupted using small molecule inhibitors and their influences on capillary organization and stability could be assessed. Of particular interest is the Rho A pathway which controls cellular migration, proliferation, and cytoskeletal organization (1). However it is highly likely that a small molecule inhibitor approach will prevent capillary formation and thus prevent migration into the lattice. More specific targeting of EC populations of could be achieved through genetic manipulation. An inducible dominant-negative (T19N) Rho-A construct could be used to disrupt Rho signaling in EC after capillaries have formed but before significant invasion has occurred into the lattice. Further, adjacent wells could be filled with separate populations of wild-type and modified ECs. This experiment could provide more concrete evidence as to whether the ECs are responding to the stresses or by factors released by adjacent ECs.

Additional experiments with wild-type ECs could use small-molecules to relax the ECs at various time points and determine the nature of the ECM stresses. Of particular interest is whether the stresses are held in the cytoskeleton, or in the ECM by means of deposited crosslinking proteins in the basement membrane. In other words, are the

cells pulling the matrix and holding it in place, or are they pulling on the matrix and tying it in place? The latter case would provide new targets for angiogenesis inhibitors as an alternative to cytoskeletal inhibitors which have numerous off-target effects.

Improvement of the resolution of the particle tracking analysis would be a promising avenue of research. In this analysis, we collected time lapse data at a resolution of one day. This uncovered interesting trends wherein stress increased during capillary migration and then dropped off. Further investigation may yield better insight as to how these stress events relate to EC organization. Increasing the time resolution to 6 or even 3 hours could be accomplished readily, but shortening intervals to 1 hour would require live-cell imaging approaches. Approaches towards EC labeling should be optimized as well. In this thesis, we utilized fluorescent proteins and probes. In chapter 3, networks lengths were quantified with both RFP (Figure 19B) and immunofluorescent staining (Figure 21A). The RFP proteins were bright, but the total network lengths were reduced by a factor of one-third. The lipophilic dye was not suitably bright to image through a thick construct. Better dye selection may provide a means to observe EC locations with finer detail. The spatial resolution of the system could be improved to provide better localization of forces. The current approach is limited to 50 μm owing to severe optical scattering. Increasing the resolution to even 10 μm would allow determination of single-cell forces within a capillary and would greatly ease the computation of cellular tractions. This could be accomplished by using a non-adhesive glass dish instead of an agarose-coated plastic dish. Further reductions in scattering would come from reducing the bead density and using more precise microscopy, such as a laser-scanning confocal.

The current approach suffers from being observational in nature. While we can measure localized stress fields, we cannot create them. Creation of localized strain fields would be applied through external mechanical loading on regions of ECM. This has been accomplished using micro-rheological approaches. The materials utilized are too stiff for passive (thermal) approaches to be useful (2), but active techniques utilizing microbeads would be appropriate. These can be embedded in the lattice and driven individually by optical tweezers or collectively by magnetic beads. Optical tweezers would be difficult to implement owing to the poor optics of the system. Furthermore, optical tweezers produce uniform strains and would have difficulty actuating stiff lattice elements (3, 4). Additionally, the optics may interact with embedded fluorescent microbeads for stress mapping. A better approach would be to embed magnetic particles (ferrous, non-charged) which would be actuated through an external magnetic field. This approach would apply a constant force to the bead and the resulting matrix stress could be determined in real time with the approaches outlined in this thesis. The forces could be controlled with distance and/or strength of the magnetic field. Further, this could be done in parallel across the entire array (with variable, but known stresses) to greatly increase throughout (5). Finally, this would be inexpensive and simple to implement as it requires only beads and a suitably large magnet placed orthogonal to the image plane.

Applications of the Approach to Other Fields of Research

Over the course of this thesis, a material platform and manufacturing process were developed. The specific application developed was in addressing the hypothesis. However, it is easy to envision other uses of the system.

One application is the influence of cellular niche on angiogenesis. A preliminary experiment was conducted to demonstrate the feasibility of the micropatterning platform. In this experiment, mesenchymal stem cells (MSC) were encapsulated in patterned PEG-collagen matrices while MSC with EC were cultured around these islands in a collagen matrix. It was hypothesized that the encapsulated EC would respond to the stiffer matrix and modulate network formation. While a modest decrease in vascular network formation with MSCs was observed, it was not found to be statistically significant (E. Chen, *unpublished work* Figure 42A). Further work could investigate an all PEG-collagen system and increasing the MSC seeding density. Similar experiments could be devised wherein the stromal cell identity is modulated to be cancer cells and their ability to recruit vasculature *in vitro* could be assessed.

Investigations were conducted into the ability of PEG-collagen lattices to support osteogenesis. In these experiments, MSCs were seeded into both phases of the assay and cultured for 21 days in osteogenic medium before staining with Von Kossa's Stain. The MSC produced robust mineralization when compared to an acellular control (S. Paris *unpublished work* Figure 42B). Thus, the system holds promise as a platform for studying various aspects of mineralization and bone formation.

Additional experiments sought to establish the parameter space for PEG-collagen photolithography. In these, it was found that increased exposure time or intensity was detrimental to small features. Conversely decreased exposure time and increased intensity allowed fabrication of smaller features. Modification of the PEG-collagen polymer solution by extraction into 0.01N acetic acid further allowed reduction of feature sizes to 125 μm. However, these lattices were unstable and dissolved after a day of culture (M. Tam, *unpublished work* Figure 42C). Further studies will be needed in order to develop PEG-collagen formulations which support reduced feature sizes. The photolithographic approach allows fabrication of any planar shape. From a design perspective it is important to know beforehand what the sizes of the smallest shapes which can be faithfully be transferred. More complex arrays could be fabricated that pose mazes or patterns for EC to follow while creating vasculature.

Further applications of the PEG-collagen photolithography system would could be in the fabrication of engineered tissues. This system allows for the construction of 3D tissues with pre-defined domains which can readily form vasculature. It is not difficult to imagine how this approach could be used to build complex vascularized tissues ex vivo for rapid implantation and perfusion. Furthermore, large sections of tissue could be laid out and rapidly fabricated using photolithography. These sections could be individually cultured and re-assembled before implantation to make thick 3D tissues. Further investigation of photolithographic tissue printing could pose a viable alternative to current cell-printing approaches.

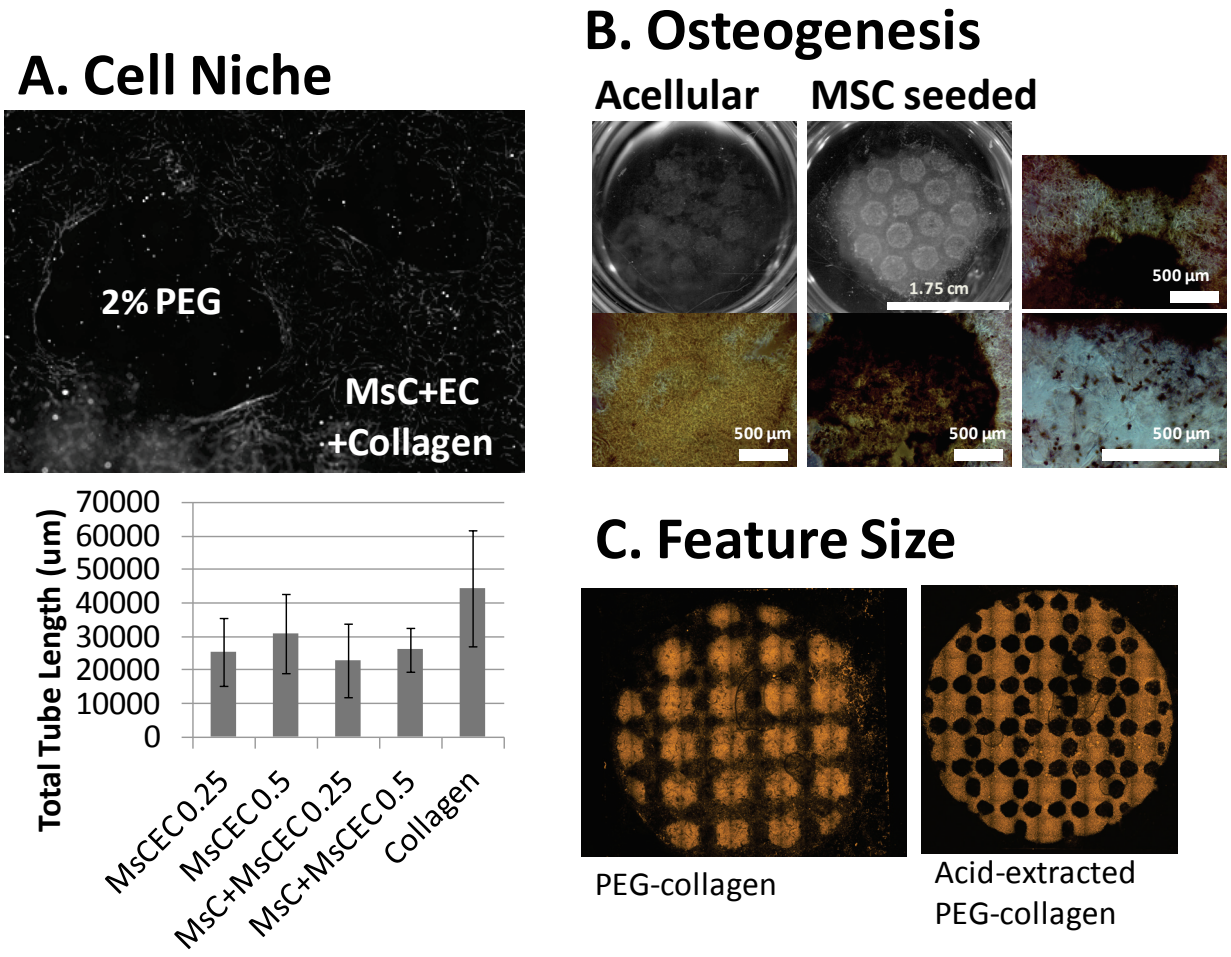

Figure 42: Future applications of PEG-collagen photolithography.

A) Vascular formation in patterned hydrogels containing MSCs in a separate phase. B) Osteogenesis of PEG-collagen lattices showed mineral deposition in the 1% phase but not in the 2% phase. C) Photolithography of PEG-collagen constructs allowed fabrication of smaller features after acid extraction of the polymer.

References

1. Bryan BA, D'Amore PA. What tangled webs they weave: Rho-GTPase control of angiogenesis. Cell Mol Life Sci. 2007;64(16):2053-65. doi: 10.1007/s00018-007-7008-z.

2. Cicuta P, Donald AM. Microrheology: a review of the method and applications. Soft Matter. 2007;3(12):1449-55. doi: 10.1039/b706004c.

3. Wilson LG, Poon WCK. Small-world rheology: an introduction to probe-based active microrheology. Physical Chemistry Chemical Physics. 2011;13(22):10617-30. doi: 10.1039/c0cp01564d.

4. Neuman KC, Nagy A. Single-molecule force spectroscopy: optical tweezers, magnetic tweezers and atomic force microscopy. Nat Meth. 2008;5(6):491-505.

5. Sniadecki NJ, Anguelouch A, Yang MT, Lamb CM, Liu Z, Kirschner SB, et al. Magnetic microposts as an approach to apply forces to living cells. Proceedings of the National Academy of Sciences. 2007;104(37):14553-8. doi: 10.1073/pnas.0611613104.

Appendicies

Appendix A Synthesis of 20kDa PEGdiacrylamide

from RS, NB 008 p6, p8 &p19 (Transcribed 1/20/15 by Rahul Singh)

Reagents:

Acetone (for washing)
20kDa polyethylene glycol
Benzene (dry) (4L)
Anhydrous dichloromethane (dry) aka DCM
Triethylamine
Diethyl ether (12L)
Whatman 113 filter paper
Ammonium Hydroxide (Saturated solution, 30%)
Acryloyl Chloride

Cleaning glassware:

All glassware should be cleaned with soap and water, then thoroughly rinsed with distilled water, Millipore water and acetone. Glassware should be dried under nitrogen to displace water. After use, glassware can be cleaned with a concentrated base solution or prolonged soaking in detergents.

Protecting PEG (Day 1)

1. Assemble distillation setup- as shown

[insert picture]

2. Weigh 50.00 g 20k polyethylene glycol (commercial source 99+% purity) aka PEGdiol
3. Add powder to 1000L round bottom flask using a plastic funnel, careful not to get any on the fritting
4. Add 500 mL benzene through the funnel and place flask in oil bath (pre-heated) at 110°C
5. Purge the trap / column with Nitrogen at 10 Pa for 1 minute
    a. Seal with clamps and distill, stir at 400 rpm
    b. After 30 minutes, increase temperature to 130°C
    c. After 45 minutes, volume should be halved (~200 mL)
6. Remove the flask from oil and detach from distillation column. Plug with septum and put under nitrogen with a bubbler.
7. Place the flask in an ice bath. place stirrer under ice bath and stir until cool (15-30 minutes)
8. While stirring, slowly add 100 mL DCM through the septum. Stir 15 minutes until mixed.
9. **Slowly** add 4.2 mL Triethylamine and stir for 30 minutes at RT (watch for phase separation)

USE AIR-FREE TECHNIQUE with Methylsulfonyl Chloride

10. **Slowly** add 2.4 mL Methylsulfonyl Chloride - pot will turn yellow cover with foil and stir slowly overnight
11. Place 4L of diethyl ether to cool at -20°C overnight

Collect PEG-MS (Day 2)

1. Set up a Buchner funnel with filter paper and a vacuum pump.
2. Filter contents of the flask to remove triethylamine salts - solution may still be yellow depending on stirrer speed
3. Add the solution to 1.2 L of ***stirred*** cold diethyl ether and shake for 1 minute
4. Dump the slurry onto a filter paper and dry with vacuum for ~5 minutes

5. Transfer the collected paste to a 1 L beaker and heat 80°C - 120°C add 50 mL benzene and stir constantly until a homogenous solution or suspension

CAUTION: Ether vapors can self-ignite and benzene can boil over if left unattended

6. Once dissolved, repeat steps 1 to 5
7. Repeat steps 1 to 4
8. Transfer the slurry (should be very dry and white) to a clean 1L beaker
9. Dry under vacuum (with a solvent trap) overnight - trap will need emptying after 30 minutes

React with Ammonia (Days 3-10)

1. Add 400 mL of ammonia water (ammonium hydroxide) and transfer to a clean 1L flask
2. Seal with kimwipes & foil and put on shaker at 300 rpm, RT with ventilation
3. React for 4 days
4. Remove foil and uncover, shake with ventilation for another 3 days
5. Transfer to a 2L beaker and dry at 40°C with gentile nitrogen flow for 6 hours
6. Adjust pH to 13.0 (from 8.5) with sodium hydroxide solution
7. Dry overnight at RT without nitrogen. **Cool 2L of ether to -20°C**

Collect PEG-diamine (Days 11-15)

1. Extract PEG into DCM
    a. Add 200 mL DCM to form an emulsion, stir 5 minutes
    b. Transfer to 50 mL centrifuge tubes and spin at 2,000 g for 10 minutes to separate
    c. Keep DCM phase in a 1L beaker
    d. Wash the remaining emulsion with 200 mL more DCM, stir 5 minutes
    e. repeat steps b & c
    f. optional: clarify DCM by further centrifugation
2. Dry the stirred DCM solution at 40°C under nitrogen to a 100 mL slurry
3. Add 200 mL benzene and precipitate with 1.2 L cold ether
4. Collect precipitate and dry on filter 5 minutes
5. Transfer to vacuum oven and dry at 40°C overnight

6. Collect product and dissolve in 150 mL distilled water
7. Transfer to a 12kDa dialysis bag (only fill 50%) against 5L distilled water - CLAMP WELL
8. Change water once and dialyze overnight

9. Carefully collect the dialyzed solution, aliquot 30 mL into 50 mL tubes, freeze sideways at -80°C
10. Lyophilize product and weigh (25-35 g is typical)
11. Re-dissolve into distilled water at 40mg / 100 mL
12. Freeze sideways and store until needed

PEG-diacryamide synthesis (days 15-21)

1. Lyophilize 20 mg PEG-diamine for 3 days
2. Prepare distillation set-up as before
3. Add PEG-diamine and 400 mL benzene to a 1 L round-bottom flask
4. Remove 100 mL Benzene by distillation (PEG should already be very dry, but can do more)
5. Cool on ice to RT and put under nitrogen
6. Add 50 mL DCM to solution through septum
7. Add 0.41 mL Tethanolamine (~1 mL)

USING AIR-FREE Technique

8. Add 0.24 mL Acryloyl Chloride (~1 mL)
9. Cover, stir at 400 rpm, foil, and react overnight
10. Place 4L of diethyl ether to cool at -20°C overnight

11. Precipitate with ether and dry overnight (see *Collect PEG-MS*)
12. Re-dissolve in distilled water to 20 g / 100 mL and freeze at -80°C (store for up to 5 years)
13. Lyophilize product and use within one year
14. Check conjugation ^{1}H NMR: (DCCl3) 3.6 ppm (1816 H, PEG), 5.6 ppm (dd, 2 H, CH2=C*H*-CON-), 6.1 ppm, 6.2ppm (dd, 4 H, C*H*2=CH-CON-).

Published Protocol

Synthesis of PEG-diacrylamide

Poly(ethylene glycol) was functionalized as described elsewhere. Briefly, poly(ethylene glycol) (20 kDa MW, 100 g, 10 mM -OH) (Fluka, Buchs, Germany) was dried azeotropically against benzene and reacted with triethylamine (4.1 mL, 30 mmol, Acros, Fair Lawn, NJ) and mesyl chloride (2.3 mL, 30 mmol, Acros) overnight under nitrogen at 20°C. The product was precipitated in cold ether (Fisher, Waltham, MA), dried under vacuum and reacted against 25% aqueous ammonia (Acros) for 4 days. After evaporating the ammonia, the pH was adjusted to 13 with 1 N NaOH, and the solution was extracted with dichloromethane (Fisher), concentrated, precipitated, and dried. The resulting poly(ethylene glycol)-di-amine was dialyzed against water and stored at -80°C. For acrylation, 20 mg of the PEG-diamine intermediate was lyophilized and dried azeotropically before addition of dichloromethane, triethylamine (0.41 mL, 3 mmol), and acroyl chloride (0.23 mL, 3 mmol, Aldrich, St. Louis, MO). The reaction proceeded overnight under nitrogen and the product was precipitated and dried. The resulting poly(ethylene glycol)-di-acrylamide (PEGDAm) was dissolved in water, lyophilized and kept at -20°C. Conversion of diols to diacrylamides was confirmed via ^{1}H NMR: (DCCl3) 3.6 ppm (1816 H, PEG), 5.6 ppm (dd, 2 H, CH2=C*H*-CON-), 6.1 ppm, 6.2ppm (dd, 4 H, C*H*2=CH-CON-).

Appendix B PEG-Collagen Conjugation

Revision 1.7 by Rahul Singh, 01/28/2014

Thioacetylation of Collagen (day 1 & 2)
Note 1: Collagen will readily gel if not kept near 4°C, ensure the reaction is kept on ice at all times!
Note 2: Use aseptic technique (work inside a biosafety cabinet) to ensure sterility. Reagents do not have to be sterile filtered (due to high stock concentrations) and PBS dialysis buffer does not need to be sterile.

- Place 4L of PBS at 4°C to chill
- Working inside a biosafety cabinet, place reagents into a STERILE 50 mL tube.
- Dilute collagen to 3 mg/mL with an equal volume of STERILE cold 2x PBS
  Adjust pH to 7.0 with 40-60uL 1N NaOH (Put the pH meter in the biosafety cabinet and CLEAN the probe before and after use. To thoroughly clean, use 0.1N HCl or pepsin after 2-3 runs)
- Remove SATA from -20°C and fully equilibrate to RT before opening .
  (stock solution at 50mg/mL in DMSO, mp=19°C)
- Add 45µL SATA solution per 10 mL collagen solution. The DMSO will freeze and fall to the bottom. Mix thoroughly; react for 24 hours at 4°C while rotated (not shaken).
- Transfer to a 12kDa MWCO dialysis bag and dialyze at 4°C against 1L *cold* 1xPBS for 12h change media three times (4L total PBS). The resulting product it is stable and can be stored at 4°C.
- A suggested dialysis scheme would be to change after: 2h, 6h, 12h or 1h, 3h, 8h, or etc...
  this isn't critical as long as reasonable diffusion times are allowed.

Thiol Exposure (day 3 & 4)

- Place 4L of PBS at 4°C to chill
- In a biosafety cabinet, collect contents of dialysis bag into a sterile 50 mL tube.
- Freshly prepare a 0.5M solution of Hydroxylamine HCl in PBS, pH to 7.4
  - for 0.5mL: 0.1737 g HyAm + 0.3mL ddH_2O + 0.2mL 10N NaOH
  - Do not save this solution - it goes bad in a couple hours
- Add 375µL of Hydroxylamine stock per 10 mL of collagen (10 molar excess) react rotated for 8h (±2h) at 4°C (side products have a foul odor).
- Add 2mg TCEP-HCl in 200uL PBS per 10mL collagen solution, continue reaction overnight (8-12h).
- Transfer to a 12kDa MWCO dialysis bag and dialyze at 4°C against 1L *cold* 1xPBS for 12h
  change media three times (4L total PBS).

- *Optional:* Measure thiol concentration with Ellman's assay

PEGylation (day 5 & 6)

- Place 4L of PBS at 4°C to chill
- Dissolve three -fold excess TCEP to thiols (2mg/10mL solution) in 100µL ddH_2O add all of it to collagen. Allow it to react for 30 minutes at 4°C, pH should be about 4.0
- Prepare 2-fold molar excess 20k PEG-diacrylamide 120mg/10mL solution in 500uL PBS
- After 30 minutes, add 200 µL of the PEG solution and mix well at 4C
- After 30 minutes, slowly add Triethanolamine to 11.5mM.
    - Prepare a stock of 1 part TEOA and 9 part ddH_2O
    - For a 10 mL batch: add 115 µLof TEOA stock
    - Adjust pH to ~8.2 (use 120µL of 1N NaOH)
    - Immediately add 200 µL of PEG solution
- After 30 minutes add final 200 µL of PEG solution
- Cover with foil; react 12hr at 4°C with agitation
- Transfer to 50kDa MWCO dialysis bag, and dialyze for 48h against 1L of 1x PBS at 4°C with four media changes (4L total)
- Once completed, treat the product as STERILE. Collect contents of the dialysis bag in a biosafety cabinet using good sterile technique

Cellular Encapsulation

- Aseptically collect contents of dialysis bag on ice transfer to 50mL centrifuge tube, keep on ice
- Homogenize Immediately before use:
    - Collect the product with an 18.5G needle into a 10cc syringe
    - Change to a 22.5G needle
    - Quickly expel product into a clean centrifuge tube; use within 5 minutes

Appendix C Immunofluorescent Staining of PEG-Collagen Gels

General Notes:

Gels are 200uL with EC and Stromal Co-culture at day 14
10x TBS: 44g NaCl + 15.75g Tris in 500mL H20
TBS+0.5% Trition X-100: 5mL 10xTBS + 0.25mL TritonX-100, q.s. to 50mL with ddH_20
TBS-T: 10mL 10x TBS + 0.1mL Trition X-100, qs to 100mL with ddH_20
Formalin: 1mL Saturated formaldehyde solution (36.5%) + 1mL 10x PBS + 8mL ddH_20
AbDil: 2% (2g/100mL) Bovine serum albumin in TBS-T

Procedure

1. Transfer gels to a fresh 24-well plate
2. Rinse thoroughly with PBS until clear (1mL three times for 5 min each at RT)
3. Fix with 0.5mL formalin @4°C for 30 minuets
4. Rinse with 1mL PBS three times for 5 min each at RT
5. Permeablize with 1mL TBS+0.5%Triton X-100 @4°C for 1 hour
6. Rinse with 1mL TBS-T three times for 5 min each at RT
7. Block with 1mL AbDil overnight @ 4°C

8. Dilute CD31 primary antibody in AbDil (1:200) and add 1mL to the well then incubate overnight @ 4°C

9. Rinse with 1mL TBS-T three times for 5 min each at RT
10. Dilute secondary antibody in AbDil (1:450) and add 1mL to the dish then incubate overnight @ 4°C

11. Rinse with 1mL TBS-T five times for 5 min each at RT and photograph. Gels can be Stored in TBS-T for up to 1 month.

12. Counter-stain with phalloidin (1:200) in TBS-T and DAPI (1:10,000) for 4 hours @ 4°C
13. Rinse with 1mL TBS-T three times for 5 min each at RT

Appendix D HUVEC Isolation from Umbilical Cords

Nov. 3 2014

Materials per cord

- 10 mL syringes
- 20 mL syringes
- 18 gauge needles
- Butterfly needles
- 0.22 µm syringe filter
- Sterile 1X PBS
- 10 mL of Collagenase solution
    - 250 units/mL in PBS
- EGM-2

Other Materials

- Large glass beaker
- Surgical tools (autoclaved or soaked in 70% ethanol)
- Ice
- Paper towels and gauze pads
- Bleach

1. Thaw cords over ice. Leave them in ice until ready to isolate
2. Prepare work space: Lay 4 layers of paper towels. Can add gauze pads on top if desired. Soak everything with bleach.
3. Sterilize collagenase solution using syringe filter. Deposit into 50 mL centrifuge tube.
4. Fill two 20 mL syringes with PBS. These will be used for washing the cords.
5. Remove cord from container. Look for clamp marks on both ends of the cords.
6. Cut off the clamped ends of the cord about 0.5 – 1 inch above the clamp.
7. Locate the umbilical vein; it is the largest vessel out of the three.
8. Remove needle from butterfly needle; should be left with rigid tube at the needle end. Insert into the vein of the cord.
9. Clamp the cord at the insertion using the surgical clamps. Make sure to create a seal between insertion and vein.
10. Remove needle from the flexible tube end of the butterfly needle and insert 20 mL syringe with PBS. Inject PBS to wash out the vein.
11. Draw up 10 mL of collagenase and slowly inject through butterfly needle tube until droplets from the other end of the cord are the color of the collagenase solution (amber).
12. Clamp the remaining end of the cord with surgical clamps and inject enough collagenase solution until the cord is full (should feel resistance to injection).

13. Place everything in a large glass beaker and place in 37°C incubator for 20 minutes.
14. Return beaker to sterile hood and remove cord. Cut the free end of the cord above the clamp to begin emptying cord into a 50 mL centrifuge tube. Push through all remaining collagenase.
15. Rinse the cord with 20 mL PBS, collecting the rinse in the same centrifuge tube. Use a relatively high flow rate. Discard the cord.
16. Centrifuge the contents of the tube at 200x g for 5 minutes.
17. Remove supernatant and re-suspend in 5 mL EGM-2. Should contain a lot of red blood cells.
18. Deposit the cell suspension into a T-25 flask.
19. After 24 hours, rinse flask with PBS as much as necessary to remove red blood cells.

Appendix E PEG-Collagen Photolithography

Version 4.0 02/12/2114
Prepared by: Evan Chen, Matthew Tam, Spencer Paris, and Rahul Singh
Total Time: 1 hour set-up and 1-2 hours per gel

Materials:

Stock Solutions

- 20kDa PEGdiacrylamide at 200 mg in 1 mL of PBS [cover with foil to protect from light]
  Prepare in a 1.5 mL microcentrifuge tube, add solvent slowly, vortex and centrifuge to degas
  Stock can be frozen at -20°C, protected from light and re-used for up to 3 months
- Irgacure 2959 at 100mg in 1 mL 70% Ethanol (with ddH2O) [cover with foil]
  Prepare in a 1.5 mL microcentrifuge tube, and vortex for 2 minutes until dissolved
  Stock must be made immediately before use and not re-used
- PEG-Collagen (1mL / gel) **keep on ice**
  Stored in aliquots of 1 ± 0.2 mL. Thawing one extra tube is helpful.
  Stocks are stored at -20°C, and cannot be re-used. Stable for up to 4 months

Tools

- Place in 100mm petri dish
  - Two treated PDMS molds (600 µm deep, treated) kept in vacuum
  - Two Acrylated coverglasses, kept in vacuum in foil, use within 30 days
  - Two masks: Hex_2x1 kept in "microfludics" drawer (Hex_2x2 and Hex_1x0.5 also work)
- Other: Tweezers, UV lamp, white stands, two coverslip boxes, 2-well test tube rack

Consumables (Per Batch)

- 2x 6-well plates (one for wash and one for culture)
- Per batch: 2x1mL slip-tip syringes, 2x 23G needles, 5x 18G needles
- Sterile: Alcohol Pads, All-Purpose Sponges, 100mm dish, 2x 60mm dish

Cells & Reagents

- DMEM, FBS, Trypsin, PBS, Growth Media (EGM 2 or Osteogenic)
- Each batch requires 1 million cells, split evenly between two exposures.

Take items to biosafety cabinet and set up using aseptic technique (sterilize everything with ethanol)

1. Assemble the lamp according to diagram and turn it on to warm up (minimum 5 minutes)
   Caution! UV light is harmful to the eyes. **DO NOT LOOK DIRECTLY INTO THE LAMP**

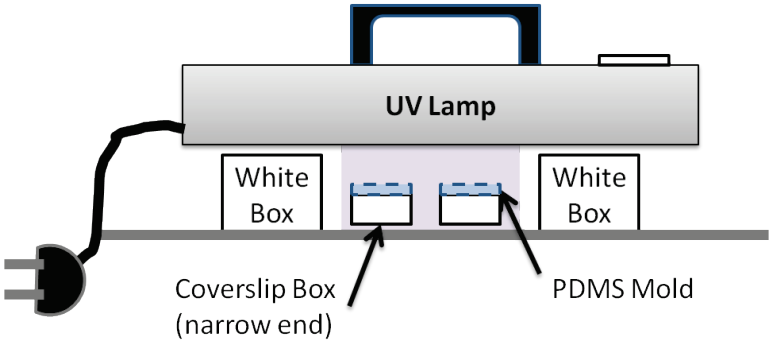

2. Sterilize the Tools
   a. Sterilize coverslips by submerging in 70% ethanol for at least 5 minutes

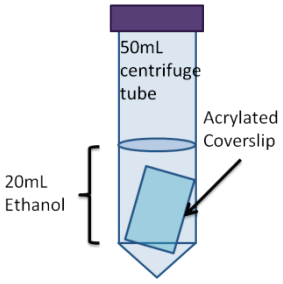

   b. Place each acrylated coverslip in a 60mm dish with a 200µL pipette tip to keep the slip off the dish, leave open to dry.
   c. Once dry, close the lid to prevent debris from falling onto the coverslip

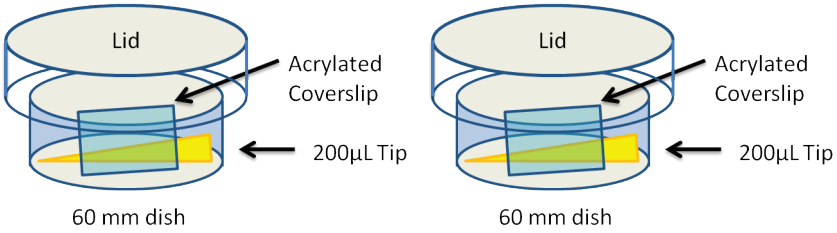

   d. Spray the masks with ethanol and place it in the 100 mm dish, once dry, close the lid
   e. Sterilize PDMS molds and place them on top of the coverslip boxes under the UV lamp

3. Prepare cells
   Each batch requires 1million cells, for a double-exposure gel, each phase requires 500k cells
   <u>If possible, only trypsinize enough cells for one batch!</u>
   a. Trypsinize and count cells
   b. Re-suspend in DMEM + 10%FBS at 1 million / mL
   c. Aliquot 0.5 mL of the suspension (500k cells) into 1.5 mL microcentrifuge tubes
   d. Cap and set aside
4. Prepare the crosslinker solutions in 1.5 mL microcentrifuge tubes
   Prepare in 500 µL batches, for a double-exposure gel, prepare both phases now, and label tubes!

<u>1% Phase</u>	Words to fill the gap	<u>2% Phase</u>
30 µL Irgacure Stock		30 µL Irgacure Stock
28.5 µL PBS		3.5 µL PBS
25 µL PEG Stock		50 µL PEG Stock

   Add the components to sterile 1.5 mL micro-centrifuge tubes and set aside
5. Prepare cell-pellet by centrifuging one aliquot of cells for 5 minutes at 200g in the microcentrifuge
6. Suspend cells in PEG-Collagen
   a. Prepare PEG-Collagen:
      i. Thaw to room temperature by gently warming the tube by hand. A clump of frozen PEG-Collagen should remain in the tube - shake the tube to see how big the clump is. Solution is thawed when half the vial is liquid.
      ii. *Homogenize* the PEG-Collagen by drawing and expelling from a 1mL syringe with an 18G needle <u>several</u> times until smooth. Use the tip to break up remaining clumps.
      iii. Draw up 420 µL of PEG-Collagen
      iv. Discard the 18G needle and replace with a 23G needle
      v. Expel PEG-Collagen into the PEG solution and homogenize several times
      vi. Draw up the solution into the syringe
      vii. Discard the 23G Needle and replace with a fresh 18G Needle, <u>do not remove the shield,</u> and set the syringe aside
   b. Prepare Cell Suspension:
      i. Aspirate the media from the centrifuged cell pellet
      ii. Tap the microcentrifuge tube to dislodge the pellet

iii. ***Gently and slowly*** add the PEG-collagen solution to the cell pellet
iv. ***Gently and slowly***, homogenize the mixture three times, and draw into the syringe
v. Replace the needle with a shielded 18G needle, and set the syringe aside.

7. First Photoencapsulation
    a. Remove the PDMS wells & coverslip box from UV
    b. Add 210 µL of cell solution to each PDMS well (any less produces air bubbles)
    c. Carefully place the acrylated coverglass on top of the well, careful to avoid forming bubbles
    if bubbles form, slide the bubble to the edge of the well and releasing them by sliding the coverslip open. If they do not release, then leave them at the edge of the well.
    d. Place the photomask on top of the coverslip - **do not press down on the coverslip**
    e. Press the mask down on areas away from the coverslip to ensure it is flat
    f. Place the assembly under the UV lamp for **EXACTLY** 5 minutes (under & parallel to lamp)

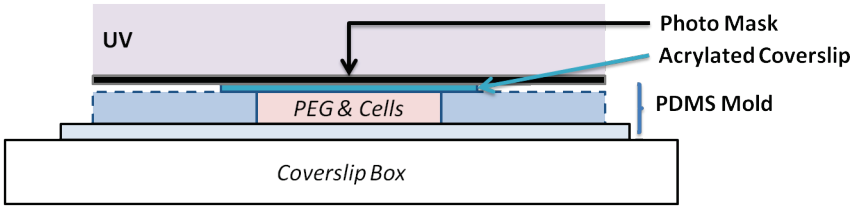

    g. Meanwhile, place 5mL PBS in two wells of 6-well plate, and place a 10 µL pipette tip at the bottom of each well.
    h. Remove the assembly from UV
    i. Using tweezers carefully release each coverslip by pressing under the glass and into the PDMS and working all around the well.
    There is a high chance of breaking the coverslip at this step
    j. Once released, gently lift each coverslip straight up out of the PDMS well and place it gel-side up into its own PBS-filled well (see below), cover and set aside.
    k. Clean the PDMS molds with an ethanol wipe and place it & the box under UV to dry.

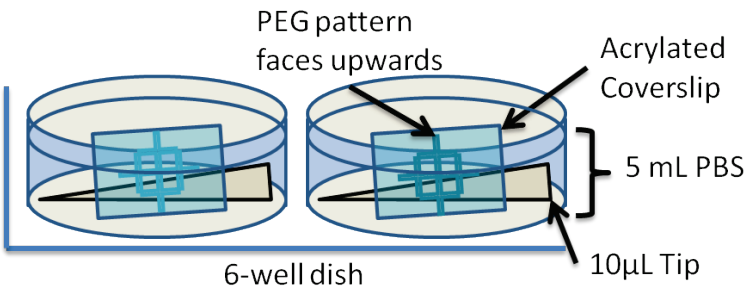

8. Second Photoencapsulation
    a. Prepare the second phase of PEG-Collagen as in §8a
    b. Prepare the second cell-suspension as in §8b
    c. Remove the PEG-covered coverslips made in §9 from the 6-well
    d. Place each coverslip back onto a mold with the PEG-sides facing up
    e. ***Gently and carefully*** wick PBS out of the first pattern with the corner of the sponge.
    f. Drop-wise add the second cell suspension over the first PEG gels
    Only use enough to fill the pattern - try to make a thin layer!
    g. Place under UV for 5 more minutes

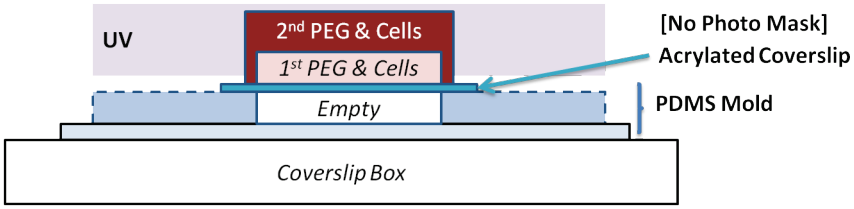

    h. Meanwhile, in a fresh 6-well plate add 5 mL of DMEM + 10% FBS in two wells
    i. After UV exposure, carefully place each coverslip gel side up in its own media well
    May have to press coverslips down with tweezers to break surface tension
9. Reset for next gel
    a. Place the newly formed gels in the 37°C incubator
    b. Use a ethanol wipe to clean the mask and place back into the 100 mm dish
    c. Use a ethanol wipe to clean the PDMS mold place back under UV
    d. Repeat steps 5-11 for the next batch
10. The DMEM should be changed to growth / experimental media after 2-6 hours

---

Notes:

Planning Cell Culture for Photoencapsulation Experiments

1. Determine the number of substrates you want to test.
    a. Each batch can make two gels.
    b. These gels will have identical compositions of PEG and cells.
    c. Gels can have different patterns.
2. For each batch of two substrates, you will need 1 million cells (500k per exposure).
3. Multiply the number of cells by the number of substrates to determine how many cells you need for photoencapsulation. Add in a safety margin of 1 million cells in case of a failed exposure.
4. Working backwards, determine the number of cells you need to plate
    a. Cells must undergo one passage between thawing and use in an experiment
    b. For MSC: One passage is 6-8 days in which the cells triple (3x)
    MSC can be passage twice or more
    MSC are typically frozen at 500k to 1 million.
    c. For EC: One passage is 5-6 days in which the cells octuple (8x)
    EC can only be passage once
    EC are frozen down at 500k
    d. e.g. Three batches (6 gels) will need 3 million MSC.
    Adding a buffer makes this 4 million MSC.
    Plate 4/3 = 1.3 million cells 7 (±1) days prior to use.
    Stocks are only 1 million, so another passage is needed[1].
    This will require 1.3 / 3 = 0.440 million cells 7 (±1) days prior to that.
    So plate 500 thousand cells 14 (±2) days prior to use[2].
    Note 1: <u>Stocks can be made at an intermediate passage to expedite this process</u>
    Note 2: It's better to have extra cells than too few!

Appendix F Bead Assay Assembly & Staining

Preparing Cytodex beads

1. Take a scoop (~1 cc) of Cytodex-3 microcarrier beads (Sigma) (diameter of 150 μm)
2. Add 15 mL of phosphate buffered saline (PBS) to a glass scintillation vial (20 mL).
3. Disperse beads in PBS and loosely attach cap before sealing with aluminum foil
4. Autoclave on standard liquids cycle - beads will swell with PBS
5. Remove and Parafilm seal cap, sterile beads last 3 years. Store at 4°C.

Count the bead concentration: place 10 μL in a hemocytometer and count the average number of beads per quadrant then multiply by 10^4 to determine concentration (beads/mL). Target is 10,000 beads / mL adjust volume if deviation is beyond 3,000 and re-count the beads.

Beads will rapidly settle, this is okay - they readily disperse. DO NOT CENTRIFUGE or VORTEX BEADS. They can be dispersed by gently inverting the vial a couple times.

Cell Preparation

Isolate HUVEC as described elsewhere and 4-6 days prior to the experiment plate at 500k / T-75 in EGM-2. Stromal cells can be plated 2-4 days prior to use depending on their growth rate. NEVER use cells directly from cryogenic storage. Culture cells at least one passage. HUVEC should be used at passage 3 (thaw P2 then assay is P3).

Bead coating (On day before setting up assay)

1. Warm the following to 37°C; PBS, EGM-2, 10mL Trypsin, Serum supplemented media (DMEM, M199, etc...)
2. Keep bead solution at 20°C, do not chill or heat.
3. Trypsinize and count HUVECs one flask should have 4-8 million cells.
    a. Remove media, add 5mL PBS and gently roack 1-3 times, remove PBS and add 5 mL trypsin. Incubate 5-10 minutes until cells form a suspension. DO NOT TAP cells off the surface - this creates clumps. Inactive trypsin with 5mL serum containing media and transfer suspension to centrifuge tube. Pellet cells at 200g for 5 minutes. Aspirate media. Resuspend in 5 mL EGM2 and count on a hemocytometer.
4. Cells should be coated at a density of 4 million cells / 10,000 beads the total volume should be 5mL. Adjust the beads to the cell number to maintain that

ratio. But do not place less than 3 million or more than 5 million HUVEC in a flask.
5. In an inverted T-25 place cells, beads and media on the bottom (lid should face the ceiling). eg. 4 million cells in 4mL EGM2 + 0.7mL beads in PBS + 0.3 mL EGM2.
6. Place flask in incubator *still inverted* and tap 2-3 times to suspend beads.
7. Every 30 minutes, shake and tap the flask to disperse beads.
8. Continue shaking for 3.5 hours.
9. After last shaking, wait 30 minutes than transfer bead + cell suspension to a clean T-25 and culture in the normal fashion overnight. Excess cells and beads will adhere to culture surface while dead cells and uncoated beads will float.

Tissue Assembly Preparation

1. Warm the following to 37°C; PBS, EGM-2, 10mL Trypsin, Serum supplemented media (DMEM, M199, etc...)
2. On ice, thaw Thrombin (50 IU/mL) and 1mL aliquot of fetal bovine serum (**F**BS)
3. Keep bead solution at 20°C, do not chill or heat.
4. Meanwhile, weigh fibrinogen to a gel concentration of 2.5 mg/mL clottable protein. Lyophilized powders are assayed for protein content and clottable fraction, Further , the stock will be diluted to make the final gel (465μL stock / 500μL gel).
   fibrinogen powder = (gel concentration) /(%clottable * % protein)*(1.075).
   do not account for bound water as this changes over time, also ~1 mL is lost in processing so round up and prepare an extra mL.
5. Place powder into a 50 mL conical tube and add PBS to desired concentration. Alternatively to PBS, serum-free EGM2 has been used by others, but it is unnecessary with this protocol.
6. Gently invert tube to wet the powder (do not vortex - this creates foam and dentures the protein) and place in the water bath for 15-30 minutes to dissolve. After 15 minutes, if bubbles are present, centrifuge 1 minute at 2,000 g to degas
7. Once dissolved, transfer to tissue culture hood and filter with a 0.22 μm PES syringe filter. Typically can filter 5-7 mL per filter unit without clogging. Place solution in a sterile centrifuge tube and keep on ice to cool.

8. Working in a tissue culture hood, and using good aseptic technique, spray down reagents and place in tissue culture hood. Ice bucket can remain outside.
9. Ignore stromal cells for now.
10. Collect coated beads: Remove media and add 5mL fresh EGM2. Vigorously tap flask against counter to dislodge beads. Collect bead suspension in a sterile 50

mL tube. Set aside and gently shake every 15 minutes to keep beads suspended.

Tissue Assembly (single-well protocol)

1. Get a sterile tissue culture treated **24-well plate** to construct assay. Use the middle row to assemble gels.
2. Shake beads to suspend. Place 200-50 μL bead suspension in a sterile **1.5mL centrifuge tube**. Place aside to let beads settle. After making the first gel, adjust volume of beads so that beads are 0.5 to 1 mm apart.
3. To another 1.5 mL centrifuge tube add 10 μL of thrombin and 50 μL of **F**BS
4. Aspirate the remaining media from the bead suspension, careful not to suck out beads. If in doubt, the bead-pellet can be visualized through the tube with an inverted microscope.
5. Withdraw 465 μL of fibrinogen solution and use it to re-suspend the beads.
6. Work as quickly as possible - fibrin clots in under a minute.
7. Add the fibrinogen-bead solution to the thrombin-FBS solution and mix well
8. Pipette this solution into a 24-well plate's well
9. Repeat procedure to fill all the desired well and place at 37°C to clot.
10. Allow 30-60 minutes for gels to clot. When set, they become translucent.
11. Meanwhile, collect stromal cells and determine concentration as previously described.
12. Each well receives 25,000 stromal cells, so suspend cells at 25k/mL in EGM2. Once clotted, add 1mL of stromal cell suspension to each well
13. **Change media after 12-18 hours** then every other day for the duration of the culture period. This is important since the EGM2 is diluted by the PBS in the clot.

Tissue Assembly (multi-well protocol for 48-96 wells)

1. Get a couple sterile tissue culture treated **24-well plate** to construct assay. Also get a uncoated **96-well U-bottom** plate.
2. Shake beads to suspend. Place 100 μL bead suspension in into wells of the **96 well U-bottom**. Place aside to let beads settle.
3. **To each well of the 24-well plate add 10 μL of thrombin and 50 μL of FBS**
4. Aspirate the remaining media from the bead suspension, careful not to suck out beads. Work in groups of 6 to prevent beads form drying out.
5. Withdraw 465 μL of fibrinogen solution and use it to re-suspend the beads form one well. Just push enough into the well to get the beads ~1/3 of the volume.
6. Add the fibrinogen-bead solution to the well with thrombin-FBS solution. Do not mix.
7. Repeat procedure to fill all the desired wells and place at 37°C to clot.
8. Allow 30-60 minutes for gels to clot. When set, they become translucent. Remember which plate you start with since it can easily be 15 minutes between placing plates in the incubator.

9. Meanwhile, collect stromal cells and determine concentration as previously described.
10. Each well receives 25,000 stromal cells, so suspend cells at 250k/mL in EGM2. Once clotted, add 1mL of EGM2 and 100uL of stromal cell suspension to each well.
11. **Change media after 12-18 hours** then every other day for the duration of the culture period. This is important since the EGM2 is diluted by the PBS in the clot.

IF Staining of Fibrin Gels (Bead Assay)

Composed by Rahul Singh 12/4/2013

from Notebook 005, pg 13

1. Rinse 3x with PBS for 5 minutes each
   all wash volumes are 2x gel volume
2. Fixation for 15 minutes with 10% Formalin at 20°C (2-4 hour at 4°C).
3. Wash 3x for 5 minutes each with PBS
4. Permeabilize with TBS+0.5% v/v TritonX-100 for 30 minutes at 4°C
5. Wash 3x with TBS-T (TBS + 0.1% v/v TritonX-100) for 5 minutes each
6. Block with Abdil (2% BSA in TBS-T) for at least 1hr at 4°C
7. Incubate with your primary antibody overnight (diluted in AbDil) at 4°C
   ie. Mouse anti-Human CD31 at a 1:250 dilution
   use a volume equivalent to the gel's volume (ie. 0.5 mL for 500uL gels)

8. Wash 3 times for 5 minutes each with TBS-T
9. Incubate with secondary antibody for 4 hours (up to overnight, but shorter is often better)
   ie. Goat anti-Mouse 594 Alexa Flour (Ab box in 4°C)
   Dilute 1:450 and use a volume equivalent
10. Wash three times for 5 minutes each with TBS-T
11. Leave in TBS-T overnight

12. DAPI stain (optional):
    a. Rinse three times for 5 minutes each with PBS
    b. Add DAPI at 1:10,000 ratio in PBS for 10 minutes at RT
    c. Rinse once with PBS for 10 minutes

Notes:

TBS: 50 mM Tris-Cl, pH 7.5 & 150 mM NaCl
To prepare, dissolve 6.05 g Tris and 8.76 g NaCl in 800 mL of ddH_2O. Adjust pH to 7.5 with 1 M HCl and make volume up to 1 L with ddH_2O. TBS is stable at 4°C for 3 mo.

Appendix G Inhibiting Rho GTPase Activity in Stromal Cells Attenuates Angiogenesis

Abstract

Previous studies have established that the ability of endothelial cells (ECs) to generate traction force depends on the small GTPase RhoA, and that these RhoA-dependent forces are necessary for angiogenic sprouting. However, if RhoA-dependent traction forces influence stromal cell support of angiogenesis remains unclear, as the majority of mechanobiological studies of angiogenesis have focused on the ECs. We hypothesize that disrupting Rho GTPase signaling pathways in stromal fibroblasts will adversely affect their ability to promote angiogenic sprouting.

Methods

Viral Constructs

The mutant RhoA and eGFP transgenes were subcloned from pcDNA3-EGFP-RhoA-Q63L (Addgene plasmid 12968), and pcDNA3-EGFP-RhoA-T19N (Addgene plasmid 12967) plasmids using a high fidelity DNA polymerase (Q5 high fidelity DNA polymerase, New England Biolabs). The subcloned transgenes were inserted into the MCS of a tetracycline inducible backbone, tetO-FUW-MCS, derived from Addgene plasmid 20321 (tetO-FUW-OSKM) to construct the plasmids tetO-FUW-eGFP-RhoA-Q63L, tetO-FUW-eGFP-RhoA-T19N, and tetO-FUW-eGFP (Fig. 1A).

To prepare viral supernatant, plasmids or a doxycycline inducible transactivator (M2rtTA) lentiviral vector (Addgene plasmid 20342) were transfected into 293FT cells (Invitrogen #R700) along with lentiviral packaging plasmids pLP1, pLP2, and pLP-VSVG (Invitrogen) in growth medium containing lipofectamine 2000 (Invitrogen #11668). Media was changed 24 hours after transfection and collected 48 hours post-transfection. Supernatant was clarified by centrifugation at 3000 rpm at 4°C for 15 minutes. Aliquots were frozen at -80°C until use.

Cell Transduction

Stromal cells (normal human lung fibroblasts) were transduced with equal parts viral supernatant containing M2rtTA and either eGFP, T19N, or Q63L. Appropriate volumes were determined by serial titration of viral particles and used at a MOI = 8. Transducation media was prepared containing 5 µg/mL polybrene (Millipore #TR-1003-G), viral supernatant, and 10% FBS with the remainder made up of DMEM. Stromal cells at passage 8-12 were plated at 833k /cm^2 in growth medium (DMEM + 10% FBS) and allowed 6 hours to attach and spread. Subsequently, cells were treated with transduction medium for 24 hours before use.

To assess expression of rho mutants, cells were subsequently induced with 120 ng/mL doxycycline (Sigma)for 48 hours. Cultures were then fixed with 10% formalin (Sigma) in PBS, permeabilized with 0.5% Triton®X-100 (Sigma), and stained with 1:400 Alexa Flour 568 phalloidin (Invitrogen, A12380)and 1:10,000 DAPI (Sigma) in 2% bovine serum albumin (BSA, Sigma A3803). Cultures were imaged with an Olympus IX81

inverted microscope equipped with a Hamamatsu ORCA-R2 (model C10600) digital CCD. The following filter sets were used with ex/em of: DsRed 562 / 641; GFP 473 / 520; DAPI 377 / 447.

For a subset of experiments, cells were treated with the proliferation inhibitor mitomycin C (Fisher Scientific). Stromal cells were transduced with lentiviral constructs as previously described. The day following transduction, media was changed to DMEM + 10% FBS. After 24 hours the media was again changed to DMEM supplemented with mitomycin C at 10 µg/mL. After 24 hours of treatment, the cells were used normally to assemble assays.

Western Blotting

Cell lysates were prepared by washing culture dishes with ice-cold TBS. For tissue constructs, the stromal cells were removed from fibrin clots by treatment with 2.5% Trypsin for 1 minute at 37°C. Cells were pelleted and washed with TBS. To prepare protein extracts, samples were treated with Garner buffer (50mM Tris, pH = 7.5, 150 mM NaCl, 1 mM phenylmethylsulfonyl fluoride, 1% Triton X-100) (1) with protease inhibitors (11.7 mM leupeptin, 0.5 M sodium orthovandate, 1.5 mM aprotinin, and 1.5 mM pepstatin A). The total protein was assessed with a bicinchoninic acid assay kit (Thermo, #23225).

Samples were loaded at 40µg of total protein and electrophoresed under reducing conditions through a 10% tris-gly gel before transfer to a PVDF membrane. Blots were

probed with a mouse monoclonal antibody against human rho A (1:200, Santa Cruz Biotech) or a mouse monoclonal antibody against human alpha smooth muscle actin (αSMA; 1:200, AbCam). Blots were subsequently probed with a horseradish peroxidase conjugated anti-mouse secondary antibody (1:2,000) before detection with an enhanced chemiluminescence detection system. Bands were identified by comparison to a known molecular mass ladder (Kaleidoscope, Bio-Rad).

Angiogenesis Assay

We adopted a previously established *in vitro* 3D angiogenesis assay (Fig. 2A) (2). Human umbilical vein endothelial cells (EC) were isolated and used at passage 3. These cells were combined with Cytodex-3 microcarrier beads (Sigma) (diameter of 150 μm) at a density of 4 million EC per 10,000 beads in an inverted T-25 culture flask with 5mL EGM-2 (Lonza). The cells were allowed to adhere to the beads over the course of 3 hours with agitation every 30 minutes. The suspension was then transferred to a new T-25 and incubated overnight. Fibrinogen solutions were prepared by dissolving lyophilized fibrinogen powder (Sigma F8630) to a final clottable protein concentration of 2.5mg/mL in PBS. These solutions were sterile filtered and chilled on ice prior to use. To assemble constructs, ~25 beads were pelleted and re-suspended in 465 μL fibrinogen solution before combining with 25 μL FBS and 10 μL of a 50 IU / mL thrombin (Sigma T6634) solution. This was quickly pipetted into a 24-well plate and allowed to clot at 37°C for 30 minutes. After clotting, stromal cells were plated at 25,000 cells/well in EGM-2. The next day EGM-2 was replaced with EGM-2 supplemented with 120 ng/mL doxycycline (Sigma #D9891) to induce expression of the plasmids. Constructs

were maintained in doxyclycline supplemented EGM-2 for 14 days with changes every 48 hours. For a subset of experiments, constructs were prepared with either 5,000; 25,000; 125,000; or 500,000 stromal cells in the same manner.

For visualization of endothelial sprouting, constructs were fixed at day 14 with 10% formalin in PBS for 15 minutes at 20°C. Constructs were washed in TBS-T, permeabilized with TBS + 0.5% TritionX-100, blocked with 2% BSA and stained with a monoclonal mouse anti human CD31 antibody (1:250 Dako M0823), washed, and stained with a monoclonal goat anti-mouse AF 594 (1:450 Invitrogen A-11005). Samples were photographed with an Olympus IX81 microscope. The total lengths of capillary networks sprouting from a single bead were quantified using the angiogenesis module in Metamorph (Molecular Devices).

For visualization of the ECM, confocal reflectance microscopy was performed on formalin fixed, unstained constructs. An Olympus FluoView 500 Laser Scanning Confocal Microscope with an argon excitation source at 488 nm and a 60x 1.2 NA water immersion objective was used to perform.

Rheology

Samples were cultured in 24 well plates which was clamped to the stage of an AR-G2 rheometer (TA Instruments, New Castle, Delaware). The lower stage was heated to 37°C and samples were tested under media. Measurements were taken with an 8 mm flat plate. The upper plate was coated with P800 wet or dry sandpaper (3M, St. Paul,

Minnesota) to prevent slip. Gaps were adjusted to accommodate the heights of the hydrogel. Gel heights were determined by micro-indentation of the upper plate on a separate set of samples from shear testing. Constructs with stromal cells that were: wild-type (WT) were tested at 3 mm; eGFP were tested at 3mm; T19N were tested at 3 mm; Q63L were tested at 2.5 mm and acellular constructs were tested at 3 mm. Heights are from the lower plate.

Collagen Deposition

A Sirius Red collagen assay (#9062 Chondrex) was performed. Briefly, fibrin gels were washed with PBS then digested for 72 hours at 4°C by pepsin in 0.05 M Acetic Acid under gentle agitation. The liquefied gel was collected into 1.5 mL micro-centrifuge tubes and centrifuged. The supernatant was collected and 100 µL was added to 500 µL of Sirius Red reagent and allowed to precipitate at 20°C for 20 minutes. The tubes were centrifuged and the pellet was washed twice and extracted. Samples were run in parallel with bovine type I collagen standards. The solutions were then photometrically measured in a 96-well microplate at 530 nm. The total protein of the samples was determined by assaying the pepsin-extracted volume with a bichronodinic acid kit (Thermo), and the total collagen was normalized to total protein in each gel.

Construct Compaction

Fibrin hydrogel constructs were created as described previously along with an acellular fibrin clot. After one day of culture, the gels were detached from the 24-well plate and

allowed to freely float in doxycycline supplemented EGM-2. On days 3, 7, and 14 the plates were imaged with an Epson Perfection V300 photo scanner and saved as high-resolution files (*.tif). Diameters of the constructs were assessed using Image J software (National Institutes of Health, Bethesda, MD).

Monolayer Density

Fibrin constructs were cultured for 3., 7, or 14 days in doxycycline supplemented media. The stromal cell monolayer was removed by digestion in 2.5% trypsin for 1 minute at 37°C. Samples from 5 wells were pooled and cell counts were taken with a hemocytometer.

Based on these cell counts, stromal cell types were plate at densities that would yield in equal numbers of stromal cells on day 14. A Low group was made to have 500k cells per well at day 14. This group had 1.3k WT, 6.63k eGFP, 25k T19N, and 25k Q63L cells. A High group was made with to have 1m cells per well at day 14. This group had 25k WT, 100k eGFP, 500k T19N, and 500k Q63L cells.

Statistics and Graphing

Graph pad prism was used to conduct statistical comparisons were appropriate an ANOVA was used to identify significant factors followed by a Bonferroni post-test ($P < 0.05$) to identify significant pairs of comparisons. The software was likewise used to prepare graphs.

Results

Cell Transduction

Stromal cells are found to uptake the viral constructs and express proteins in doxycycline containing media. Fluorescence imaging of transduced stromal cells shows marked GFP emission attributable to the eGFP or eGFP-Rho A fusion protein expression. Further, the eGFP-positive Q63L mutants have pronounced stress fibers and a compacted phenotype. In contrast, the eGFP-positive T19N mutants are more elongated (Fig 1B). Western blotting at multiple viral titers shows the relative expression of the Rho A mutants to native Rho A. Immunoblotting for total Rho A revealed the expected band at 22 kDa for the native protein (Fig. 1C). In the Q63L and T19N mutants, there is a secondary band above 50 kDa which would be expected for a Rho-eGFP fusion protein. This band is absent in the eGFP transduced control.

Angiogenesis Assay

Stromal cells support angiogenic sprouting to varying degrees (Fig. 2B). ANOVA reveals that genotype is a significant factor, and post-tests show multiple significant comparisons. Capillary networks supported by wild-type (WT) and eGFP transduced stromal cells are not significantly different. However, networks supported by Q63L stromal cells were found to be significantly shorter than WT, and networks produced by T19N stromal cells were found to be significantly shorter than both WT and eGFP stromal cells. Further quantification of the mean segment lengths (A measure of how

branched the network is) reveals that the T19N stromal cells promote networks that are significantly shorter than the other conditions.

In the angiogenesis model, the stromal cell monolayer continued to express eGFP in the transduced cells for the duration of the experiment (Fig 2C). Further, the Q63L stromal cells adopted a phenotype wherein they formed dense clusters instead of spreading into a uniform layer.

Western blotting confirmed the expression of Rho A and eGFP-Rho A in the stromal cells (Fig 2D). Further, alpha-SMA was also fund to be expressed by all stromal cell types throughout the duration of the experiment with no apparent differences between the stromal cells.

Matrix Characterization

Confocal reflectance imaging of the constructs shows the fibrin matrix surrounding endothelial cell sprouts in all four conditions (Fig 3A). However, the reflectance signal in the T19N condition is qualitatively less pronounced than the other three conditions.

Rheological measurements of the cultured constructs reveals differences in mechanical properties with respect to stromal cells (Fig 3B). The acellular control was found to be significantly softer than the WT, eGFP, and Q63L conditions, but not significantly different from the T19N condition. The Q63L gels were found to be both the stiffest and

the shortest gels. The heights of the other conditions did not significantly differ from each other (Fig 3B).

The cultured constructs had varying levels of protein deposition with WT and eGFP having significantly more than T19N and Q63L (not shown). However, the total collagen deposition is reversed, with the T19N and Q63L having significantly more collagen than the WT and eGFP constructs. The normalized data (Fig 3C) reflects these trends.

[compaction blurb goes here - the data makes no sense! - redo the experiment!]

Monolayer Density

Stromal cell proliferation is attenuated by the expression of Rho A mutants. At day 14, The T19N condition has 1/3 the number of cells than the WT and Q63L conditions has 1/5 the number of than the WT condition (Fig. 4A). Both differences were statistically significant. Additionally, the eGFP condition is not significantly different from the WT while the Q63L was significantly reduced. The Q63L and T19N conditions are not significantly different from each other.

The growth rate of the stromal cells are expected to be exponential at early time points and logistic as the maximum capacity of the well is reached. Further, we observe that the maximum capacity of a well is approximately 1 million cells. Using the initial

seeding density of 25,000 and the densities of cells, we can solve the exponential growth equation: Y = Y0 exp(k t) to provide growth rates (k) for the stromal cells: WT = 0.9452, eGFP = 0.8891, T19N = 0.1923, and Q63L = 0.1498. It is also apparent from the logistic fits that the maximum capacity of the WT wells are reached sometime before 7 days. Solving the inverse equation at day 4, we can determine how many time greater the initial seeding density must be for all the cells types to reach the same density as the WT: eGFP = 1.3, T19N = 20, and Q63L = 24.

The stromal cell densities in the monolayer are tiered by an increasing (High) and decreasing (Low) order of 20 from the original seeding density of 25k / well. Further, the data is normalized to the WT condition seeded at 25k to account for variability between EC batches. Between the Low and Equal groups, the WT is significantly different while the other conditions are comparable which is expected due to the equivalent seeding densities. Between the Equal and High groups, the Q63L is significantly increased while the other conditions are not changed. Finally, between the Low and High groups, both the eGFP and Q63L conditions are increased. Within the low group there are significant differences between the WT and eGFP conditions and between the WT and Q63L conditions. Within the Equal group, there were significant differences between the eGFP and T19N and between the eGFP and Q63L conditions, but the difference between the WT and mutant conditions were not significant. The same statistical trend was observed within the High group.

Conclusions

Stromal cells were transduced with constitutively active (Q63L) or inactive (T19N) RhoA and utilized to support angiogenic sprouting of EC to form capillaries in vitro. RhoA was stably expressed in NHLFs with expression controlled by doxycycline induction. Inactive RhoA mutants had decreased proliferation on fibrin constructs. Expression of inactive RhoA produced softer constructs and shorter networks. After accounting for stromal cell proliferation Altering seeding density showed effects due to RhoA activity at high cell densities. Mitotically inactive stromal cells supported capillary formation with T19N mutants supporting shorter networks at high seeding density.

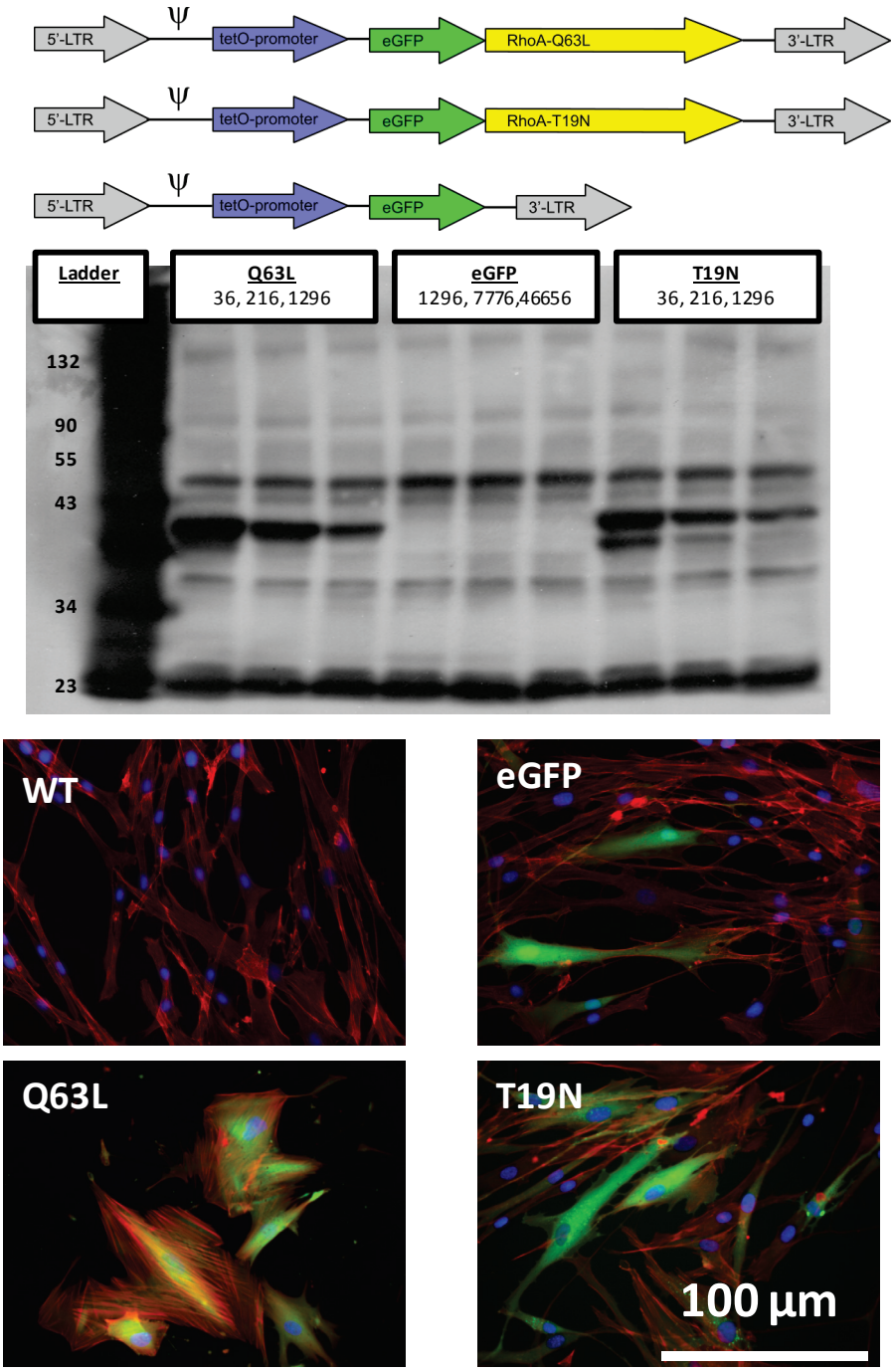

Figure 43: Verification of Rho A modulation in stromal cells

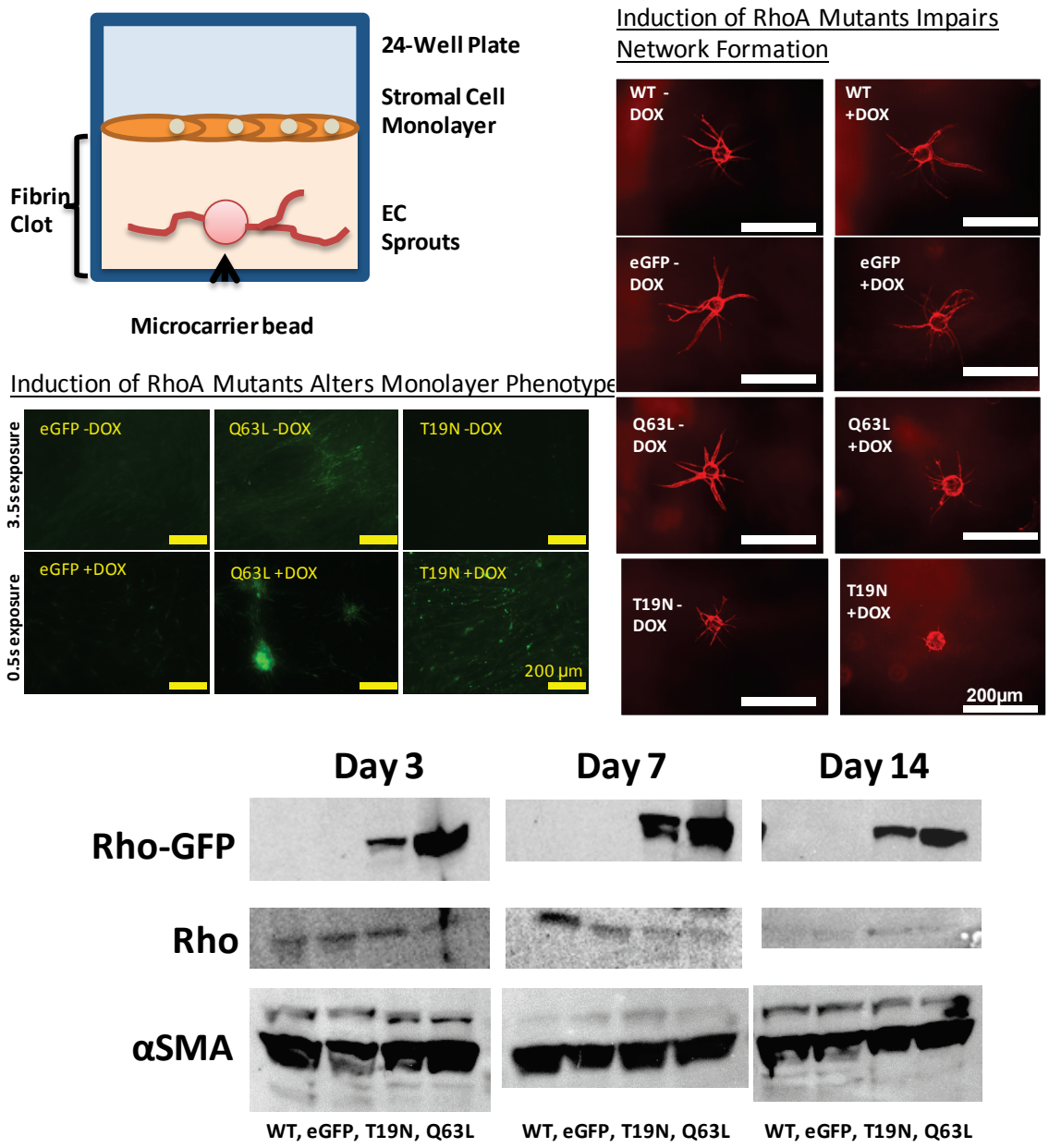

Figure 44: Incorporation of modified stromal cells into a sprouting angiogenesis assay.

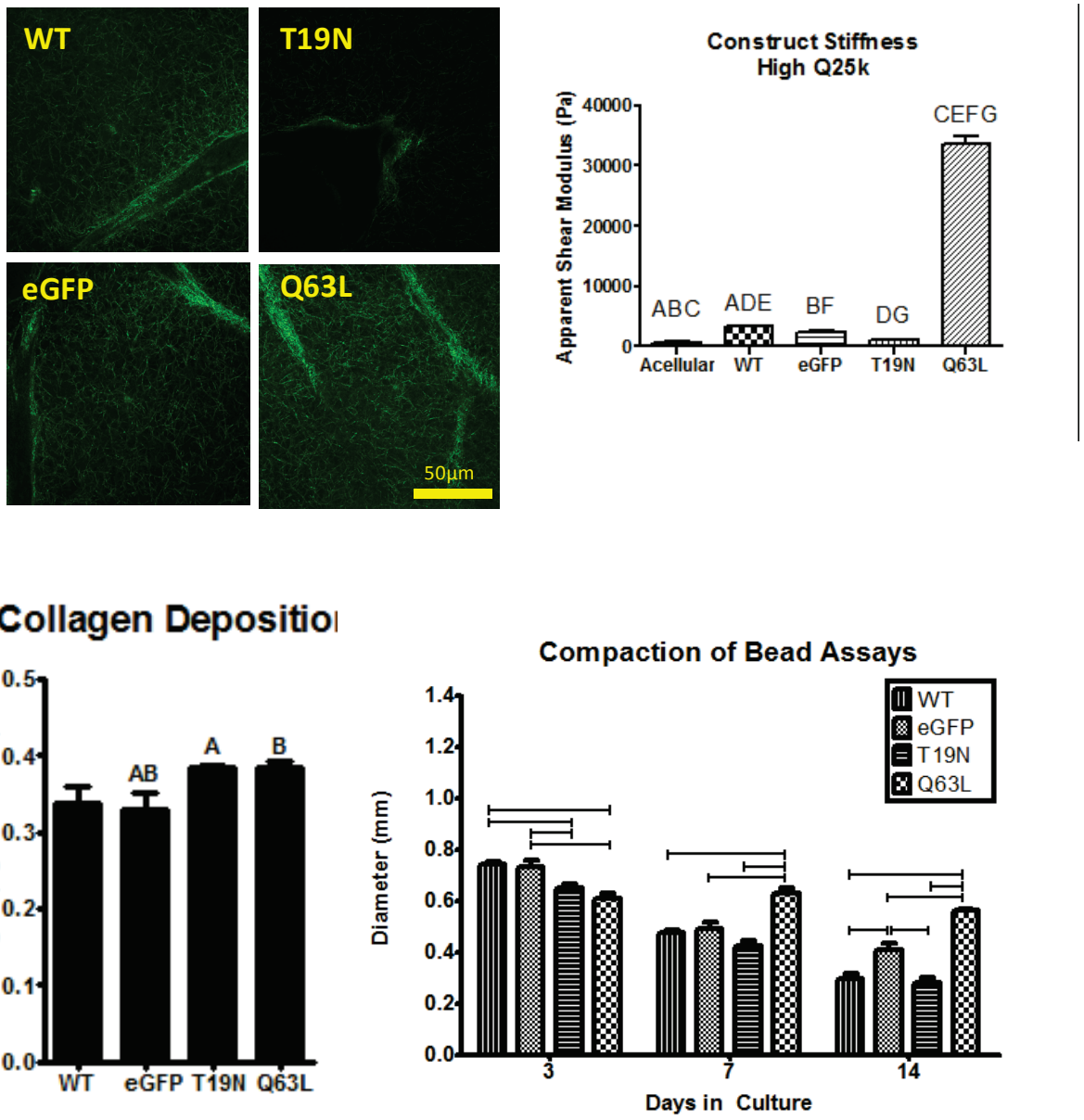

Figure 45: Rho A modulation in stromal cells alters the ECM deposited around capillaries.

Monolayer proliferation depends on RhoA Activity

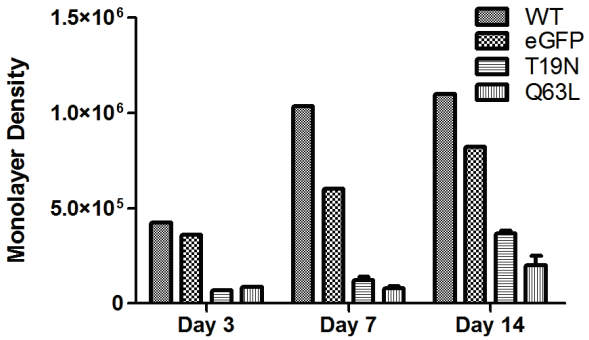

Tukey's Multiple Comparison Test, Repeated Measures (Days)	Significant, P < 0.05
WT vs eGFP	No
WT vs T19N	Yes
WT vs Q63L	Yes
eGFP vs T19N	No
eGFP vs Q63L	Yes
T19N vs Q63L	No

Compensating for Proliferation Rates

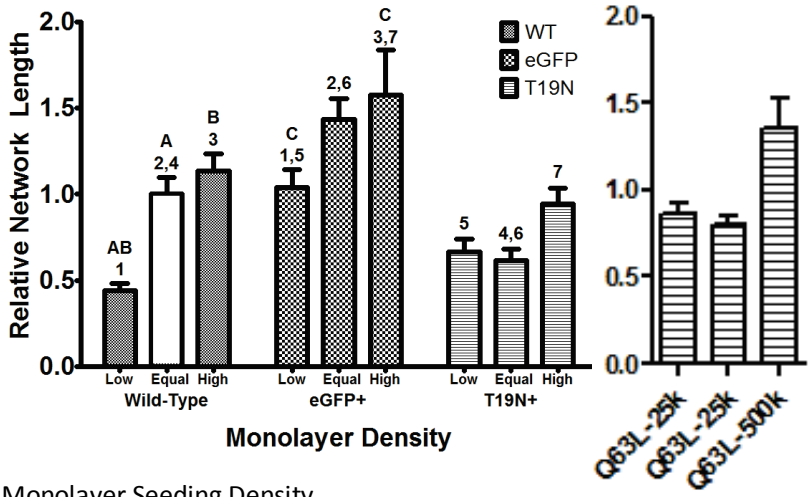

	WT	eGFP	T19N	Q63L
Low	1.3k	6.3k	25k	25k
Equal	25k	25k	25k	25k
High	25k	100k	500k	500k

Monolayer Seeding Density

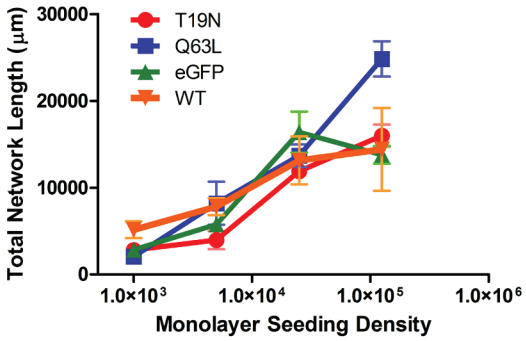

MitoC treated & Pre Induced (d7)

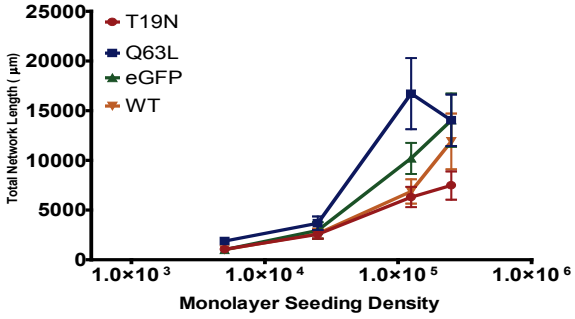

Figure 46: Rho A modulation alters proliferation of stromal cells

References

1. Ghajar CM, Chen X, Harris JW, Suresh V, Hughes CCW, Jeon NL, et al. The Effect of Matrix Density on the Regulation of 3-D Capillary Morphogenesis. Biophysical Journal.94(5):1930-41. doi: 10.1529/biophysj.107.120774.

2. Ghajar CM, Blevins KS, Hughes CCW, George SC, Putnam AJ. Mesenchymal Stem Cells Enhance Angiogenesis in Mechanically Viable Prevascularized Tissues via Early Matrix Metalloproteinase Upregulation. Tissue Engineering. 2006;12(10):2875-88. doi: 10.1089/ten.2006.12.2875.

3. Qi W, Anindita B, Jessamine PW, Arjun Y, Paul AJ. Local and global deformations in a strain-stiffening fibrin gel. New Journal of Physics. 2007;9(11):428.

Appendix H Western Blotting

Western Blotting Protocol v3.0 From Jake on 8/19/13, Transcribed by Rahul

Prepare modified RIPA Buffer: (50mM Tris, pH 7.6; 150mM NaCl; 10mM MgCl2; 1% Triton; & inhibitors)

2x lysis buffer (100 mL) lasts 30 days, grows brown mold!

10 mL	1M Tris, pH 7.6	12.11g / 100mL

(Titrate with 7-10 mL 10N HCl)

6 mL	5M NaCl	29.22g / 100mL
2 mL	1M MgCl2	20.33g / 100mL (Hexahydrate salt)
20 mL	10% TritonX-100	1:9 in water
62 mL	ddH2O	

Working Solution (10 mL)

5 mL	2x lysis buffer		
5 mL	ddH2O		
40 µL	250 mM PMSF	in Methanol	(4°C box)
20 µL	5mg/mL leupeptin	in ddH_2O	(-20°C box)
20 µL	0.5 M Na3VO4	in ddH_2O	(-20°C box)
10 µL	10mg/mL aprotinin	in ddH_2O	(-20°C box)
5 µL	1mg/mL pepstatin A	in 9:1 EtOH:AA	(-20°C box)

Cell Extract Preparation

Chill cells, lysis buffer, and TBS on ice for 5 min

10xTBS: 1.5M NaCl (88g/L) & 0.2M Tris-Cl (31.5g/L) in ddH2O

Wash cells with TBS 1-2 times and drain well then lyse cells in 500µL lysis buffer per T-75

Scrape cells rapidly and transfer lysates into chilled 1.5 mL eppendorf tube

Clear lysates by centrifuging for 5 minutes in 4°C microcentrifuge (Stegemann Lab) at max speed

Transfer supernatants to pre-chilled tubes (can store at -80°C for 1 month)

Measure Total Protein by BCA

Use 1%BSA in ddH2O as to prepare standard curve.

1% BSA	0	2.5	5	10	20	30	40
ddH2O	50	47.5	45	40	30	20	10

Add 20µL supernatant to 30µL ddH2O

Add 1mL BCA reagent (1 pt. B and 50 pt A) to each tube & incubate 45 min in 37°C water bath

Run SDS-PAGE

Adjust sample concentrations to be equal and as high as possible (see spreadsheet)

Reduce in Lamelli sample buffer and boil 5 min

Running buffer 10x Stock

25mM Tris 30.3g / L ddH2O
190mM Glycine 144.2g / L ddH2O
0.1% SDS 10g / L ddH2O

Run 10% or 16% gel for 1:30 at 125 V

Transfer to Membrane

Get PVDF membrane from envelope; cut to the size of a gel; remove blue backing; do not touch the membrane.

Soak PVDF membrane in methanol for 2 min then transfer to a tray with western buffer

10x Western Buffer:

25mM Tris	30.3g
190mM Glycine	144.2g
ddH20	1L

1x Transfer Buffer

10x Western Buffer	100mL
Methanol	200mL
ddH20	700mL

Immerse fiber pads (4) and filter papers (2) in trays of transfer buffer. Let soak 10-30 min

Remove gel from cassette and trim off excess

Assemble blotting sandwich:

U-shaped tray
Fiber Pad
Fiber Pad
Filter Paper
SDS-PAGE gel
PVDF Membrane
Filter Paper
Fiber Pad
Fiber Pad
Flat Lid

Place in blot module (same as SDS), clamp and fill inside with transfer buffer

Fill outside of module with dH2O and run at 25V for 3 hours (can leave overnight)

Remove the PVDF membrane form the blot module

Place the membrane in a tray and block with 5% BSA in TBS-T for at least 2 hours at RT on rocker

(Alternatively, block overnight at 4°C without agitation)

TBS-T: 1:10 of 10xTBS + 1:1000 of TritonX-100

Day 2

Immunostaining

Prepare 3mL of antibody (1:200 for RhoA, 1:500 for aSMA) in 5% BSA

Cut a 15 cm^2 sheet of thermoset plastic (one side should be sealed to make a flap)

Place the PVDF membrane in the plastic flap

Seal other two sides of the thermoset plastic to make a puch
Add the antibody solution to the pouch
Press out air bubbles & seal the remaining side
Put pouch on rotator (rotate not rock) at slowest speed for 2 hours

Transfer to a tray with TBS-T and place on rocker. Change buffer every 10 min for 1 hour (6x).

Prepare 6 mL 5% BSA with secondary (mouse-HRP) at 1:2,000 (or up to 1:5,000 if background is high)

Prepare a new thermoset plastic flap, add membrane, seal two more, add buffer, remove bubbles, seal

Put pouch on rotator (rotate not rock) at slowest speed for 2 hours

Remove from pouch and transfer to tray. Wash every 10 minutes for 1 hour

Chemiluminescence

Prepare solutions

DS1: 5mL 100mM Tris, pH8.6 + 50uL Luminol + 22uL p-Coumeric Acid

DS2: 5mL 100mM Tris, pH8.6 + 3uL Hydrogen Peroxide

Luminol Stock: 0.44g in 10mL DMSO Keep dark, lasts 2-3 wk

p-Coumaic Stock 0.15g in 10mL DMSO Keep dark, lasts 2-3 wk

DO ALL OF THE FOLLOWING IN THE DARK

Drain excess buffer from membrane, add DS1 & DS2 shake 1 minute

Wrap in bag, removing air bubbles then place in developing cassette with film - do quick

Expose 1 minute to 15 minutes - longer for weak signal

Transfer to developer for 5 min- should see bands when done

Rinse in water, place in fixer until film is transparent, rinse in water again

Photograph film

Appendix I Generating Lentiviruses in T-225 flasks

Protocol version 2.0

Authors: Rahul Singh (05/27/14), Yen Kong (12/17/12)

Follow all BSL 2+ safety precautions. Do not attempt this protocol without proper training!

These lentiviral constructs require both a target protein (eGFP, T19N, Q63L, ...) and a transcription activator (M2rtTA) in order to work. **Each viral stock must be prepared separately.** So to prepare a virus for transduction **perform the protocol twice** (in parallel) for both the protein of interest and the transcription activator. Full expression is achieved by exposure to >100 ng/mL Doxycycline.

1. Plate 5 million (HEK) 293FT cells in a T-75 flask. Growth medium is DMEM + 10%FBS.
2. Grow 293FT cells for up to 48 hrs, then passage cells to a T-225 flask.

Continue to culture the cells for 24-48 hours, until 70% confluent.
Do not let the cells reach confluence in the T-225; it will abrogate virus production.

3. Prepare the plasmids in 4.5 mL unsupplemented Optimem:
    a. M2rtTA 14.5 µg (**or** eGFP, **or** T19N, **or** Q63L)
    b. PLP1 16 µg
    c. PLP2 7.6 µg
    d. PLP-VSVG 10.6 µg
4. Add 146 µL Lipofectamine2000 (L2K) to a separate tube of 4.5 mL Optimem.
5. After 5 mins, mix the L2K containing Optimem with the plasmid containing Optimem.
6. After 20 mins, change 293FT media with 25 mL of fresh DMEM + 10%FBS.
7. Add the 9 mL Optimem from (5) dropwise onto the media in the T-225 flask.

8. Change 293FT media the next day with 35 mL fresh DMEM + 10%FBS.

9. Next day, (48 hrs after transfection), collect supernatant and centrifuge at 3000 rpm, 15min, 4 deg. C. Discard the cells (treat with bleach before disposal).
10. Aliquot 1.2 mL into screw top vials and store at -80 deg. C. Aliquots will last for 6-12 months.

Appendix J Rheological Characterization of Biomaterials

Consider a simple tensile test. By Hooke's law, the mechanical resistance of a material is proportional to the elongation in response to a force. In a tension test, the sample is stretched and thereby exposed to a range of strains until it breaks. The force and extension required to do this is measured. Using a uniform, known sample geometry (e.g. dog bone) this can be converted to a stress-strain curve. The slope along some region is defined as the modulus. In a non-destructive variation of this test, the same sample can be elongated to a lesser degree, the force measured, and then returned to resting. The slope of that curve would give an approximation of the modulus. If we assume the sample is unchanged in this small loading, we could repeat this test over-and-over by applying a sawtooth elongation (strain) profile. Of course, the slope at each 'peak' is undefined. Instead we can use a sine wave for the loading profile instead of a pointy sawtooth wave. That way, we'll get a continuous slope function and a continuous estimation of the modulus. Indeed, this is dynamic mechanical analysis (DMA). We apply a sinusoidal strain to the sample (in shear this time) and we get a sinusoidal strain response back. We could perform an extension test a across large range of strains by applying a sinusoidal wave with progressively increasing amplitude, or a strain sweep.

Simple tension / compression were commonly done on hard materials, but do not work on soft materials or fluids. In the study of fluids (rheology), the mechanical resistance, or viscosity, of a fluid is proportional to the shear rate (the changes in shear stress with

respect to time) by Newton's law of viscosity. Traditionally, this was tested by applying a constant force to a fluid and measuring the velocity of the fluid. The most convenient approach is a ball-viscometer in which a steel ball is dropped into a fluid and accelerated by gravity to a constant velocity. Thus, the viscosity could be determined by measuring the velocity of the ball. For a thick fluid, this ball could take weeks to fall to an appreciable extent. Another approach to measure viscosity would be to place the fluid between parallel plates and apply a known torque to one plate and measure the rotation of the other plate. This is the essence of the parallel-pate rheometer (modern systems have one moving part). As before, we can apply a dynamic load to quickly measure the fluid's properties. However, the resistance to shear stress would be constant. Instead, we would notice a marked change in properties of the fluid to changes in shear rate, so we will apply a sinusoidal wave with varying frequency. This is known as a frequency sweep.

Now that we have a dynamic means of loading our material, we can predict how our rheometer will respond to solids and liquids. First consider a perfectly elastic material. The loading profile is a sinusoidal oscillation which goes left then right. The material instantly responds by twisting left and right thereby returning our exact sine wave to the force transducer. Form the amplitudes, we can determine the modulus. Now consider a perfect fluid under the same loading. When we twist it to the right it will flow in that direction, and some initial force will be required to start the flow but it will continue to flow without any further force. However, when we try to make it flow to the left, it will resist this change in direction. That resistance to change in flow

will be the (dynamic) viscosity of the fluid. In our force transducer, we will instead see our sine wave exactly 90 degrees out-of-phase from our input.

What about a material that is a "soft solid" or a "thick liquid" or a mixture of a solid and liquid or some sort of goo? The mechanical response of this material will be a mixture as well. It will resist force with some modulus and will resist flow with some viscosity. We will see a response somewhere in between these two extremes and we would call it "viscoelastic". Thus with a sine-wave loading, we would measure a displacement with sine wave with some degree of delay.

The delta is the delay in getting back our sine wave (0 for elastic and 90 for viscous). Whatever energy we put in loading that is not returned immediately is considered to have dissipated. So the delta also tells us how well the material dissipates energy. Looking at the magnitudes as well as the phase of the returned wave, we can determine how much of this energy has been 'stored' and returned later versus how much has been 'lost' for good. Quantifying these modes of energy dissipation are how we get the storage (G') and loss (G") moduli. We can observe how these two values change in response to various strain rates and amplitudes to learn about the structure of the material. Further, we can vary the temperature and number of cycles to learn about the thermodynamic properties. Further, we could superimpose multiple waveforms to quickly test loading conditions with one 'run'. These effects are of great interest to soft-matter physicists, rheologists, polymer scientists, and other people you'd rather avoid at parties.

Now we can derive expressions for these quantities. Consider the case of simple shear we have σ = γ*G, where sigma is the shear stress and gamma is the shear strain. They are related by a quantity called the shear modulus which describes the material under simple shear.

However, we are testing the material under oscillatory loading so our stress function looks like this: σ = σ0 cos(ωt) and the strain function looks like γ = γ0 cos(ωt - δ) with ω being the angular frequency and δ being the phase delay. The modulus would still be the ratio of the stress and strain: σ/γ = [σ0 cos(ωt)] / [γ0 cos(ωt - δ)] which we can re-write using Euler's formula as σ/γ = [σ0 exp(iωt)] / [γ0 exp(iωt) exp(-iδ)] = σ0/γ0 [exp(iδ)] or back to trig notation: σ0/γ0 [cos(δ) + i sin(δ)] thus our modulus is complex (hence, "complex modulus") and defined as G* = σ0/γ0 [cos(δ) + i sin(δ)] further if we define G' = σ0/γ0 cos(δ) as the "storage modulus" and G'' = σ0/γ0 sin(δ) as the "loss modulus" we get: G* = G' + iG'' finally, we can look at the total dissipation by taking the magnitude: |G*| = sqrt(G'^2 + G''^2) = σ/γ this is the absolute shear modulus and is analogous to the shear modulus, G, under simple shear.

Likewise, if we consider the viscosity σ = η dγ/dt we can derive a similar relation for sinusoidal loading. Specifically, dγ/dt = iωγ so we end up with the relation σ0/iωγ0 exp(i δ). This is the complex viscosity η* = iG'/ω + G''/ω = iη'' + η' note, this is the conjugate of the modulus with the "dynamic viscosity": η' = G''/ω and the "out-of-phase viscosity" η'' = G'/ω. Likewise we can take the magnitude as: |η*| = sqrt(η'^2 + η''^2). However, |η*| is not the total viscous dissipation; rather, it is the total resistance to changes in velocity. While G' and |G*| are largely interchangeable for small δ, η' and |η*| are not

since the complex portion of η* includes the out-of-phase term which is realistically the compliance of *reversing* the flow.

Now knowing the physical framework of DMA, we can design tests to study common bioengineering materials. Many biologic materials have a response known as "strain hardening" (or strain stiffening) wherein the modulus increases as a function of strain magnitude. This arises from the multiscale (often fibrillar) structure of the materials. In a simple tension test, this will cause a 'J-shaped' strain response. This is commonly seen in fibrin clots and to a lesser degree in collagen gels and is a form of hyper-elasticity. PEG hydrogels do not behave in this manner. They are linear-elastic and will not undergo significant strain dependent effects. In a simple tension test this means that the slope will be constant with respect to strain until it begins to yield and fail. Polymer melts (or dense solutions) will also have strain dependent effects wherein they tend to soften at high strain magnitudes. This effect is known as a form of plasticity. It is caused by polymer chains sliding past one another. The presence of cross-links in the polymer will tie the material together and prevent such sliding. PEG gels are highly crosslinked and thus do not behave like polymer solutions either. Thus, by applying a strain sweep, we can draw conclusions about the microstructure form the modulus. A fibrillar structure will strain harden, a crosslinked gel will remain constant, and an un-crosslinked solution will strain-soften.

All biologic materials display some degree of viscoelasticity. This is due to plastic deformations that occur during loading. In a fibrous matrix, this is due to displacements of the fibers. Fibers can move in affine (shape preserving) or non-affine modes. In an affine deformation, the fibers elongate, bend, rotate, or translate *as a rigid body*. In a non-affine deformation fibers move independently by sliding past each other. Naturally, crosslinking the fibers together will prevent sliding. Remarkably, the fibers can re-organize in response to stresses. De-polymerization of actin and collagen filaments has been observed wherein they adapt to loadings by permanently elongating. Further introducing inter-fibrillar crosslinking will prevent this effect, and for each fibrous material there is an enzyme whose role is to do this. PEG hydrogels, are by nature, highly crosslinked and will not display viscoelasticity in the same manner as fibers. Instead, their viscous properties are largely attributable to the bulk flow of water. These materials exist in an equilibrium wherein the osmotic pressure of solvating the polymer is balanced by the mechanical tension of the crosslinked polymer chains. Adding mechanical loading will *decrease* the tension in the polymer network, decrease the polymer's interaction with the water, and decrease the osmotic pressure thus forcing water out of the gel. Naturally, an excessive force will break the polymer network and the material will be able to engorge more water. Remarkably, a PEG hydrogel with many 'dangling ends' will have a surprising ability to flow despite a high modulus simply by shifting this physiochemical equilibrium. Finally, a dense polymer solution or melt will have predictable viscous properties. It will flow - eventually. These materials behave like supercooled fluids and will undergo a phase transition wherein they suddenly begin to flow. To trigger this change, the solution needs to be heated past its glass transition,

or it needs to be sheared at a sufficiently high rate. This is in accordance with time-temperature superposition theory.

But what will the shear-rate, or frequency response, of the other materials tell us? For fibrous materials, the frequency response will have multiple regions depending on the bending modes of the network. At extremely low frequencies, the intermolecular forces holding the fibers will dissipate energy, but this is difficult to do experimentally with a rheometer. At intermediate frequencies, the material will show another region wherein the bending modes of fibers dissipate energy. At higher frequencies, the materials stiffen as they cannot respond to the load quickly enough to dissipate energy. For a weakly-crosslinked fibrous material, the non-affine motions will manifest as a softening at higher frequencies and eventual 'failure' of the material as it begins to flow. This may or may not be reversible depending on whether the crosslinks are reversible. For a PEG hydrogel the frequency response has two regions. At low frequencies, the bulk flow of water predominates, and the material flows easily. At higher frequencies, water cannot flow fast enough out of the gel to reestablish equilibrium. This pressurizes the gel applies more stress on the polymer network. Thus, the bending modes of the polymer network dominate and the gel stiffens. Note that this is the *opposite* of what happens to a uncrosslinked polymer solution. Thermodynamically this is driven by the entropy of the polymer-solvent interaction.

In conclusion, rheology can reveal much about the physical properties of a material beyond how stiff it is. Designing a test to interrogate the strain and frequency dependent behavior of a material can shed light on unique properties of the

microstructure of the material. These structural properties can, in turn, further the understating of biologic studies.

Appendix K Brief Introductory Guide to Operation of a TA AR-G2 Rheometer

Adapted from Protocol by Fred Mazzeo, Ph.D. TA Instruments

1. Turn on the air supply (house air) and ensure the pressure is 30 psi. Air will be leaving the regulator. Close the blue valve connecting the pressure regulator to the rheometer.
2. Turn on the rheometer power supply (silver box). Wait 1 minute for system to initialize. If the machine starts beeping, turn off the power and proceed to step 3. Then turn the power back on.
3. Remove the black bearing lock by holding it in place and turning the draw rod knob on top counter-clockwise. Doing this without adequate air supply will damage the instrument.
4. Ensure the water supply is turned on (same supply as rheometer). Ensure the tank is filled with distilled water and clean. Do not add "clear bath" as this corrodes the pump. If adequate water flow is not maintained, the stage will not cool below 15°C. If this occurs, turn off the machine, and clean out the lines and connectors to the peliter stage - they get clogged with lint.
5. Turn on the TA "AR instrument control" software. This only runs on Windows XP, so don't mess with the OS.
6. Look at the "instrument status page" and ensure that communication has been established. The status variables will be live and changing.
7. Select bearing type. Select *Instrument > set bearing mode*. For hydrogels or fibrin clots select 'soft' for dense gels or polymer melts choose 'hard' the cutoff is about G=10,000 Pa.
8. Determine the instrument inertia by selecting *Options>Instrument>Inertia* and press the 'Calibrate' button. An acceptable range for this value is ~17-19 μNms^2
9. Attach test geometry* by sliding it up the drive shaft and hold it stationary while **turning the draw rod knob** at the top in a clockwise direction. If the geometry file was previously created, choose the appropriate geometry (Geometry>Open…), or create a new geometry by selecting Geometry>New, and follow the New Geometry dialogue window.
   **If applying sandpaper do this now, before calibrating the machine.*
10. Calibrate the geometry inertia by pressing the 'Calibrate' button that is found in the Geometry Page >Settings>Inertia: Calibrate. It is important to calibrate the inertia value for every geometry, particularly if high frequency oscillations are being used, or if low viscosity fluids are being measured.
11. Bearing friction correction: *Options>Instrument>Miscellaneous*, check the '*bearing friction correction*' box and press the '*Calibrate*' button. A magnetic bearing is used to float the drive shaft. It contributes ~1% of a low viscosity sample's torque and an acceptable value is between ~0.25-0.3 $\mu N\ mrad^{-1}s$
12. Peltier stage temperature. *Options>Instrument>Temperature* Set the stage to the experimental temperature and wait for equilibration.

13. Zero the geometry gap: *Instrument>Gap>Zero Gap* and follow the directions on screen. Ensure the upper plate is heated to the same temperature as the lower plate. This can be done by pacing them 10 μm apart for a couple minutes.
14. Gap compensation. If testing over a temperature range, it is important to determine this value. Once determined, the value can be re-used between experiments with he same set-up. *Geometry Page > Settings > Gap Temperature Compensation: Calibrate*
15. Mapping (Calibrations)
    a. Rotational Mapping: The instrument will rotate through one revolution and compensate for discrepancies in the optical encoder. Go to *Instrument > Rotational Mapping* select a default of TWO iterations on STANDARD. If making low-torque measurements then use 'precision'. If performing Creep experiments, use four iterations. Setting iterations greater than three has diminishing returns.
    b. Oscillation Mapping: Performs baseline subtraction only when running continuous controlled strain mode and will improve performance for low torque, low displacement data. Go to *Instrument > Oscillatory mapping* Up to 10 mappings can be stored and the software will pick the closest to the experimental procedure automatically. Otherwise, enter parameters that span the experimental procedure about to be run.
16. Procedure: Create a new procedure by selecting *Procedure > New* or open one
17. Experimental notes: *Notes > New* These are embedded in the data file for recovery later on.
18. Sample loading: The amount of sample volume that is required, based on the dimensions entered in the *Geometry page>Dimensions* tab for cone, parallel and concentric cylinder systems, can be found in *Geometry page>Settings: Approximate sample volume*.
    a. For a solution, set the gap to the appropriate value then engage the bearing lock and pipette the sample between parallel plates. To prevent drying, add a solvent trap of mineral oil around the top plate.
    b. For a pre-cast hydrogel, place the gel below the upper plate and slowly lower it to make contact with the gel. Either run all samples with a uniform compression (Normal force) or at a uniform gap. Use buffer as a solvent trap, a puddle can be made on the lower stage.
19. Gap closure: *Instrument > gap > enter gap*
20. Run test: *Experiment > run* It will prompt for a saving location.

Cleaning up

21. Do not use solvents on the lower stage - this will damage the seals. Ethanol and water will remove most samples.
22. All settings can be conveniently saved with *File > Save session* and re-loaded prior to calibration (step 7) in the future.
23. Close the rheology software.
24. Loosely attach the black bearing lock by holding it in place and turning the draw rod knob on top clockwise. Spindle should still freely rotate. If the rheometer will be moved, tighten this fully.
25. Turn off the power supply

26. Open the blue air valve to let air bypass the rheometer. Turn off air supply valve. To view data offline use 'TA Data Analysis' - there are a staggering amount of help files and tutorials in here.

Appendix L MATLAB Code for particle tracking

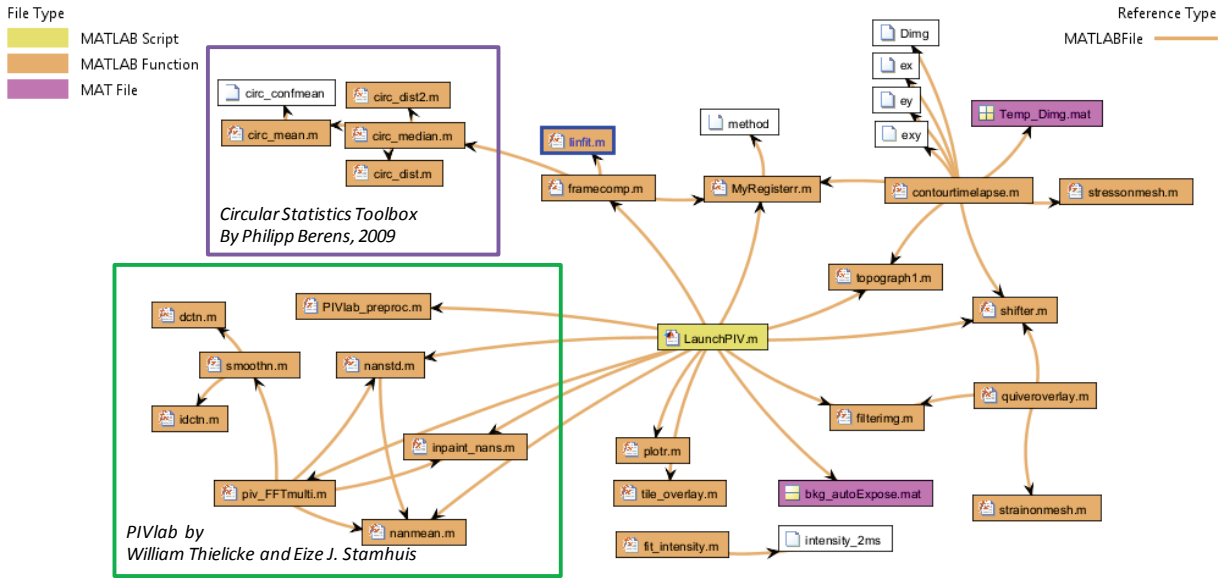

Figure 47: Overview of file dependencies in image processing and PIV algorithm.

This appendix is an overview of PIV analysis program as of 02/16/15. Scripting was performed in MATLAB r2014b with image processing, curve fitting, statistics, neural network, and parallel computing toolboxes. This application is built around PIVlab - Digital Particle Image Velocimetry Tool for MATLAB developed by Dipl. Biol. William Thielicke and Prof. Dr. Eize J. Stamhuis programmed with MATLAB 7.1.0.246 (R14) Service Pack 3 (August 02, 2005) on March 09, 2010. Additionally, this app uses the Circular Statistics Toolbox for Matlab By Philipp Berens, 2009. These files are freely available online with a BSD license and are not included in this appendix. The LaunchPIV script converts image pairs in the current directory into a .mat file which contains the aligned image. Contourtimelapse.m compiles the image pairs and computes stress and strain vectors. Quiveroverlay produces plots of stress and strain overlaid on image files. Other files support these three core files.

```
function contourtimelapse
%     make_files

%     [Dsmooth, shift_log, img] = load_files;
%     [Dimg] = align_stack(Dsmooth, shift_log, img);
%     save('Temp_Dimg.mat', 'Dimg')

    load('Temp_Dimg.mat', 'Dimg')
    DimgC = crop(Dimg);
    draw_plot(DimgC)
end

function make_files
%%Generate the filtered strain maps from stored files and save
(manually)
    a = dir;
    loc = cellfun(@(x) (regexp(x,'fixmask')), {a.name},
'UniformOutput', false);
    indx = cellfun(@(x) ~isempty(x), loc);
    b = {a(indx).name};
    for ind = 1:length(b)
        display(['Loading file: ' b(3) '  ...']);
        S = load(b(3));
        x = S.x; y = S.y; u_filt = S.u_filt; v_filt = S.v_filt;
        shift_log = S.shift_log;
        % create a maximum intensity projection for later
aligment
        img = max(S.img{1}{5},S.img{1}{4});
        display('   Computing strains & stresses');
%         [ex, ey, exy] = strainonmesh(x, y, u_filt,v_filt);
%         D{1} = abs(sqrt(ex{1}.^2 + ey{1}.^2));
        [sx, sy, sxy] = stressonmesh(ex, ey, exy, 1);
        D{1} = sx{1}; D{2} = sy{1}; D{3} = sxy{1};
        ext{1} = '_s1'; ext{2} = '_s2'; ext{3} = '_theta';
        for indp = 1:3
            display('   Generating image');
            [Xq,Yq] = meshgrid(1:2048,1:2048);
            Di = interp2(x{1},y{1},D{indp},Xq, Yq, 'cubic');
            n = 16*4; %interpolation is 16px, so want to span
multiple original points
            % h = 1/(n^2)*ones(n);
            % h = fspecial('gaussian',n,0.75);
            % Dsmooth = filter2(h,Di);
            Dsmooth = wiener2(Di,[n,n]);
            figure
    %         contour(Dsmooth, [0.1], 'r') %0.1 good for strain
and 5 good for stress
```

```
    %         set(gca,'ydir','reverse')
            if indp < 3
                imagesc(Dsmooth, [0, 7000])
            else
                imagesc(Dsmooth, [-45, 45])
            end
            colorbar
            print(gcf, ['g4f', num2str(ind), ext{indp}], '-
dpng', '-r200');
            if indp == 1
            save(['g4f',
num2str(ind)],'Dsmooth','shift_log','x', 'y',
'u_filt','v_filt','img')
            end
        end
        display('   Done!')
        close all
    end
end

function [Dsmooth, shift_log, img] = load_files
    %Load the files you manually generated
    a = dir;
    loc1 = cellfun(@(x) (regexp(x,'g4f')), {a.name},
'UniformOutput', false);
    indx1 = cellfun(@(x) ~isempty(x), loc1);
    loc2 = cellfun(@(x) (regexp(x,'.mat')), {a.name},
'UniformOutput', false);
    indx2 = cellfun(@(x) ~isempty(x), loc2);
    indx = indx1 & indx2;
    b = {a(indx).name};
    %clear a loc ind
    Dsmooth = cell(length(b),1);
    shift_log = cell(length(b),1);
    img = cell(length(b),1);
    for ind = 1:length(b)
        S = load(b(3));
        Dsmooth(3) = S.Dsmooth;
        shift_log(3) = S.shift_log;
        img(3) = S.img;
    end
end

function [Dimg] = align_stack(Dsmooth, shift_log, img)
    %align the image stack
    Dimg = cell(length(Dsmooth),1);
    Mimg = cell(length(Dsmooth),1);
```

```
    Dimg{1} = Dsmooth{1};
    Mimg{1} = img{1};
    for ind = 1:(length(Dsmooth)-1)
        display(['Aligning stack - Image #' num2str(ind)])
        Theta = sum(shift_log{ind+1}(:,3));
        if ind == 1
            Ds2 =
imrotate(Dsmooth{ind+1},Theta,'nearest','crop');
            DsM = imrotate(img{ind+1},Theta,'nearest','crop');
        else
            DrTmp = shifter(Dimg(3), Dsmooth{ind+1}, [0, 0
,Theta], 0);
            Dimg(3) = DrTmp{1};
            Ds2 = DrTmp{2};

            MrTmp = shifter(Mimg(3), img{ind+1}, [0, 0 ,Theta],
0);
            Mimg(3) = MrTmp{1};
            DsM = MrTmp{2};
        end
        topores = 3;
        [m, n] = size(img(3));
        [Mm, Mn] = size(DsM);
        mi = [floor(Mm/2+1)-floor(m/2):floor(Mm/2)+floor(m/2)];
        ni = [floor(Mn/2+1)-floor(n/2):floor(Mn/2)+floor(n/2)];
        mapBt = topograph1(DsM(mi,ni), topores);
        if ind == 1
            for indt = 1:5
                if indt == 1
                    mapAt = topograph1(img(3), topores);
                else
                    [m, n] = size(img(3));
                    [Mm, Mn] = size(MiTmp{2});
                    mi = [floor(Mm/2+1)-
floor(m/2):floor(Mm/2)+floor(m/2)];
                    ni = [floor(Mn/2+1)-
floor(n/2):floor(Mn/2)+floor(n/2)];
                    mapAt = topograph1(MiTmp{2}(mi,ni), 3);
                end
                [Dx, Dy, Dt] = MyRegisterr(mapAt, mapBt, 0, 1);
                DiTmp = shifter(Dsmooth(3), Ds2, [Dx, Dy, Dt],
0);
                MiTmp = shifter(img(3), DsM, [Dx, Dy, Dt], 0);
            end
        else
            for indt = 1:5
                if indt ==1
```

```
                    [m, n] = size(img(3));
                    [Mm, Mn] = size(Mimg(3));
                    mi = [floor(Mm/2+1)-
floor(m/2):floor(Mm/2)+floor(m/2)];
                    ni = [floor(Mn/2+1)-
floor(n/2):floor(Mn/2)+floor(n/2)];
                    mapAt = topograph1(Mimg(3)(mi,ni), topores);
                else
                    [m, n] = size(img(3));
                    [Mm, Mn] = size(MiTmp{2});
                    mi = [floor(Mm/2+1)-
floor(m/2):floor(Mm/2)+floor(m/2)];
                    ni = [floor(Mn/2+1)-
floor(n/2):floor(Mn/2)+floor(n/2)];
                    mapAt = topograph1(MiTmp{2}(mi,ni), 3);
                end
                [Dx, Dy, Dt] = MyRegisterr(mapAt, mapBt, 0, 1);
                DiTmp = shifter(Dimg(3), Ds2, [Dx, Dy, Dt], 0);
                MiTmp = shifter(Mimg(3), DsM, [Dx, Dy, Dt], 0);
            end
        end
        if ind == 1
            Dimg{1} = DiTmp{1};
            Mimg{1} = MiTmp{1};
        end
        Dimg{ind+1} = DiTmp{2};
        Mimg{ind+1} = MiTmp{2};
    end
end

function  DimgC = crop(Dimg)
    [mx, nx] = size(Dimg{1});
    %Quick and dirty cropping - NEED BETTER ALIGMENT - fix
shifter?
    DimgC = cellfun(@(x) x(1:mx,1:nx), Dimg, 'UniformOutput',
false);
    for ind = 1:length(DimgC)
        DimgC(3)(DimgC(3)<0.01) = NaN;
    end
end

function draw_plot(DimgC)
    display('Overlaying plots...')
    cmap = colormap(jet(7)); close(gcf)
    figure
    hold on
    for ind = 1:length(DimgC)
```

```
        [~, hc1] = contour(DimgC(3), [0 200], 'k');
        nc1 = get(hc1, 'Children');
        set(nc1,'EdgeColor',cmap(ind,:))
    end

    hh = get(gca,'children');
    set(hh, 'LineWidth',2)
    set(gca,'ydir','reverse')
    colormap(jet(7));
    colorbar
    colorbar('yticklabel',{'D1','D2','D3','D4','D5','D6','D7'})
    print(gcf, 'Contour', '-dpng', '-r400');
end
% [~, hc1] = contour(Dimg{1}, [0.1], 'k');
% nc1 = get(hc1, 'Children');
% set(nc1,'EdgeColor',cmap(1,:))
%
% [~, hc2] = contour(Dimg{2},[0.1],'g');
% nc2 = get(hc2, 'Children');
% set(nc2,'EdgeColor',cmap(3,:))
% % save('g4f5','Dsmooth')
%
% % Dimg = shifter(Dsmooth, Dsmooth2, shift_log(1,:), 0);
% % for ind = 2:size(shift_log,1)
% %     Dimg = shifter(Dimg{1}, Dimg{2}, shift_log(ind,:), 0);
% % end
%
```

```
function [sx, sy, sxy] = stressonmesh(ex, ey, exy, ps)
% Operates on outputs form strainonmesh
% Uses Hooke's law for plane stress (thin plates)
frames = length(ex);
sx = cell(frames,1);
sy = cell(frames,1);
sxy = cell(frames,1);

nu = 0.49;
G = 334;
mMat = [1-nu, nu, 0;
        nu, 1-nu, 0;
        0, 0, (1-2*nu)];
E = 2*G*(1+nu);
a = E/((1-2*nu)*(1+nu));

for ind = 1:frames
    [m, n] = size(ex(3));
    [S] = a.*mMat*[ex(3)(:), ey(3)(:), exy(3)(:)]';
    sx(3) = reshape(S(1,:),m,n);
    sy(3) = reshape(S(2,:),m,n);
    sxy(3) = reshape(S(3,:),m,n);

end

if ps == 1
    ps1 = cell(frames,1);
    ps2 = cell(frames,1);
    th = cell(frames,1);

    for ind = 1:frames
%         sx(3) = abs(sx(3));
%         sy(3) = abs(sy(3));
%         sxy(3) = abs(sxy(3));
%
        A = (sx(3)+sy(3))./2;
        B = sqrt(((sx(3)-sy(3))./2).^2+sxy(3).^2);
        ps1(3) = abs(A+B);
        ps2(3) = abs(A-B);
        th(3) = real(0.5.*atand(2.*sxy(3)./(sx(3) - sy(3))));
    end
    sx = ps1;
    sy = ps2;
    sxy = th;
end
```

```
function [mapA] = topograph1(imgA, lineres)
%load the image
imgA = uint8(imgA);
% imgB = uint8(imgB);

% Intensity capping & re-map
imgA(imgA > 155) = 155;
% imgB(imgB > 155) = 155;
imgA = imadjust(imgA);
% imgB = imadjust(imgB);

mapA = uint8(zeros(size(imgA,1),size(imgA,2)));
% mapB = uint8(zeros(size(imgA,1),size(imgB,2)));

roll = [10, 50, 100, 200, 300];
roll = roll(roll>5*lineres);
dI = uint8(floor(255./length(roll)));
% level = 0.2;
for ind = 1:length(roll)
    backgroundA = imopen(imgA,strel('disk',roll(ind)));
%     backgroundB = imopen(imgB,strel('disk',roll(ind)));

%     bwA = im2bw(backgroundA,level);
%     bwB = im2bw(backgroundB,level);
    EDA = edge(backgroundA, 'sobel');
    OLA = uint8(255*imdilate(EDA,strel('disk',lineres)));
%     OLB = uint8(255*imdilate(edge(backgroundB,
'canny'),strel('disk',lineres)));

%     bwA2 = imdilate(bwA,strel('disk', 150, 4)).*(~bwA);
%     bwB2 = imdilate(bwB,strel('disk', 150, 4)).*(~bwB);

%     OLA2 = uint8(255*imdilate(edge(bwA2),strel('disk',10)));
%     OLB2 = uint8(255*imdilate(edge(bwB2),strel('disk',10)));

    mapA = mapA + OLA./255.*dI;
%     mapB = mapB + OLB./255.*dI;
end
```

```
% RegisterFourierMellin see RegisterFM (Register.m) for comments
/ attrubutation

function [Tx, Ty, Theta, img] = MyRegisterr(I1, I2, showpic,
shift_limit)
% only genreates an img if showpic is true; use shifter.m to
shift images around.
if nargin < 4;
    shift_limit = 0;
end
% convert all NaN to 0
I1(isnan(I1))=0;
I2(isnan(I2))=0;
    % MAXIMUM SHIFTS ARE LIMITED!!! tp +/-5% in x & y
    %   Set thresholds to 30deg rotation and 10% shift in x or y

    % dx is the sub-sampleing region
    % showpic is logical to show the overlayed images
    % I1 and I2 are uint8 images (not filenames this version
doesn't load
    % images from the disk)

    % Convert both to FFT, centering on zero frequency component
    SizeX = size(I1, 1);
    SizeY = size(I1, 2);

    FA = fftshift(fft2(I1));
    FB = fftshift(fft2(I2));

    % Output (FA, FB)
    % -------------------------------------------------------------
-----------
    % Convolve the magnitude of the FFT with a high pass filter)
    IA = hipass_filter(size(I1, 1),size(I1,2)).*abs(FA);
    IB = hipass_filter(size(I2, 1),size(I2,2)).*abs(FB);
    % TO see the fourier-space images:
    % imshow(log10(abs(IA)),[1 7])

    % Transform the high passed FFT phase to Log Polar space
    L1 = transformImage(IA, SizeX, SizeY, SizeX, SizeY,
'nearest', size(IA) / 2, 'valid');
    L2 = transformImage(IB, SizeX, SizeY, SizeX, SizeY,
'nearest', size(IB) / 2, 'valid');
clear IA IB
%     a1 = L1';
%     a2 = L2';
% %     ThetaCorr = normxcorr2(a1,a2);
```

```
% %     [max_c, imax] = max(abs(ThetaCorr(:))); %max_c=1 means
the img a contain img b (overlapping)
% %     [Theta, Phi] = ind2sub(size(ThetaCorr),imax(1));
%
%     % Try MATLAB's Cross-power function
%     win = size(a1,2);
%     fs = win^2;
% %     [Pxy, F] =
mscohere(a1(:),a2(:),hamming(win*50),win*40,win,fs);
%     [Pxy, F] = mscohere(a1(end:-1:(length(a1(:))-
100*win)),a2(end:-1:(length(a2(:))-
100*win)),hamming(floor(1/4*win)),[],180);
% %     plot(F,Pxy)
% %     Pxy_trunc = [Pxy(1:floor(win/10)); zeros(length(Pxy)-
2*floor(win/10)-1,1); Pxy((length(Pxy)-floor(win/10)):end)];
%     %rotations are not that big (but can be negative)
%     [pks,loc] = findpeaks(Pxy,'Threshold',0.1);
%     if numel(loc) > 0
%         THETA_Y = loc(1);
%     else
%         [~, THETA_Y] = max(Pxy(2:end));
%     end
%     DPP = 180 / pi;
%     Theta = DPP * (F(THETA_Y) - 0);
% if ~exist('Theta', 'var')
% Convert log polar magnitude spectrum to FFT
    THETA_F1 = fft2(L1);
    THETA_F2 = fft2(L2);

% Compute cross power spectrum of F1 and F2
    a1 = angle(THETA_F1);
    a2 = angle(THETA_F2);

    THETA_CROSS = exp(1i * (a1 - a2));
    THETA_PHASE = real(ifft2(THETA_CROSS));

    % Find the peak of the phase correlation
%     THETA_SORTED = sort(THETA_PHASE(:));  % TODO speed-up, we
surely don't need to sort
%     SI = length(THETA_SORTED):-1:(length(THETA_SORTED)-100);
%     for ind = 1:length(SI)
%         [THETA_X(ind), THETA_Y(ind)] = find(THETA_PHASE ==
THETA_SORTED(SI(ind)));
%     end
    [THETA_X, THETA_Y] = find(THETA_PHASE ==
max(max(THETA_PHASE)));
%     % Compute angle of rotation
```

```
    DPP = 360 / size(THETA_PHASE, 2);
    Theta = DPP * (THETA_Y - 1);
    % Rotations are not big, so wrap to [0, 90]
    Tvec = (repmat(Theta,1,5) - repmat([0 90 180 270
360],length(Theta),1));
    [~, Tin] = min(abs(Tvec),[],2);
    Theta = Tvec(Tin);
%     theta_w = Theta_d';
%     theta_w = min(abs(repmat(theta_w,1,5) - repmat([0 90 180
270 360],length(theta_w),1)),[],2);
%     Theta = circ_mean(theta_w(theta_w < 30));
%     s = sinfit(THETA_PHASE);
%     Theta = s(2)/(2*pi)*360;
    % Output (Theta)
    % ------------------------------------------------------------
-----------
% cut out the +/- 180 test since images NEVER flip
    % Rotate image back by theta and theta + 180
% end
    R = imrotate(I2, -Theta, 'nearest', 'crop');
%     R2 = imrotate(I2,-(Theta + 180), 'nearest', 'crop');
%
%     % Output (R1, R2)
    % ------------------------------------------------------------
-----------

    % Take FFT of R1
    R1_F2 = fftshift(fft2(R));

    % Compute cross power spectrum of R1_F2 and F2
    a1 = angle(FA);
    a2 = angle(R1_F2);
%     a1 = abs(FA);
%     a2 = abs(FR);
%     c = a1*conj(a2)
%     c = xcorr2(a1,a2);
%     [~, imax] = max(abs(c(:))); %max_c=1 means the img a
contain img b (overlapping)
%     [y, x] = ind2sub(size(c),imax(1));
    R1_F2_CROSS = exp(1i * (a1 - a2)); %quick and dirty way to
cmpoute cross-correlation
    R1_F2_PHASE = real(ifft2(R1_F2_CROSS));
%     h = fspecial('disk', 16); FD = filter2(h, R1_F2_PHASE);
%imagesc(FD);
if shift_limit == 0;
    [y, x] = find(((R1_F2_PHASE) == max(max((R1_F2_PHASE)))));
else
```

```
%         R = R1;
    win = floor(size(a1,2)./20);
    phaseclip = zeros(size(a1,1),size(a1,2));
    phaseclip(1:win,1:win) = R1_F2_PHASE(1:win,1:win);
    phaseclip(1:win,(end-win):end) = R1_F2_PHASE(1:win,(end-
win):end);
    phaseclip((end-win):end,1:win) = R1_F2_PHASE((end-
win):end,1:win);
    phaseclip((end-win):end,(end-win):end) = R1_F2_PHASE((end-
win):end,(end-win):end);
    [y, x] = find(((phaseclip) == max(max((phaseclip)))));
end
%     [Pshfty, Fshfy] =
mscohere(a1(:),a2(:),hamming(win*5),win*4,win,win*2);
%     [~, Iy] = max(Pshfty(1:floor(win/10))); %rotations are not
that big
%     y = Fshfy(Iy);
%     a1 = a1';
%     a2 = a2';
%     [Pshftx, Fshfx] =
mscohere(a1(:),a2(:),hamming(win*5),win*4,win,win*2);
%     [~, Ix] = max(Pshftx(1:floor(win/10))); %rotations are not
that big
%     x = Fshfx(Ix);
%     DPP = 360 / win;
%     Theta = DPP * (F(THETA_Y) - 1);

    % ---------------------------------------------------------
-----------

    % Ensure correct translation by taking from correct edge
    % Translation is Frame1 - Frame2 (for plotter script) so '-'
is right
    Tx = x - 1;
    Ty = y - 1;
%
    if (x > (size(I1, 2) / 2))
        Tx = Tx - size(I1, 2);
    end

    if (y > (size(I1, 1) / 2))
        Ty = Ty - size(I1, 1);
    end
if showpic == 1
    % ---------------------------------------------------------
-----------
    % FOLLOWING CODE TAKEN DIRECTLY FROM fm_gui_v2
```

```
    % Combine original and registered images

    input2_rectified = R; move_ht = Ty; move_wd = Tx;

    total_height =
max(size(I1,1),(abs(move_ht)+size(input2_rectified,1)));
    total_width =
max(size(I1,2),(abs(move_wd)+size(input2_rectified,2)));
    combImage = zeros(total_height,total_width); registered1 =
zeros(total_height,total_width); registered2 =
zeros(total_height,total_width);

    % if move_ht and move_wd are both POSITIVE
    if((move_ht>=0)&&(move_wd>=0))
        registered1(1:size(I1,1),1:size(I1,2)) = I1;

registered2((1+move_ht):(move_ht+size(input2_rectified,1)),(1+mo
ve_wd):(move_wd+size(input2_rectified,2))) = input2_rectified;
    % if translations are both NEGATIVE
    elseif ((move_ht<0)&&(move_wd<0))

registered2(1:size(input2_rectified,1),1:size(input2_rectified,2
)) = input2_rectified;

registered1((1+abs(move_ht)):(abs(move_ht)+size(I1,1)),(1+abs(mo
ve_wd)):(abs(move_wd)+size(I1,2))) = I1;
    elseif ((move_ht>=0)&&(move_wd<0))

registered2((move_ht+1):(move_ht+size(input2_rectified,1)),1:siz
e(input2_rectified,2)) = input2_rectified;

registered1(1:size(I1,1),(abs(move_wd)+1):(abs(move_wd)+size(I1,
2))) = I1;
    elseif ((move_ht<0)&&(move_wd>=0))

registered1((abs(move_ht)+1):(abs(move_ht)+size(I1,1)),1:size(I1
,2)) = I1;

registered2(1:size(input2_rectified,1),(move_wd+1):(move_wd+size
(input2_rectified,2))) = input2_rectified;
    end
    % Plant the FIRST Image and shift the next (change form
original)
    % This puts Frame A below Frame B
```

```
    % % % find the image with the greater number of zeros - we
shall plant that one and then bleed in the other for the
combined image
%     if sum(sum(registered1==0)) > sum(sum(registered2==0))
%         plant = registered1;    bleed = registered2;
%     else
%         plant = registered2;    bleed = registered1;
%     end

    img = cell(1,3);
    img{1} = registered1;
    img{2} = registered2;
    img{3} = combImage;
else
    img = cell(1,3); %return an empty array
end

    % Show final image
    if showpic == 1
        imgRGB = cat(3, combImage, combImage, combImage);
                mx1 = max(max(img{1}));
        mx2 = max(max(img{2}));
        for p=1:total_height
            for q=1:total_width
                if (combImage(p,q)==0)
                    imgRGB(p,q,1) = img{1}(p,q)./mx1;
                    imgRGB(p,q,2) = img{2}(p,q)./mx2;
                end
            end
        end
        img{3} = combImage;

        figure
        imshow(imgRGB);

%         combImage = plant;
%         for p=1:total_height
%             for q=1:total_width
%                 if (combImage(p,q)==0)
%                     combImage(p,q) = bleed(p,q);
%                 end
%             end
%         end
%         img{3} = combImage;

%         figure
%         title('Cross-power spectra')
```

```
% %         subplot(3,1,1)
%             plot(F.*DPP,Pxy)
%             xlabel('Theta')
%         subplot(3,1,2)
%             plot(Fshfy, Pshfty)
%             xlabel('y shift')
%         subplot(3,1,3)
%             plot(Fshfx, Pshftx)
%             xlabel('x shift')

%         figure
%         imshow(combImage, [0 255]);
%         figure
%         subplot(1,2,1)
%         imshow(registered1, [0 255])
%         title('Frame A')
%         subplot(1,2,2)
%         imshow(registered2, [0 255])
%         title('Frame B')
    end




% ------------------------------------------------------------
-------
% Performs Log Polar Transform

function [r,g,b] = transformImage(A, Ar, Ac, Nrho, Ntheta,
Method, Center, Shape)

% Inputs:   A       the input image
%           Nrho    the desired number of rows of transformed
image
%           Ntheta  the desired number of columns of transformed
image
%           Method  interpolation method
(nearest,bilinear,bicubic)
%           Center  origin of input image
%           Shape   output size (full,valid)
%           Class   storage class of A

global rho;

theta = linspace(0,2*pi,Ntheta+1); theta(end) = [];

switch Shape
```

```
case 'full'
    corners = [1 1;Ar 1;Ar Ac;1 Ac];
    d = max(sqrt(sum((repmat(Center(:)',4,1)-corners).^2,2)));
case 'valid'
    d = min([Ac-Center(1) Center(1)-1 Ar-Center(2) Center(2)-
1]);
end
minScale = 1;
rho = logspace(log10(minScale),log10(d),Nrho)';  % default 'base
10' logspace - play with d to change the scale of the log axis

% convert polar coordinates to cartesian coordinates and center
xx = rho*cos(theta) + Center(1);
yy = rho*sin(theta) + Center(2);

if nargout==3
  if strcmp(Method,'nearest'), % Nearest neighbor interpolation
    r=interp2(A(:,:,1),xx,yy,'nearest');
    g=interp2(A(:,:,2),xx,yy,'nearest');
    b=interp2(A(:,:,3),xx,yy,'nearest');
  elseif strcmp(Method,'bilinear'), % Linear interpolation
    r=interp2(A(:,:,1),xx,yy,'linear');
    g=interp2(A(:,:,2),xx,yy,'linear');
    b=interp2(A(:,:,3),xx,yy,'linear');
  elseif strcmp(Method,'bicubic'), % Cubic interpolation
    r=interp2(A(:,:,1),xx,yy,'cubic');
    g=interp2(A(:,:,2),xx,yy,'cubic');
    b=interp2(A(:,:,3),xx,yy,'cubic');
  else
    error(['Unknown interpolation method: ',method]);
  end
  % any pixels outside , pad with black
  mask= (xx>Ac) | (xx<1) | (yy>Ar) | (yy<1);
  r(mask)=0;
  g(mask)=0;
  b(mask)=0;
else
  if strcmp(Method,'nearest'), % Nearest neighbor interpolation
    r=interp2(A,xx,yy,'nearest');
  elseif strcmp(Method,'bilinear'), % Linear interpolation
    r=interp2(A,xx,yy,'linear');
  elseif strcmp(Method,'bicubic'), % Cubic interpolation
    r=interp2(A,xx,yy,'cubic');
  else
    error(['Unknown interpolation method: ',method]);
  end
  % any pixels outside warp, pad with black
```

```
  mask= (xx>Ac) | (xx<1) | (yy>Ar) | (yy<1);
  r(mask)=0;
end


% ------------------------------------------------------------------
-------
% Returns high-pass filter

function H = hipass_filter(ht,wd)
% hi-pass filter function
% ...designed for use with Fourier-Mellin stuff
res_ht = 1 / (ht-1);
res_wd = 1 / (wd-1);

eta = cos(pi*(-0.5:res_ht:0.5));
neta = cos(pi*(-0.5:res_wd:0.5));
X = eta'*neta;

H=(1.0-X).^1.*(2.0-X).^1;
% H = (1-X).*(4-X).*(32-X).*(128-X);
```

```
% Master function to perform image registration
% Transforms Pitures in directory to u, v vectors
% Calls:
%   framecomp.m (in turn calls MyRegisterr.m)
%   shifter.m
% Analysis only needs to run ONCE per image stack
% Saves the result to Vectors.m
%
%
% Example script how to use PIVlab from the commandline
% You can adjust the settings in "s" and "p", specify a mask and
a region of interest
% clc; clear all
showplots = false; %shows the grayscale quiver plots ov vectors
saveheatmap = true; %saves a heatmap to cd

% %% Create list of images inside specified directory
% % close all
% % Parallel is 30% to 50% faster!
isOpen = matlabpool('size') > 0;
if  ~isOpen
    % change this to local cluster size, my laptop is 4-core
    matlabpool(8)
end

if ~exist('img', 'var')
    % find all the .TIF images in the directory
    % NAMES MUST BE SEQUENTIAL!!!
    a = dir;
    % loc = cellfun(@(x) (regexp(x,'.TIF')), {a.name},
'UniformOutput', false);
    loc = cellfun(@(x) (regexp(x,'r.tif')), {a.name},
'UniformOutput', false);
    indx = cellfun(@(x) ~isempty(x), loc);
    b = {a(indx).name};
    c = b(2:end);
    nopix = sum(cellfun(@numel, loc));
    img = cell(nopix-1, 1);
    imgw = cell(nopix-1, 1);
    imgh = cell(nopix-1, 1);
    display('Loading Images...')
    for photo = 1:(length(b)-1)
        img{photo}{1} = uint8(imread(b{photo})./16);
        img{photo}{2} = uint8(imread(c{photo})./16);
        imgh{photo} = size(img{photo}{1},1);
        imgw{photo} = size(img{photo}{1},2);
    end
```

```
    %subtract background mask
    load('bkg_autoExpose.mat');
    for photo = 1:(length(b)-1)
        bkgtile = tile_overlay(bkg,imgw{photo},imgh{photo});
        img{photo}{1} = double(img{photo}{1}).*bkgtile;
        img{photo}{2} = double(img{photo}{2}).*bkgtile;
    end
    clear bkgtile bkg
        g_dx = [0*205]';
        g_dy = [0*618]';
        g_th = [0*1.1]';
    guess = [g_dx, g_dy, g_th];
    shift_log = guess;
    if sum(guess.^2) > 0
        img{photo} = shifter(img{photo}{1}, img{photo}{2},
guess, 0);
    end
%     if sum(guess) == 0;
         for photo = 1:(length(b)-1)
            display(['Registering Photos #', num2str(photo), ' &
#' num2str(photo+1)])
            % Approximate shift locations
            total_shift = zeros(nopix-1, 3);
            total_shift = total_shift + guess;
            display('   Computing shift angle')
%
plotr(img{1}{1},imrotate(img{1}{2},4,'nearest','crop'))
%             lineres = [1];
%             lineres = [3, 2, 2, 1, 1, 1];
%             lineres = [7, 5, 5, 3, 3, 1, 1, 1]; %figure 1
            lineres = [30, 20, 20, 15, 15, 10, 10]; %, 7, 5, 4,
3, 3, 2, 1, 1];
            dm = 2048; %Can't go bigger than 4096 even 6144
locks up computer an takes 2 hr / topo call
%             dm = 2048;
            cr = floor(size(img{photo}{1},1)./2);
            cc = floor(size(img{photo}{1},2)./2);
            mapA = uint8(img{photo}{1}(cr-dm:cr+dm-1,cc-
dm:cc+dm-1));
            mapB = uint8(img{photo}{2}(cr-dm:cr+dm-1,cc-
dm:cc+dm-1));
            shift_log = [shift_log; zeros(length(lineres),3)];
            for pass = 1:length(lineres)
                predict = zeros(1,3);
                display(['   Pass #', num2str(pass)]);
                display('      Computing topographic
projection...')
```

```
%                 [mapAt, mapBt] = topograph(mapA, mapB,
lineres(pass));
                [mapAt] = topograph1(mapA, lineres(pass));
                [mapBt] = topograph1(mapB, lineres(pass));
                display('      Computing shift...')
        %current bottleneck
                [predict(photo,1), predict(photo,2),
predict(photo,3)] = MyRegisterr(mapAt, mapBt, 0, 1);
                display('      Re-aligning images')
                total_shift = total_shift + predict;
                img{photo} = shifter(img{photo}{1},
img{photo}{2}, predict(photo,:), 0);
                display(['   Total shifts: ',
num2str(total_shift)])
%                 plotr(img{photo}{1},img{photo}{2});
                shift_log(pass+1,:) = predict;
%                 clear mapAt mapBt
            end
            last_line = size(shift_log,2);
            shift_log = [shift_log; zeros(5,3)];
            for pass = 1:5 %Maximum of 5 will span whole image
                display('   Aligning images');
                display(['      Pass #', num2str(pass)]);
                dm = 1024*pass; %size of sub-sampling window use
factors of 2 to save A LOT of time
                pos = zeros(nopix-1, 5);
                display('      Computing shifts...')
                cr = floor(size(img{photo}{1},1)./2);
                cc = floor(size(img{photo}{1},2)./2);
                mapA = uint8(img{photo}{1}(cr-dm:cr+dm-1,cc-
dm:cc+dm-1));
                mapB = uint8(img{photo}{2}(cr-dm:cr+dm-1,cc-
dm:cc+dm-1));
                if dm <= 2048
                    [predict(photo,1), predict(photo,2),
predict(photo,3)] = MyRegisterr(mapA, mapB, 0, 1);
                else
                    [~, pos(photo,:)] = framecomp(mapA, mapB,
(2048)); %framecomp includes image filtering
                    predict = pos(:,1:3);
                end
                total_shift = total_shift + predict;
                img{photo} = shifter(img{photo}{1},
img{photo}{2}, predict(photo,:), 0);
                display(['         Total shifts: ',
num2str(total_shift)])
                shift_log(last_line+pass,:) = predict;
```

```
            end
            % Convergence vector - weighted absolute diagonal
shifts
            if numel(lineres) > 1
                Converge = (sqrt(shift_log(:,1).^2 +
shift_log(:,2).^2) + abs(tan(shift_log(:,3))).*dm);
%.*[lineres(1), lineres, ones(1,pass)]'./dm;
            else
                Converge = [];
            end
         end
% else
%          total_shift = guess;
% %     end
%     % Line up the pictures for further processing, re-load to
ensure no
%     % errors propegate down
%     display('   Final Alignment...')
%     clear img
%     img = cell(nopix-1, 1);
%     for photo = 1:(length(b)-1)
%         img{photo}{1} = uint8(imread(b{photo})./16);
%         img{photo}{2} = uint8(imread(c{photo})./16);
% %         [Tx(photo), Ty(photo)] = MyRegisterTheta(imgA, imgB,
0, Theta(photo));
%         img{photo} = shifter(img{photo}{1}, img{photo}{2},
total_shift(photo,:), 0);
%     end
%     display('Done registering!')
% end
end
crop_bkg = 1;
sub_mesh = 1;
if sub_mesh == true
    cx = 7700-200; % x cordinate of interrogation window
    cy = 7100-000; % y cordinate of interrogation window
    wi = floor(2048/2); % half-width of window

    display('Filtering images...')
    for photo = 1:(length(b)-1)
%         %for some reason this doesn't like rectangular images?
--> due to
%         %FFT properties, also a low-factor (ie power of 2)
size is way faster
        [img{photo}{4}, img{photo}{5}] =
filterimg(img{photo}{1}((cy-wi):(cy-1+wi),(cx-wi):(cx-1+wi)),
...
```

```
            img{photo}{2}((cy-wi):(cy-1+wi),(cx-wi):(cx-1+wi)),
crop_bkg);
    end
else
        display('Filtering images...')
    for photo = 1:(length(b)-1)
        [img{photo}{4}, img{photo}{5}] =
filterimg(img{photo}{1}, img{photo}{2}, crop_bkg);
    end
end

    plotr(img{1}{1},img{1}{2}, [cx,cy,wi]); %shows a cropped
region of the image

%% Standard PIV Settings

s = cell(10,2); % To make it more readable, let's create a
"settings table"
% it's way faster to do more iterations (w successively smaller
windows) than to
% have smaller windows on fewer itratations.
%Parameter                      %Setting          %Options
s{1,1}= 'Int. area 1';          s{1,2}=1*128;        % window
size of first pass, default is 128
s{2,1}= 'Step size 1';          s{2,2}=3*128;        % step of
first pass, default is 3x128
s{3,1}= 'Subpix. finder';       s{3,2}=1;         % 1 = 3point
Gauss, 2 = 2D Gauss (makes no differnece)
s{4,1}= 'Mask';                 s{4,2}=[];        % If needed,
generate via: imagesc(image);
[temp,Mask{1,1},Mask{1,2}]=roipoly;
s{5,1}= 'ROI';                  s{5,2}=[];        % Region of
interest: [x,y,width,height] in pixels, may be left empty
s{6,1}= 'Nr. of passes';        s{6,2}=3;         % 1-4 nr. of
passes ***NaN are due to too many passes!
s{7,1}= 'Int. area 2';          s{7,2}=64;        % second
pass window size
s{8,1}= 'Int. area 3';          s{8,2}=32;        % third pass
window size
s{9,1}= 'Int. area 4';          s{9,2}=16;        % fourth
pass window size
s{10,1}='Window deformation';   s{10,2}='*linear'; % '*spline'
is more accurate, but slower than '*linear'

%% Standard image preprocessing settings
p = cell(8,1);
%Parameter                      %Setting          %Options
```

```
p{1,1}= 'ROI';                    p{1,2}=s{5,2};     % same as in
PIV settings
p{2,1}= 'CLAHE';                  p{2,2}=0;          % 1 = enable
CLAHE (contrast enhancement), 0 = disable
p{3,1}= 'CLAHE size';             p{3,2}=8;          % CLAHE
window size
p{4,1}= 'Highpass';               p{4,2}=0;          % 1 = enable
highpass, 0 = disable
p{5,1}= 'Highpass size';          p{5,2}=64;          % highpass
size
p{6,1}= 'Clipping';               p{6,2}=0;          % 1 = enable
clipping, 0 = disable
p{7,1}= 'Clipping thresh.';       p{7,2}=0;          % 0-255
clipping threshold
p{8,1}= 'Intensity Capping';      p{8,2}=0;          % 1 = enable
intensity capping, 0 = disable

%% PIV analysis loop
amount = length(img)*2;
% if mod(amount,2) == 1 %Uneven number of images?
%     disp('Image folder should contain an even number of
images.')
%     %remove last image from list
%     amount=amount-1;
%     filenames(size(filenames,1))=[];
% end
x=cell(amount/2,1);
y=x;
u=x;
v=x;
typevector=x; %typevector will be 1 for regular vectors, 0 for
masked areas
counter=0;
% for i=1:2:amount
display('Initializing PIV loop')
for indi=1:length(img)
    counter=counter+1;
%     image1=imread(fullfile(directory, filenames{i})); % read
images
%     image2=imread(fullfile(directory, filenames{i+1}));
%     img{AB pair}{sub-image #}(1=imageA)
%     img{AB pair}{sub-image #}(2=imageB)
    display(['Pre-processing PIV #' num2str(indi) ' of '
num2str(length(img))] )
    image1 = PIVlab_preproc
(img(3){4},p{1,2},p{2,2},p{3,2},p{4,2},p{5,2},p{6,2},p{7,2},p{8,
2}); %preprocess images
```

```
    image2 = PIVlab_preproc
(img(3){5},p{1,2},p{2,2},p{3,2},p{4,2},p{5,2},p{6,2},p{7,2},p{8,
2});
    [x{counter}, y{counter}, u{counter}, v{counter},
typevector{counter}] = piv_FFTmulti
(image1,image2,s{1,2},s{2,2},s{3,2},s{4,2},s{5,2},s{6,2},s{7,2},
s{8,2},s{9,2},s{10,2});
%     clc
    display([int2str(indi/amount*2*100) ' %']);

    % Graphical output (disable to improve speed)
    if showplots == 1
        imagesc(double(image1)+double(image2));colormap('gray');
        hold on

quiver(x{counter},y{counter},u{counter},v{counter},'g','AutoScal
eFactor', 1.5);
        hold off;
        axis image;
    %     title(filenames(3),'interpreter','none')
        set(gca,'xtick',[],'ytick',[])
        drawnow;
    end
end

%% PIV postprocessing loop
% Settings
umin = -100; % minimum allowed u velocity %default fr all are 10
umax = 100; % maximum allowed u velocity
vmin = -100; % minimum allowed v velocity
vmax = 100; % maximum allowed v velocity
stdthresh=6; % threshold for standard deviation check %defaut is
6
epsilon=0.15; % epsilon for normalized median test default is
0.15
thresh=3; % threshold for normalized median test default is 3

u_filt=cell(amount/2,1);
v_filt=u_filt;
typevector_filt=u_filt;
display('Post-prcessing PIV')
for PIVresult=1:size(x,1)
    u_filtered=u{PIVresult,1};
    v_filtered=v{PIVresult,1};
    typevector_filtered=typevector{PIVresult,1};
    %vellimit check
    u_filtered(u_filtered<umin)=NaN;
```

```
    u_filtered(u_filtered>umax)=NaN;
    v_filtered(v_filtered<vmin)=NaN;
    v_filtered(v_filtered>vmax)=NaN;
    % stddev check
    meanu=nanmean(nanmean(u_filtered));
    meanv=nanmean(nanmean(v_filtered));

std2u=nanstd(reshape(u_filtered,size(u_filtered,1)*size(u_filter
ed,2),1));

std2v=nanstd(reshape(v_filtered,size(v_filtered,1)*size(v_filter
ed,2),1));
    minvalu=meanu-stdthresh*std2u;
    maxvalu=meanu+stdthresh*std2u;
    minvalv=meanv-stdthresh*std2v;
    maxvalv=meanv+stdthresh*std2v;
    u_filtered(u_filtered<minvalu)=NaN;
    u_filtered(u_filtered>maxvalu)=NaN;
    v_filtered(v_filtered<minvalv)=NaN;
    v_filtered(v_filtered>maxvalv)=NaN;
    % normalized median check
    %Westerweel & Scarano (2005): Universal Outlier detection
for PIV data
    [J,I]=size(u_filtered);
    medianres=zeros(J,I);
    normfluct=zeros(J,I,2);
    b2=1;
    for cc=1:2
        if cc==1; velcomp=u_filtered;else;velcomp=v_filtered;end
%#ok<*NOSEM>
        for indi=1+b2:I-b2
            for j=1+b2:J-b2
                neigh=velcomp(j-b2:j+b2,indi-b2:indi+b2);
                neighcol=neigh(:);

neighcol2=[neighcol(1:(2*b2+1)*b2+b2);neighcol((2*b2+1)*b2+b2+2:
end)];
                med=median(neighcol2);
                fluct=velcomp(j,indi)-med;
                res=neighcol2-med;
                medianres=median(abs(res));

normfluct(j,indi,cc)=abs(fluct/(medianres+epsilon));
            end
        end
    end
```

```
info1=(sqrt(normfluct(:,:,1).^2+normfluct(:,:,2).^2)>thresh);
    u_filtered(info1==1)=NaN;
    v_filtered(info1==1)=NaN;

    typevector_filtered(isnan(u_filtered))=2;
    typevector_filtered(isnan(v_filtered))=2;
    typevector_filtered(typevector{PIVresult,1}==0)=0; %restores
typevector for mask

    %Interpolate missing data
    u_filtered=inpaint_nans(u_filtered,4);
    v_filtered=inpaint_nans(v_filtered,4);

    u_filt{PIVresult,1}=u_filtered;
    v_filt{PIVresult,1}=v_filtered;
    typevector_filt{PIVresult,1}=typevector_filtered;
end
%% Save presentation pics & clean up
if saveheatmap == 1
%     display('Saving files')
    for PIVresult=1:size(x,1)
        A = abs(sqrt(u_filt{PIVresult}.^2 +
v_filt{PIVresult}.^2));
        D =
atand(real(v_filt{PIVresult})./real(u_filt{PIVresult}))+[sign(re
al(v_filt{PIVresult}))<0].*[sign(real(u_filt{PIVresult}))<0].*(-
180-90);
%         A = abs(sqrt(u{PIVresult}.^2 + v{PIVresult}.^2));
        colormap('jet');
        figure
        imagesc(x{PIVresult}(:), y{PIVresult}(:), (A));
        % Cropped result
%         imagesc(x{PIVresult}(:), y{PIVresult}(:),
(A).*(img{1}{5}(x{1}(1,:),y{1}(:,1))>0), [0 50]);
        grid on
        colorbar
        saveres = 2^ceil(log2(max(size(x{PIVresult}))));
%         hgexport(gcf, ['figure',num2str(PIVresult),'.jpg'],
hgexport('factorystyle'), 'Format', 'jpeg');
        print(gcf, ['figure',num2str(PIVresult)], '-dpng', ['-
r',num2str(saveres)]); % '-r1200')
    end
end
% clearvars -except pos img p s x y u v typevector directory
u_filt v_filt typevector_filt
% save('Vectors.mat')
```

```
% save('fig2_v2.mat','-v7.3')

%overlay the quiver plot on the image and save the data as 2
plots and a CSV Table
% quiveroverlay(x, y, u_filt, v_filt, img, cx, cy, wi,
shift_log, 1)
% colorquiver(x{1},y{1},abs(ex{1}),abs(ey{1}))
% [counts, bins] = hist(sqrt(ex_filt(:).^2 + ey_filt(:).^2),
[0:0.01:1]);
```

```
function [Gimg, ex, ey] = quiveroverlay(x, y, u_filt, v_filt,
img, cx, cy, wi, shift_log, no)
% load fig7_fixmask.mat
% no = 7; load(['fig',num2str(no),'_fixmask.mat']);
% quiveroverlay(x, y, u_filt, v_filt, img, cx, cy, wi,
shift_log, no)

display('Shifting GFP image')
photo = 1;
cfname = ['100614_1m_g4_F',num2str(no)];
Gimg{photo}{1} = uint8(imread(['g4d',num2str(no+7-
1),'g.tif'])./16);
Gimg{photo}{2} =
uint8(imread(['g4d',num2str(no+7),'g.tif'])./16);

for ind = 1:size(shift_log,1)
    Gimg{photo} = shifter(Gimg{photo}{1}, Gimg{photo}{2},
[shift_log(ind,:)], 0);
end
Gimg{photo}{4} = imadjust(uint8(Gimg{photo}{1}((cy-wi):(cy-
1+wi),(cx-wi):(cx-1+wi))));
Gimg{photo}{5} = imadjust(uint8(Gimg{photo}{2}((cy-wi):(cy-
1+wi),(cx-wi):(cx-1+wi))));
[maskA, maskB] = filterimg(img{photo}{1}((cy-wi):(cy-1+wi),(cx-
wi):(cx-1+wi)), ...
    img{photo}{2}((cy-wi):(cy-1+wi),(cx-wi):(cx-1+wi)), 1);
maskA = imfill(maskA>0, 'holes');
maskB = imfill(maskB>0, 'holes');
roiA = uint8(double(Gimg{photo}{4}).*maskA);
roiB = uint8(double(Gimg{photo}{5}).*maskB);
% plotr(roiA, roiB)

display('Computing Strains')
[ex, ey, exy] = strainonmesh(x, y, u_filt,v_filt);
Gimg_comb = uint8(roiA./2+roiB./2);

%subtract the offset
roi = Gimg_comb(x{1}(1,:),y{1}(:,1))==0;
[em, en] = size(ex{1});
ex{1} = ex{1} - repmat(median(real(ex{1}(roi(:)))), em, en);
ey{1} = ey{1} - repmat(median(real(ey{1}(roi(:)))), em, en);

figure;
hold on;
imagesc(Gimg_comb, [0,255]);
bd = 255; %bit depth of grayscale
```

```
imagesc(Gimg_comb, [0,bd]); colormap([zeros(bd+1,1),
([0:1:bd]./bd)', zeros(bd+1,1)]); %Particles in ROI 'gray' is
grayscale
% imagesc(x{PIVresult}(:), y{PIVresult}(:), (A));
colormap('gray'); %Strain magnitude
% Loop plots vectors on multiple length scales tom ake smaller
ones eastier
% to see

th = [0 0.001, 0.01, 0.1, Inf];
asf = [0.1, 0.5, 1];
% cm = 'rgb';
cm = [255, 255, 102;
      255, 178, 102;
      255, 102, 102]./255;
emag = sqrt(abs(ex{1}).^2 + abs(ey{1}).^2);
c_lutM = zeros(size(ex{1},1),size(ex{1},2));

for ind = 1:3
    emag_lut = (emag < th(ind+1) | emag > th(ind+2)) |
(Gimg_comb(x{1}(1,:),y{1}(:,1))==0);
    ex_filt = ex{1};
    ex_filt(emag_lut(:)) = NaN;
    ey_filt = ey{1};
    ey_filt(emag_lut(:)) = NaN;
    c_lut = ~emag_lut;

quiver(x{1}(c_lut(:)),y{1}(c_lut(:)),ex_filt(c_lut(:)),ey_filt(c
_lut(:)), ...

'color',cm(ind,:),'linewidth',0.25,'AutoScaleFactor',asf(ind),
'MaxHeadSize', 0.9)
    c_lutM = c_lut + c_lutM;
end
c_lutM = c_lutM > 0; %convert to logical
set(gca,'ydir','reverse')
axis([0, max(x{1}(:)), 0, max(y{1}(:))])
hold off
display('Saving QuiverPlot')
saveres = 2^ceil(log2(max(size(x{1}))));
%         hgexport(gcf, ['figure',num2str(PIVresult),'.jpg'],
hgexport('factorystyle'), 'Format', 'jpeg');
print(gcf, [cfname,'_QuiverPlot'], '-dpng', ['-
r',num2str(saveres*16)]); % '-r1200')

display('Saving Distributions')
g = figure;
```

```
poz = get(g,'Position');
set(g,'Position',[poz(1),poz(2)-500,800,800])
subplot(2,1,1)
% compass(ex_filt(c_lut(:))./ey_filt(c_lut(:)))
% Sang = real(ex_filt(c_lut(:))./ey_filt(c_lut(:)));
Sang = atan2(real(ey{1}(c_lutM(:))), real(ex{1}(c_lutM(:))));
%4-quadrant anfge in radians
[tout, rout] = rose(Sang, 24);

% sets the axis of polar plot (makes a blank one in background)
theta = linspace(0,2*pi,100);
r_max  = 500;
h_fake = polar(theta,r_max*ones(size(theta)));
hold on;
set(h_fake, 'Visible', 'Off');

polar(tout, rout);
[xout, yout] = pol2cart(tout, rout);
set(gca, 'nextplot', 'add');
h = fill(xout, yout, 'r');
set(h,'LineWidth',3)
title('Vector directional distribution')

subplot(2,1,2);
Smag = real(sqrt(ex{1}(c_lutM(:)).^2 + ey{1}(c_lutM(:)).^2));
hist(log10(Smag), 20);
hh = get (gca, 'children');
set(hh, 'LineWidth',3)
set(hh, 'FaceColor','c')
xlabel('Log_1_0 Strain Maganitude')
axis([-3, 0, 0, 2000]);
ylabel('Counts')
set(findall(g,'-
property','FontSize'),'FontSize',12,'FontWeight','bold')
print(g, [cfname,'_StrainDistribution'], '-dpng', ['-
r',num2str(saveres*4)]); % '-r1200')

csvwrite([cfname,'_Data_Angle,Magnitude.csv'],[Sang, Smag])

display(num2str(mean(Smag)));
% ED = sqrt(abs(ex{1}).^2+abs(ey{1}).^2);
% ED_lut = (ED > 0.1) & (ED < 10);
% hold on; imagesc(x{1}(:), y{1}(:),
sqrt(abs(ex{1}).^2+abs(ey{1}).^2))
% colormap(autumn)
% streamline(x{1},y{1},ex{1},ey{1},x{1}(ED_lut),y{1}(ED_lut));
set(gca,'ydir','reverse'); axis tight;
```

```
% D(:,1) = real(atan(ey{1}(:)./ex{1}(:)));
% D(:,2) = real(angle(ey{1}(:)./ex{1}(:)));
%
% Dl(:,1) = D(:,1) >= 0;
% Dl(:,2) = D(:,1) < 0;
% Dl(:,3) = D(:,2) > pi/2;
% Dl(:,4) = D(:,2) < -pi/2;
% Dl(:,5) = ~(Dl(:,3) | Dl(:,4));
%
% q1 = D(Dl(:,3),1).*D(Dl(:,3),2);
%
%
% figure
% rose(real(D)) %angular distribution, complex should map to an
angle
```

```
function fit_intensity
% script to compute a background mask to fix uneven illumination
% the script takes in an intensity matrix wit columns:
% Image Region  Area    Mean    Min Max X   Y
% This can be made in imageJ by measuring illumination in either
white
% or black images. It even work on lattice images as long all
regios are
% *supposed* to be the same illumination
% It is easiest to make the matrix in matlab.

load('intensity_2ms')
nc = size(intensity,2);
nr = size(intensity,1);
ni = max(intensity(:,1));
LUT_mat = zeros(nr,ni);
indc = 1;
indi = 1;
a(:,1) = intensity(:,1);
a(:,2) = [diff(intensity(:,1));0];
for ind = 1:nr
    LUT_mat(ind,indc) = 1;
    if a(ind,2)
        indc = indc+1;
    end
end
int_norm = intensity(:,4)./intensity(:,3);
LUT_int = LUT_mat.*repmat(int_norm,1,ni);
LUT_intn = LUT_int./repmat(max(LUT_int,[],1),nr,1);
int = sum(LUT_intn,2);
xmax = 1344;
ymax = 1024;
x = intensity(:,7);
y = intensity(:,8);
plot(x, y, 'bo')

figure
sf = fit([x,y],int, 'poly23');
plot(sf, [x,y],int)

[xx, yy] = meshgrid(1:xmax, 1:ymax);
bkg = sf(xx, yy);
save('bkg','bkg')
```

```
function [ex, ey, exy] = strainonmesh(x, y, u_filt,v_filt)
    % Operates on outputs from
    % Regular mesh, so nearest neighbors to Xi,j are Xi+1,j and
Xi,j+1
    frames = length(u_filt);
    ex = cellfun(@(x) x.*0, u_filt, 'UniformOutput', false);
    ey = cellfun(@(x) x.*0, v_filt, 'UniformOutput', false);
    exy = cellfun(@(x) x.*0, u_filt, 'UniformOutput', false);

    cal = 1.6074; %um/pixel - gets divided out anyway
    for ind = 1:frames
    %     % compute forward-difference, zero-pad last column
%         du = [(u_filt(3)(:,2:end)-u_filt(3)(:,1:end-1)),
zeros(size(u_filt(3),1),1)];
%         dv = [(v_filt(3)(2:end,:)-v_filt(3)(1:end-1,:));
zeros(size(u_filt(3),2),1)'];
        du = CNM1(u_filt(3),2)./cal;
        dv = CNM1(v_filt(3),1)./cal;
        dx = [diff(x(3),1,2),  (x(3)(:,end) - x(3)(:,end-
1))]./cal; %convert to microns
        dy = [diff(y(3),1,1); (y(3)(end,:) - y(3)(end-
1,:))]./cal; %convert to microns
        ex(3) = du./dx;
        ey(3) = dv./dy;
        % can use orthogonal vectors and gradient also
        % [du dv] = gradient((abs(u_filt{1})+i.*abs(v_filt{1})),
mode(mode((diff(x(3),1,1)))), mode(mode((diff(y(3),1,1)))));
        % ex = real(dv); ey = imag(dv);
        exy(3) = 1/2.*(du./dy + dv./dx);
    %     exy(3) = du(1:end-1,:)./dy(:,1:end-1) - dv(:,1:end-
1)./dx(1:end-1,:);
        ex(3)(isnan(ex(3)(:))) = 0;
        ey(3)(isnan(ey(3)(:))) = 0;
        exy(3)(isnan(exy(3)(:))) = 0;
    end
end

function dx = CNM1(x,n) %second order central difference formula
    nr = size(x,2);
    nc = size(x,1);
    dx = zeros(nr,nc);
    if n == 1; %deravative across rows (y-dimension)
        for indi = 3:(nr-2)
            dx(indi,:) = (-x(indi+2,:) + 8.*x(indi+1,:) -
8.*x(indi-1,:) + x(indi-2,:))./12;
        end
        %forward difference for left edge
```

```
        dx(1,:) = (x(2,:) - x(1,:));
        dx(2,:) = (-x(4,:) + 6.*x(3,:) - 3.*x(2,:) -
2.*x(1,:))./6; %2nd order
        %backward difference for right edge
        dx(nr,:) = (x(nr,:) - x(nr-1,:));
        dx(nr-1,:) = (2.*x(nr,:) + 3.*x(nr-1,:) - 6.*x(nr-2,:) +
x(nr-3,:))./6; %2nd order
    elseif n == 2; %deravative across columns(x-dimenstion)
        for indi = 3:(nc-2);
            dx(:,indi) = (-x(:,indi+2) + 8.*x(:,indi+1) -
8.*x(:,indi-1) + x(:,indi-2))./12;
        end
        %forward difference for left edge
        dx(:,1) = (x(:,2) - x(:,1));
        dx(:,2) = (-x(:,4) + 6.*x(:,3) - 3.*x(:,2) -
2.*x(:,1))./6; %2nd order
        %backward difference for right edge
        dx(:,nc) = (x(:,nc) - x(:,nc-1));
        dx(:,nc-1) = (2.*x(:,nc) + 3.*x(:,nc-1) - 6.*x(:,nc-2) +
x(:,nc-3))./6; %2nd order
    end
end

function dx = CNM2(x) %function comuptes the 2nd order
deravitive!
    nr = size(x,2);
    nc = size(x,1);
    dx = zeros(nr,nc);
    for indi = 2:(nr-1) %rows
        for indj = 2:(nc-1) %columns
            dx(indi,indj) = 1/2.*(x(indi+1,indj) + x(indi-
1,indj) + x(indi,indj+1) + x(indi,indj-1) - 4.*x(indi,indj));
        end
    end
end
```

```
function bkgtile = tile_overlay(bkg,imgw,imgh)
%generate the mask by running fit_intensity.m
%for debugging use the size of g4d14r.tif
% load('bkg.mat')
% imgw = 13453;
% imgh = 12113;

%invert the background mask
bkg = 2*ones(size(bkg,1),size(bkg,2)) - bkg; %./max(max(bkg));

% size of single image in the title, set by microscope camera
xmax = 1344;
ymax = 1024;

xtile = round(xmax*0.91);
ytile = round(ymax*0.91);

nx = round(imgw./xtile)-1;
ny = round(imgh./ytile)-1;

% start locations of each tile
xstart = [1, floor([1:(nx)].*xtile), imgw];
ystart = [1, floor([1:(ny)].*ytile), imgh];
    dys = diff(ystart)+1;
    dxs = diff(xstart)+1;
[ys, xs] = meshgrid(ystart, xstart);
bkgtile = zeros(imgh,imgw);
tmp_mask = zeros(imgh,imgw);

for indx = 1:(nx+1)
    for indy = 1:(ny+1)
%         display([num2str(indx),' , ' ,num2str(indy)])
        fill_r = ys(indx,indy):(ys(indx+1,indy+1));
        fill_c = xs(indx,indy):(xs(indx+1,indy+1));
        tmp_mask(fill_r,fill_c) = bkg(1:dys(indy), 1:dxs(indx));
        ww = 2;
        blendy = ys(indx+1,indy+1):(ys(indx,indy)+ymax-1);
        tmp_mask(ys(indx,indy):(ys(indx,indy)-
1+(ww*length(blendy))),xs(indx,indy):(fill_c(1)+xmax-1)) = ...
            1.*(bkg(end:-1:end-(ww*length(blendy)-1),:) +
bkg(1:(ww*length(blendy)),:))./2; % the mean
%             bsxfun(@max, bkg(end:-1:end-(ww*length(blendy)-
1),:) , bkg(1:(ww*length(blendy)),:)); % the max
        blendx = xs(indx+1,indy+1):(xs(indx,indy)+xmax-1);
        tmp_mask((ys(indx,indy)-
1+(ww*length(blendy))):(ys(indx+1,indy+1)),
xs(indx,indy):(xs(indx,indy)-1+(ww*length(blendx))))...
```

```
            = 1.*(bkg((ww*length(blendy)-1):(dys(indy)-
1),1:(ww*length(blendx))))...
            + bkg((ww*length(blendy)-1):(dys(indy)-1),end:-
1:(end-(ww*length(blendx)-1)))))./2;
%             = bsxfun(@max, bkg((ww*length(blendy)-
1):(dys(indy)-1),1:(ww*length(blendx))), ...
%             bkg((ww*length(blendy)-1):(dys(indy)-1),end:-
1:(end-(ww*length(blendx)-1))));


bkgtile(ys(indx,indy):(ys(indx+1,indy+1)),xs(indx,indy):(xs(indx
+1,indy+1)))...
            =
tmp_mask(ys(indx,indy):(ys(indx+1,indy+1)),xs(indx,indy):(xs(ind
x+1,indy+1)));

tmp_mask(ys(indx,indy):(ys(indx+1,indy+1)),xs(indx,indy):(xs(ind
x+1,indy+1)))...
            = zeros(dys(indy),dxs(indx));
    end
end

% imagesc(bkgtile)
```

```
function [sharpA, sharpB] = filterimg(imgA, imgB, crop)
%load the image
% imgA = uint8(imread(b{photo})./16);
% photo = 1; imgA = img{photo}{1}; imgB = img{photo}{2};
% find beam location
imgA = uint8(imgA);
imgB = uint8(imgB);
% Intensity capping
% cap = 200;
% imgA(imgA > cap) = cap;
% imgB(imgB > cap) = cap;
imgA = imadjust(imgA);
imgB = imadjust(imgB);

% figure; imshow(bw)
%tophat to remove stitching seams
% A_background = imopen(imgA,strel('ball',250,5));
% imgA = imgA - A_background;
% B_background = imopen(imgB,strel('ball',250,5));
% imgB = imgB - B_background;
imgAf = imtophat(imgA,strel('disk',256));
imgBf = imtophat(imgB,strel('disk',256));
imgAf = imadjust(imgAf);
imgBf = imadjust(imgBf);

% crops out the dim regions of the image
if crop == 1
    backgroundA = imopen(imgA,strel('disk',128)); %default is
256 smaller beams need a smaller value
    backgroundB = imopen(imgB,strel('disk',128));
    level = min([0.2, (graythresh(backgroundA)./2 +
graythresh(backgroundB)./2)]);
    bwA = im2bw(backgroundA,level);
    bwB = im2bw(backgroundB,level);
    % Add a bit to return only the biggest region
    CCA = bwconncomp(bwA); SA = regionprops(CCA, 'Area'); LA =
labelmatrix(CCA);
    bwA2 = ismember(LA, find([SA.Area] == max([SA.Area])));
    CCB = bwconncomp(bwB); SB = regionprops(CCB, 'Area'); LB =
labelmatrix(CCB);
    bwB2 = ismember(LB, find([SB.Area] == max([SB.Area])));

    bwAB = ~((~bwA2).*(~bwB2));
%     bwA2 = imdilate(bwA,strel('disk', 128, 4)).*(~bwA);
%     bwB2 = imdilate(bwB,strel('disk', 128, 4)).*(~bwB);

    %crop the ROI from the images
```

```
    sharpA = imgAf.*uint8(bwAB); %+ 0*imgA.*uint8(bwA2) +
0.0*imgA.*uint8(~(bwA + bwA2));
    sharpB = imgBf.*uint8(bwAB); %+ 0*imgB.*uint8(bwB2) +
0.0*imgB.*uint8(~(bwB + bwB2));
else
    sharpA = imgA;
    sharpB = imgB;
end

%sharpen the image to undo blurring form tophat
% H = padarray(2,[4 4]) - fspecial('gaussian' ,[9 9],2);
% sharpA = imfilter(imgA,H);
% sharpB = imfilter(imgB,H);

% imshow(sharpened)

% imagesc(img{1}{1}); figure; imagesc(img{1}{2});
```

```
function plotr(imgA, imgB, loc)
% creates an RGB overlay of two images
if nargin > 2;
    cx = loc(1);
    cy = loc(2);
    wi = loc(3);
    cimgA = imgA((cy-wi):(cy+wi),(cx-wi):(cx+wi));
    cimgB = imgB((cy-wi):(cy+wi),(cx-wi):(cx+wi));
    imgRGB = uint8(cat(3, cimgA, cimgB,
zeros(size(cimgA,1),size(cimgA,2))));
    h = figure;
    image(imgRGB)
    truesize(h, [1024,1024])
    grid on
else
    nl = floor(size(imgA,1)/8);
    h = figure;
    imgRGB = uint8(cat(3, imgA, imgB,
zeros(size(imgA,1),size(imgA,2))));
    image(imgRGB(2*nl:6*nl,2*nl:6*nl,:))
    truesize(h, [1024,1024])
    grid on
end
```

```
function s = linfit(x, y)
fit = @(b,x) b(1).*x + b(2);
fcn = @(b) sum((fit(b,x) - y).^2);      % Least-Squares cost
function
s = fminsearch(fcn, [1, 0]);          % Minimise Least-Squares
% xp = linspace(min(x),max(x),1000);
% figure
% plot(x,y,'bo',  xp,fit(s,xp), 'r')
% grid
```

```
function [img, shift] = framecomp(imgA, imgB, dm)
% Calls MyRegisterr.m
% dm specifies number of divisions e.g. dm = 3 will chop image
into a 3*3
% grid of 9 images
% dm = 3;
% imgA = 'TCPS1_10uL_1uL_none_d1_4x_1_w1mCherry-DSU_s10.tif';
% imgB = 'TCPS1_10uL_1uL_none_d2_4x_1_w1mCherry-DSU_s10.tif';
% A = imread(imgA);
[Xdim, Ydim] = size(imgA);
x = [1:(dm-1):Xdim];
y = [1:(dm-1):Ydim];
ind = 1;
dx = cell(length(x), 1);
for indx = 1:(length(x)-1)
    for indy = 1:(length(y)-1)
        dx(3) = {[x(indx), x(indx+1)] [y(indy), y(indy+1)]};
        ind = ind + 1;
    end
end
clear ind indx indy
% parfor saves time if dx > 4
dxm = length(dx);
if dxm == 2;
    dxm = 1;
end
sind = 1:dxm;

SimgA = cell(dxm,1);
SimgB = cell(dxm,1);
img = cell(dxm,1);
xshift = zeros(dxm,1);
yshift = zeros(dxm,1);
theta = zeros(dxm,1);
for ind = 1:dxm
    SimgA(3) = imgA(dx{sind(ind)}{1}(1):dx{sind(ind)}{1}(2),
dx{sind(ind)}{2}(1):dx{sind(ind)}{2}(2));
    SimgB(3) = imgB(dx{sind(ind)}{1}(1):dx{sind(ind)}{1}(2),
dx{sind(ind)}{2}(1):dx{sind(ind)}{2}(2));
end

for ind = 1:dxm
%     display(['region: ' num2str(dx(3)) '  ' num2str(dx{2})])
%     A_bkg = imopen(SimgA(3),strel('disk',5));
%     A = SimgA(3) - A_bkg;
    A = (SimgA(3));
%     B_bkg = imopen(SimgB(3),strel('disk',5));
```

```
%     B = SimgB(3) - B_bkg;
    B = (SimgB(3));
    [xshift(ind), yshift(ind), theta(ind), img(3)] =
MyRegisterr(A, B, 0);
end
% figure out which sub-images have the most information (pixel
intensity)
imsum = cell2mat(cellfun(@(x) sum(sum(x)), SimgA,
'UniformOutput', false));
% drop the higher rotations - pics are not moving that much!
% wrap the angle back to 0 to 90
theta = min(abs(repmat(theta,1,5) - repmat([0 90 180 270
360],length(theta),1)),[],2);
% figure; hold on; plot(imsum./max(imsum), 'r');
plot(theta./max(theta), 'g'); plot(xshift./max(xshift), 'b');
hold off
theta_filt = imsum > max(imsum)*0.5;
% xshift = xshift(theta_filt);
% yshift = yshift(theta_filt);
% theta = theta(theta_filt);
% if pictures are (angularly) alinged, the slope will be zero --
> shift is uniform
% across the image offset is the amount that still needs to be
moves
[con] = linfit([1:length(xshift)],xshift');
xlin = median(con(1).*[1:0.1:length(xshift)]+con(2)); %for a
large n, the linfit approaches the mean
ov = [xlin, median(xshift)];
[~, iout] = min(abs(ov));
xout = round(ov(iout)); %shifts must be intergers

[con] = linfit([1:length(yshift)],yshift');
ylin = median(con(1).*[1:0.1:length(yshift)]+con(2));
ov = [ylin, median(yshift)];
[~, iout] = min(abs(ov));
yout = round(ov(iout)); %shifts must be intergers

shift = [xout, yout, circ_median((theta./360*2*pi))./(2*pi)*360,
numel(theta)./numel(theta_filt), var(xshift)];
% display(['Shift X: ' num2str(shift(1)) ' Shift Y: '
num2str(shift(2))])
% imshow(img{1}{1,3},[0, 255])
```

```
% FOLLOWING CODE TAKEN DIRECTLY FROM fm_gui_v2
% Combine original and registered images
function img = shifter(ImgA, ImgB, pos, showpic)
    Tx = pos(1); %x shift
    Ty = pos(2); %y shift
    Tt = pos(3); %rotation angle
%     if Tt > 30
%         Ttt(1) = -(Tt - 90);
%         Ttt(2) = -(Tt - 180);
%         Ttt(3) = -(Tt - 270);
%         Ttt(4) = -(Tt - 360);
%         [~, I] = min(abs(Ttt));
%         Tt = -Ttt(I);
%     end
    input2_rectified = imrotate(ImgB, Tt); %MUST ROTATE THE
IMAGE FIRST!!!
    move_ht = Ty; move_wd = Tx;

    total_height =
max(abs(move_ht)+size(ImgA,1),(abs(move_ht)+size(input2_rectifie
d,1)));
    total_width =
max(abs(move_wd)+size(ImgA,2),(abs(move_wd)+size(input2_rectifie
d,2)));

    combImage = zeros(total_height,total_width);
    registered1 = zeros(total_height,total_width);
    registered2 = zeros(total_height,total_width);

    % if move_ht and move_wd are both POSITIVE
    if((move_ht>=0)&&(move_wd>=0))
        registered1(1:size(ImgA,1),1:size(ImgA,2)) = ImgA;

registered2((1+move_ht):(move_ht+size(input2_rectified,1)),(1+mo
ve_wd):(move_wd+size(input2_rectified,2))) = input2_rectified;
    % if translations are both NEGATIVE
    elseif ((move_ht<0)&&(move_wd<0))

registered2(1:size(input2_rectified,1),1:size(input2_rectified,2
)) = input2_rectified;

registered1((1+abs(move_ht)):(abs(move_ht)+size(ImgA,1)),(1+abs(
move_wd)):(abs(move_wd)+size(ImgA,2))) = ImgA;
    elseif ((move_ht>=0)&&(move_wd<0))

registered2((move_ht+1):(move_ht+size(input2_rectified,1)),1:siz
e(input2_rectified,2)) = input2_rectified;
```

```
registered1(1:size(ImgA,1),(abs(move_wd)+1):(abs(move_wd)+size(I
mgA,2))) = ImgA;
    elseif ((move_ht<0)&&(move_wd>=0))

registered1((abs(move_ht)+1):(abs(move_ht)+size(ImgA,1)),1:size(
ImgA,2)) = ImgA;

registered2(1:size(input2_rectified,1),(move_wd+1):(move_wd+size
(input2_rectified,2))) = input2_rectified;
    end
    if numel(registered1) ~= numel(registered2)
        error('uneven matricies!')
    end
    % Plant the FIRST Image and shift the next (change form
original)
    % This puts Frame A below Frame B
    % % % find the image with the greater number of zeros - we
shall plant that one and then bleed in the other for the
combined image
%     if sum(sum(registered1==0)) > sum(sum(registered2==0))
%         plant = registered1;    bleed = registered2;
%     else
%         plant = registered2;    bleed = registered1;
%     end

    img = cell(1,2);
    img{1} = registered1;                %planted image
%     img{2} = imrotate(registered2, Tt);  %bled image
    img{2} = registered2;
%     img{3} = combImage;

    % Show final image
    if showpic == 1
        imgRGB = cat(3, combImage, combImage, combImage);
%         m = size(img{1},2);
%         n = size(img{1},1);
%         combImage = cat(3, img{1}./max(max(img{1})),
img{2}./max(max(img{2})), zeros(n,m));
        mx1 = max(max(img{1}));
        mx2 = max(max(img{2}));
        for p=1:total_height
            for q=1:total_width
                if (combImage(p,q)==0)
                    imgRGB(p,q,1) = img{1}(p,q)./mx1;
                    imgRGB(p,q,2) = img{2}(p,q)./mx2;
```

```
%                       combImage(p,q,:) = cat(3,
img{1}(p,q)./mx1, img{2}(p,q)./mx2, 0);
                    end
                end
            end
%           img{3} = combImage;

            figure
            imshow(imgRGB);
% %             figure
% %             subplot(1,2,1)
% %             imshow(registered1, [0 255])
% %             title('Frame A')
% %             subplot(1,2,2)
% %             imshow(registered2, [0 255])
% %             title('Frame B')
    end
end
```

```
function quiveroverlay2
% Draw white arrows over the imagesc map
close all;

load('Temp_quiverolverlay2.mat')
if ~exist('x','var')
    % get the compliled mat files (LaunchPIV)
    [x, y, u_filt, v_filt] = loadr;
    x = cellfun(@(t) t{1}, x, 'UniformOutput', false);
    y = cellfun(@(x) x{1}, y, 'UniformOutput', false);
    u_filt = cellfun(@(x) x{1}, u_filt, 'UniformOutput', false);
    v_filt = cellfun(@(x) x{1}, v_filt, 'UniformOutput', false);
    save('Temp_quiverolverlay2.mat')
end

display('Computing Strains')
[ex, ey, exy] = strainonmesh(x, y, u_filt,v_filt);
bkg = cell(1,length(x));
for ind = 1:length(x)
    bkg(3) = abs(sqrt(ex(3).^2 + ey(3).^2));
end

for ind = 1:length(x)
    imagesc(x(3)(1,:), y(3)(:,1), bkg(3),[0,1])
    hold on
    emag = sqrt(abs(ex(3)).^2 + abs(ey(3)).^2);

    emag_lut = (emag < 0.03 | emag > 1);
    ex_filt = ex(3);
    ex_filt(emag_lut(:)) = NaN;
    ey_filt = ey(3);
    ey_filt(emag_lut(:)) = NaN;
    % set arrows to 1;
    ex_filt = ex_filt./emag;
    ey_filt = ey_filt./emag;
    c_lut = ~emag_lut;

quiver(x(3)(c_lut(:)),y(3)(c_lut(:)),ex_filt(c_lut(:)),ey_filt(c
_lut(:)), ...
        'color','w','linewidth',0.3,'AutoScaleFactor',0.2,
'MaxHeadSize', 1)

    set(gca,'ydir','reverse')
    axis([0, max(x(3)(:)), 0, max(y(3)(:))])
    hold off
    display('Saving QuiverPlot')
    saveres = 2^ceil(log2(max(size(x(3)))))*8;
```

```
    print(gcf, ['figure',num2str(ind),'_QuiverPlot'], '-dpng',
['-r',num2str(saveres)]); % '-r1200')
end
display('Done!')
end

function [x, y, u_filt, v_filt] = loadr
    a = dir;
    loc = cellfun(@(x) (regexp(x,'fixmask')), {a.name},
'UniformOutput', false);
    indx = cellfun(@(x) ~isempty(x), loc);
    b = {a(indx).name};
    if isempty(b);
        display('No Data in Directory!  Please place mat files
(output of LaunchPIV) in dir')
    end
    n = length(b);
    x = cell(1,n); y = cell(1,n);
    u_filt = cell(1,n); v_filt = cell(1,n);
    for ind = 1:n
        display(['Loading file: ' b(3) '  ...']);
        S = load(b(3));
        x(3) = S.x; y(3) = S.y;
        u_filt(3) = S.u_filt; v_filt(3) = S.v_filt;
%         shift_log = S.shift_log;
%         % create a maximum intensity projection for later
aligment
%         img = max(S.img{1}{5},S.img{1}{4});
    end
end
```